



UNIVERSITY OF TRENTO - Italy

PhD Program in Biomolecular Sciences
Centre for Integrative Biology
XXVIII Cycle

**DEVELOPMENT OF AN
ASSAY TO STUDY THE KINETICS OF
HIV-1 CAPSID UNCOATING**

Tutor: Prof. Anna Cereseto

Centre for Integrative Biology (CIBIO)

Laboratory of Molecular Virology

Ph.D. Thesis of

Stephen Findlay-Wilson

Centre for Integrative Biology, CIBIO

Laboratory of Molecular Virology

Academic Year 2015-2016

DECLARATION

I, Stephen Findlay-Wilson, confirm that this is my own work, and the use of all material from other sources has been properly and fully acknowledged.

A handwritten signature in black ink, reading "S. Findlay-Wilson". The signature is written in a cursive style with a large, sweeping initial "S" and a checkmark-like flourish at the end.

ABSTRACT

The acquired immune deficiency syndrome (AIDS) has caused over 60 million deaths since the etiological agent, human immunodeficiency virus type 1 (HIV-1), was first discovered in 1981. Over 6000 new HIV-1 infections are reported every day, predominantly in economically deprived regions of sub-Saharan Africa. Despite impressive developments in antiretroviral therapy, current medical intervention is unable to prevent or cure HIV-1 infection, necessitating expensive life-long treatment. Difficulties in establishing a vaccine or cure, arise from its capacity to cause life-long latent infection, and its extraordinary ability to evolve resistance to therapeutic intervention.

Capsid uncoating is the process by which p24^{CA} proteins (CA) disassemble from the viral ribonucleoprotein during the early phase of the HIV-1 lifecycle. Despite intensive investigation, much is yet unknown about the spatial and temporal occurrence of this process within the cell, and the viral or host cellular factors involved. However, studies investigating p24^{CA} mutations which alter the stability, and consequently the kinetics of capsid uncoating, have shown that timely capsid uncoating is crucial for efficient HIV-1 infection.

Recent advancements in microscopic techniques have enabled high resolution analysis of cellular protein interactions, including the *in situ* localisation and dynamics of these events. We have developed three imaging techniques for the analysis of different aspects of HIV-1 capsid uncoating: 1) a dual-fluorescently labelled virus 2) a fluorescently labelled antibody targeting a capsid internalised repeat peptide array, and 3) a split-luciferase system tagging an internalised component of the capsid core.

Fluorescent labelling of both the CA and IN proteins enabled the sensitive and specific analysis of uncoating in response to both restriction factors and CA mutations, and the visualisation of CA colocalised pre-integration complexes (PICs) within the nucleus. This system is ideally suited for studying the longer-term kinetics of uncoating, and the *in situ* visualisation of protein interactions. The use of the repeat peptide array in conjunction with fluorescently labelled antibodies, reinforced reports of an initial uncoating event early after viral fusion. This system enabled the rapid and reproducible imaging of uncoating events in real-time, within the same cell sample population. Finally, the split-luciferase

system added further weight to a primary early uncoating stage, and showed capsid disassembly responses specific to mutations within the p24^{CA} that affect the stability of the viral core.

Put together, these three assays support a model of uncoating involving an initial early phase of uncoating, followed by a more gradual disassembly of CA from the PICs during cytoplasmic trafficking towards the nucleus. The colocalisation of these components within the nucleus suggests incomplete uncoating at the time of nuclear docking.

The user-friendliness of the split-luciferase system, along with its capacity for high-throughput, real-time analysis, support great potential for its use as a screening assay for testing antiviral compounds targeting capsid uncoating events.

AIM OF THESIS

The CA monomer is one of the most conserved of the HIV-1 proteins, with studies suggesting it to be stretched to the limit by pressures to produce capsid cores of optimal stability, which are still able to interact with the numerous host factors necessary for productive infection. This genetic inflexibility, unlike that of other HIV-1 proteins, make CA and the process of capsid uncoating, attractive targets for therapeutic intervention.

Studies utilising mutations in the p24^{CA} protein, which alter the stability and consequently the kinetics of capsid uncoating, have shown that timely capsid uncoating is crucial for the productive infection of HIV-1. Although multiple techniques have been employed to understand this process, the fragility of the capsid core makes it very sensitive to external manipulation. As such, much is yet unknown about the *in situ* temporal and spatial kinetics of uncoating, and the cellular factors involved.

The principal aim of this thesis was to develop, optimise and evaluate an imaging-based system for studying the kinetics of capsid uncoating within the 3-D spatial context of the cell. This system would be used to visualise the subtle cellular/capsid interactions necessary for functional viral core disassembly within the cellular environment, to help further the understanding of this complex process.

An additional objective of this project was to adapt the system for the high-throughput analysis of capsid uncoating for use in the identification of compounds which impede the normal process of uncoating, as an alternative strategy for pharmaceutical intervention.

ACRONYMS/ABBREVIATIONS

2-LTR	Two-long-terminal-repeat
A3F	APOBEC3F
A3G*	APOBEC3G Mutant
AIDS	Acquired Immune Deficiency Syndrome
APOBEC	Apolipoprotein B mRNA editing enzyme, catalytic polypeptide-like protein
AU	Airy unit
BI-1/2	Boehringer-Ingelheim pyrrolopyrazolone compounds 1 and 2
CA	p24 capsid monomers
C-A1	Coumermcin-A1
Capsid/core	The fullerene capsid core
CPSF6	Cleavage and polyadenylation specificity factor 6
CsA	Cyclosporine A
CTD	Carboxyl-terminal domain
CypA	Cyclophilin A
D110E	Reverse transcriptase mutant
E128A/R132A	CA mutant which stabilises the capsid core
E45A	CA mutant which stabilises the capsid core
EGFP	(Enhanced) Green fluorescent protein
FEZ1	Fasciculation and Elogation Factor zeta 1
Flash	Fluorescein arsenical hairpin
Gag	Group specific antigen
HiBiT	NanoBiT HiBiT
IFN	Interferon
IN	Integrase
K203A	CA mutant which destabilises the capsid core
LEDGF	Lens epithelium-derived growth factor
LgBiT	NanoBiT Large BiT
LTR	Long terminal repeat
MDM	Monocyte derived macrophages
MHR	Major homology region
mKO	Monomeric Kusabira Orange
MTOC	Microtubule-organising centre
Mx2	Myxovirus-resistance 2
NC	Nucleocapsid
Nef	Negative factor
NNRTI	Non-nucleoside reverse transcriptase inhibitor

NPC	Nuclear pore complex
NTD	Amino-terminal domain
Nup	Nucleoporin
PAMP	Pathogen associated molecular patterns
PF74	Pfizer-3450074
PIC	Pre-integration complex
pNL4-3	pNL4-3.Luc.R ⁻ E ⁻
PR	Protease
p.s.	Post-Spinoculation
PSF	Point spread function
Rev	Regulator of viral gene expression
RLU	Relative luminescence units
RT	Reverse transcriptase
RTC	Reverse transcription complex
RTU	Reverse transcription units
sfGFP	Superfolder GFP
shRNA	Short hairpin RNA
SIM	Structured illumination microscopy
siRNA	Short interfering RNA
SIV	Simian immunodeficiency virus
SNR	Signal to noise ratio
SP1/2	Spacer peptide 1/2
SU	Surface protein
Tat	Transactivator of transcription
TM	Transmembrane protein
TNPO3	Transportin 3/transportin-SR2
TRIM-Cyp	Tripartite motif-containing protein-cyclophilin
Vif	Viral infectivity factor
VLP	Virus-like particle
VNC	Viral nucleoprotein complex
Vpr	Viral protein R
Vpu	Viral protein U
VSV-G	Vesicular stomatitis virus glycoprotein
WHO	World Health Organisation
WT	Wild Type

CONTENTS

DECLARATION.....	iii
ABSTRACT.....	v
AIM OF THESIS.....	vii
ACRONYMS/ABBREVIATIONS.....	ix
CONTENTS.....	xi
INTRODUCTION.....	1
1.1 AIDS.....	1
1.2 HIV-1.....	1
1.2.1 Genomic structure.....	2
1.2.2 Replication cycle.....	3
1.2.3 Maturation.....	5
1.3 Capsid structure.....	5
1.3.1 CA p24 monomer.....	5
1.3.2 Capsid structure – capsid core.....	6
1.4 Capsid – roles in the early phase of infection.....	8
1.4.1 Housing of the viral ribonucleoprotein.....	8
1.4.2 Immune evasion.....	8
1.4.3 Reverse transcription.....	9
1.4.4 Trafficking towards the nucleus.....	10
1.4.5 Nuclear entry.....	10
1.4.6 Integration.....	11
1.5 Models of capsid uncoating.....	12
i) Rapid uncoating.....	13
ii) Gradual/biphasic uncoating.....	13
iii) Uncoating at the nuclear pore.....	14
1.6 Capsid uncoating – why study?.....	16
1.7 Systems for studying uncoating.....	17
1.7.1 In vitro core-stability and disassembly assay.....	17
1.7.2 Fate of capsid assay.....	18
1.7.3 Cyclosporine A washout assay.....	18
1.7.4 Imaging assays.....	19

1.8 Factors affecting the kinetics of uncoating.....	20
1.8.1 Capsid mutations	20
1.8.2 Restriction compounds	21
1.8.3 Protein knockdowns – CA interaction with host proteins	23
1.9 The role of imaging methods in studying uncoating.....	29
1.9.1 Imaging within living cells – Vpr-GFP	29
1.9.2 Fluorescently labelled integrase.....	30
1.9.3 Cyclosporine A washout and internalised GFP (iGFP)	31
1.9.4 Evidence of a biphasic model of capsid uncoating	32
1.9.5 Live imaging of HIV-1 uncoating	33
1.9.6 Capsid within the nucleus.....	33
1.10 Novel labelling systems	35
1.10.1 Intra-capsid core labelling using APOBEC3F and G	35
1.10.2 SUpErNova Tagging (SunTag).....	36
1.10.3 NanoBit.....	37
1.11 Summary.....	39
METHODS	41
2.1 Cell lines.....	41
2.1.1 Stable cell lines:	41
2.2 Virus production	42
2.3 Virus quantification	43
2.4 Infectivity assay	44
2.5 Immunostaining.....	44
2.6 Restriction compounds.....	45
2.7 Preparation of capsid mutants	45
2.8 Capsid uncoating assays:.....	46
2.8.1 Dual-labelled system:.....	46
2.8.2 SunTag – capsid-Tag.....	47
2.8.3 SunTag – repeat peptide array.....	49
2.8.4 NanoBiT	50
2.9 Operetta High-Content screening.....	52
2.9.1 Harmony High-Content Imaging and Analysis Software	52
2.10 Confocal Microscopy.....	54
2.10.1 Semi-automatic colocalisation.....	55

2.10.2 Bleed-through	56
2.10.3 DeconvolutionLab	57
RESULTS	59
3.1 A dual-fluorescent virus for studying uncoating.....	59
3.1.1 Colocalisation of CA-GFP with IN-mCherry in CD4 ⁺ cells.....	61
3.1.2 Development of a time course for studying uncoating	63
3.1.3 Effects of restriction compounds and capsid mutants.....	65
3.1.4 High-throughput analysis of uncoating	68
3.1.6 Colocalisation of capsid with integrase within the nucleus.....	75
3.2 SunTag capsid-tag (CA-SunTag)	77
3.3 Studying capsid uncoating with Vpr-IN-24xSunTag	81
3.3.1 24xSunTag analysis with Operetta High-Content Imaging	84
3.4 Studying uncoating with APOBEC3-24xSunTag.....	88
3.5 Operetta High-Content Imaging using a 60x objective.....	90
3.6 NanoBiT luciferase analysis of HIV-1 uncoating	92
DISCUSSION.....	95
4.1 A dual-fluorescent system for studying uncoating	96
4.1.1 Validation of dual-labelled virus	97
4.1.2 High-throughput analysis of uncoating	100
4.1.3 Colocalisation within the nucleus.....	102
4.2 SUpErNova tagging (SunTag) system – CA-SunTag.....	102
4.3 Non-capsid based reporter assays.....	104
4.4 High-throughput analysis of uncoating.....	105
4.4.1 Analysis of the 24xSunTag with High-content imaging.....	105
4.4.2 Luciferase analysis of capsid uncoating using the NanoBiT.....	107
CONCLUSION.....	111
FUTURE PERSPECTIVES	113
REFERENCES	115
SUPPORTING INFORMATION.....	141
ACKNOWLEDGEMENTS.....	143

INTRODUCTION

1.1 AIDS

The Acquired Immune Deficiency Syndrome (AIDS) first came to light as a new disease in 1981, with the reports of unusual occurrences of *pneumocystis carinii* pneumonia and Kaposi sarcoma in previously healthy, young homosexual men [1][2][3]. The causative agent was subsequently isolated and characterised as a human T-lymphotropic virus III (HTLV III) in 1983, and was officially named as the human immunodeficiency virus (HIV) by the International Committee on the Taxonomy of Viruses in May 1986 [4][5][6][7]. Since then the pandemic form of HIV-1, also known as the main (M) group, has infected at least 60 million people and caused more than 35 million deaths [8] (who.int/mediacentre/factsheets). According to World Health Organisation (WHO) statistics, there were approximately 36.7 million people worldwide living with HIV-1 by the end of 2015, but it is estimated that only 54% of people actually know they are infected (who.int/mediacentre/factsheets).

1.2 HIV-1

The HIV-1 virus is a group VI member of the *Retroviridae* family. These are enveloped viruses characterised by their ability to reverse transcribe their RNA genome into double-stranded DNA intermediates, through use of their own reverse transcriptase (RT) enzyme, and integrate their genome into host chromosomal DNA [9]. The resultant 'provirus' then serves as a template for the transcription and translation of the genomic RNA and proteins required for the development of future viral progeny. These defining features enable the virus to maintain a persistent infection within the host despite the activation of antiviral immunity. HIV-1 is further categorised as a lentivirus, which are complex viruses characterised by having a long incubation period (*lente* meaning slow in Latin) and a unique virion morphology, demarcated by the conical capsid cores [9].

1.2.1 Genomic structure

The HIV-1 genome is primarily a coding RNA that contains nine open reading frames, which translate into 16 proteins, flanked by two long terminal repeats (LTR) (**Fig. 1**) [10]. The three primary translational products (Gag, Pol and Env) encode structural proteins which are initially synthesised as polyprotein precursors, and subsequently processed into mature particle associated proteins through the action of viral or cellular proteases [9]. The 55 kDa group-specific antigen (Gag) precursor is cleaved into the matrix (MA), capsid (CA), nucleocapsid (NC) and p6 proteins. Autocatalysis of the 160 kDa Gag-pol polyprotein generates protease (PR), the heterodimeric reverse transcriptase (RT) and the integrase (IN) proteins. The 160 kDa envelope (Env) precursor is cleaved into the gp120 surface (SU) and gp41 transmembrane (TM) proteins through proteolytic digestion by cellular enzymes. The six remaining regulatory proteins (trans-activator of transcription (Tat) and regulator of the expression of the virion (Rev)) and accessory proteins (viral infectivity factor (Vif), viral protein R (Vpr), viral protein U (Vpu) and negative regulatory factor (Nef)) are translated from spliced mRNA transcribed from the integrated provirus [9].

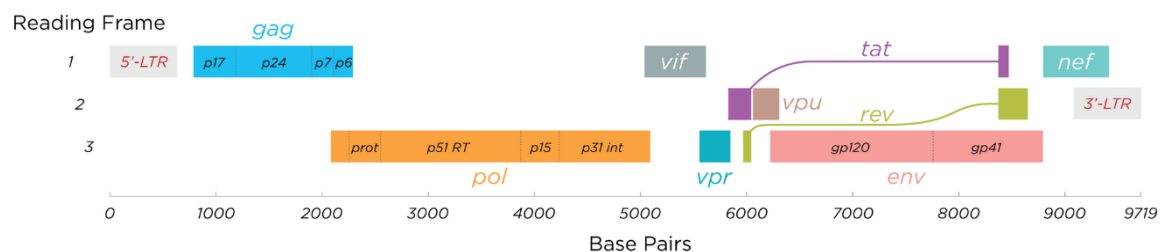


Figure 1. Genomic organisation of HIV-1. Illustration depicting the ~9.7 kb HIV-1 genome, highlighting the three main open reading frames coding for 16 proteins [11]. Long terminal repeats (LTRs) flank the genome of the integrated viruses, and contain important regulatory regions for transcription initiation and polyadenylation. The main structural proteins and regulatory enzymes (Gag, Gag-Pol and Env) are initially synthesised as polyprotein precursors, which are subsequently cleaved by viral proteases and cellular proteases (Env) into 11 subunits (Gag = MA, CA, sp1, NC, sp2 and p6; Pol = PR, RT (containing RNase H) and IN; and Env = SU and TM). Ribosomal frame-shifting permits the expression of the 160 kDa Gag-Pol protein precursor at a ratio of roughly 1:20 of that of the Gag polyprotein [12][13].

Illustration by Thomas Spletstoeser (www.scistyle.com).

1.2.2 Replication cycle

The HIV-1 replication cycle is generally characterised by two stages – the early and late phases of infection (**Fig. 2**). The early phase encompasses the initial steps of HIV-1 cellular entry. Primarily, the HIV-1 Env glycoprotein (gp41/gp120) sequentially binds with the CD4 receptor and co-receptors (CCR5 or CXCR4) present on the surface of the receptive host cell, which initiates fusion with the cellular membrane, releasing the viral core into the cellular cytoplasm [14]. A series of transformational steps occurs commencing with the reverse transcription of the two copies of positive-sense single-stranded viral RNA, at this point known as the reverse transcription complex (RTC), into double stranded copy DNA (cDNA) to form the pre-integration complex (PIC) [15]. The PIC is a ~28 nm particle containing the cDNA and various viral (MA, CA, NC, IN, RT and Vpr) and host proteins [16][17]. The PIC is then transported through the nuclear pore complex, whereupon the cDNA is integrated into the host genome through catalases by IN, to produce the provirus [17]. At some point between fusion with the cellular membrane and nuclear entry, the viral capsid core goes through a process of progressive disassembly from the viral nucleoprotein, in a process known as uncoating. This process will be the main subject of this study.

In the late phase of HIV-1 infection, proviral DNA is transcribed by host RNA polymerase into full length viral RNA. A subset of the transcripts are spliced and exported into the cytoplasm where they are translated into the regulatory proteins transactivator of transcription (Tat), which promotes transcription elongation, and the regulator of viral gene expression (Rev) [18]. The Rev protein mediates the export of singly spliced and unspliced viral RNAs from the nucleus. A conformational switch in the 5' untranslated region (UTR) of RNA determines whether it is translated for the expression of the Gag, Pol and Env gene products, or dimerised for packaging into new viral particles [19][20]. The Pr⁵⁵Gag precursor polyprotein (Gag) binds to dimerised genomic RNA (gRNA) through two zinc finger motifs present within NC [21][22][23] and the gRNA/Gag subcomplex traffics through the cytoplasm towards the cellular membrane for attachment and assembly [24]. The MA domain undergoes myristoylation at the N-terminal domain enabling the gRNA/Gag subcomplex to embed into the plasma membrane for early virion assembly [25][26]. This is followed by a rapid

accumulation of Gag, which forms higher-order structures (multimerisation) mediated by contacts between adjacent MA, CA and NC domains [27][28]. Viral budding is mediated through the interaction of two motifs on the p6 domain of Gag (PTAP and YPXnl) with the ‘host endosomal sorting complexes required for transport’ (ESCRT) machinery [29][30]. Interactions with the p6 domain also mediate the incorporation of Vpr into the assembling viral particle [31].

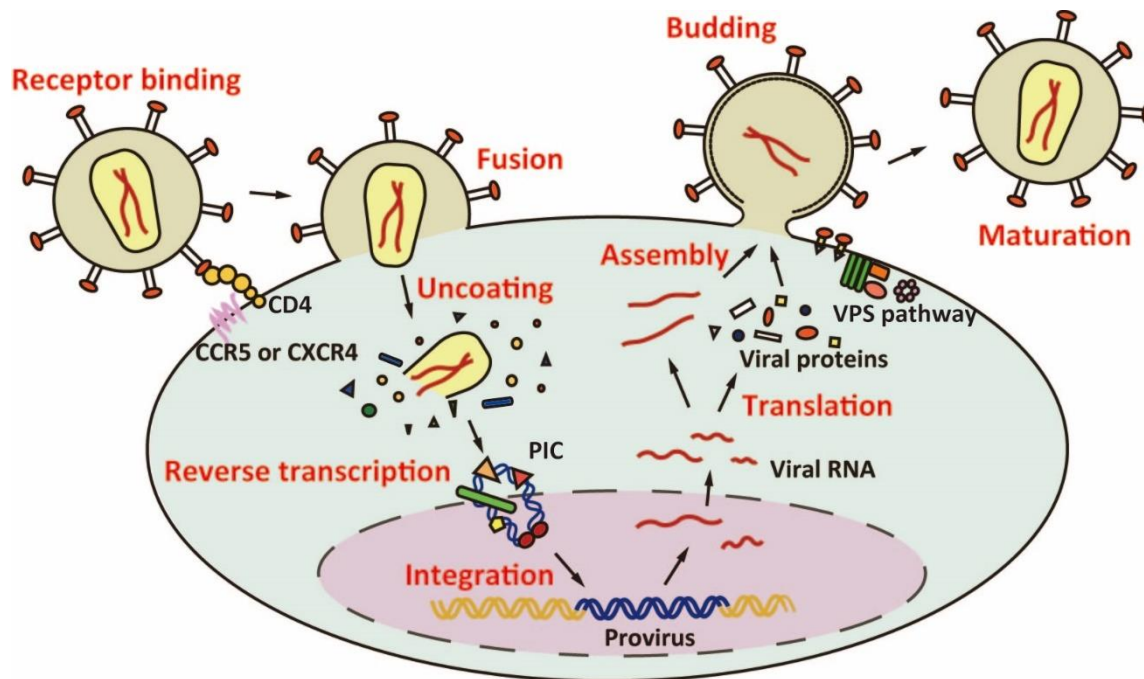


Figure 2. Schematic depicting the principal stages of the HIV-1 replication cycle [32]. A mature virion binds to a CD4 receptor and co-receptors (CCR5/CXCR4) present on the surface of a receptive cell, instigating fusion with the cellular membrane and release of the capsid core within the cytoplasm. The viral RNA is then reverse transcribed (reverse transcription complex) into double stranded linear DNA to form the pre-integration complex, which is translocated into the nucleus. At some point during these events the capsid core disassembles, in a process known as uncoating. The viral DNA integrates into the host genome forming the provirus, which is subsequently transcribed and translated into new viral RNA and protein molecules. These are trafficked across the cytoplasm and assembled at the cellular membrane, initiating budding and release of the immature virions. Viral proteases cleave the structural polyproteins to create the distinctive fullerene capsid core surrounding the viral nucleoprotein complex (VNC), in the formation of a mature HIV-1 virus.

1.2.3 Maturation

Viral maturation occurs concomitantly with the budding and release of the immature virion from the plasmid membrane [33][34][35]. It consists of a series of coordinated cleavages of the Gag-Pol polyprotein by the viral protease at ten different sites, producing the fully processed MA, CA, NC, p6, Pr, RT and IN proteins [36]. Proteolytic processing is a highly regulated event, with the timing and sequence of cleavage shown to be critical for the formation of infectious viral particles [37]. The cleavage of spacer peptide 1 (SP1) from the CTD of CA marks the final step in this process, and is known to be particularly important for structural rearrangement from a spherical immature core to the mature conical morphology [38]. The exact means by which rearrangement occurs have yet to be fully defined. The MA proteins remain associated with the inner layer of the viral membrane, whilst the CA monomers form a geometric lattice composed of ~250 CA hexamers, with 12 CA pentamers defining the curvature of the core and its typical cone shaped appearance [36]. The capsid core surrounds the two single strands of positive-sense RNA and the various enzymes and accessory proteins required for successful HIV-1 replication.

1.3 Capsid structure

The HIV-1 'capsid' is a term which is often used to refer to both the p24^{CA} monomers and the capsid fullerene core. To reduce confusion, 'CA' will be used to describe the p24^{CA} protein monomers, and 'capsid' to describe the assembled conical core.

1.3.1 CA p24 monomer

The HIV-1 CA monomer (p24^{CA}) is composed of two independently folded domains, a ~150 amino acid (aa) amino-terminal domain (CA_{NTD}) and an ~80 aa carboxyl-terminal domain (CA_{CTD}), bound by a 5-residue flexible linker [39] (**Fig. 3**). Both domains have a predominantly α -helical secondary structure: the CA_{NTD} is arrowhead shaped, with seven α -helices (numbered 1–7) and an amino-terminal β -hairpin, whilst the CA_{CTD} is more spherical, with a short single-turn 3_{10} -helix followed by an extended strand and four α -helices (numbered 8–11) [39][40]. The alpha helices act as stabilisers for the CA subunits. The CA_{NTD}, or

core domain, contains the exposed cyclophilin binding loop and is located on the outer surface of the mature capsid core, whilst the CA_{CTD}, also known as the dimerisation domain, is orientated towards the interior of the capsid core. The CA protein is relatively well conserved amongst the Gag proteins, with the major homology region in the N-terminus of CA_{CTD} displaying significant aa identity between divergent retrovirus genera [41].

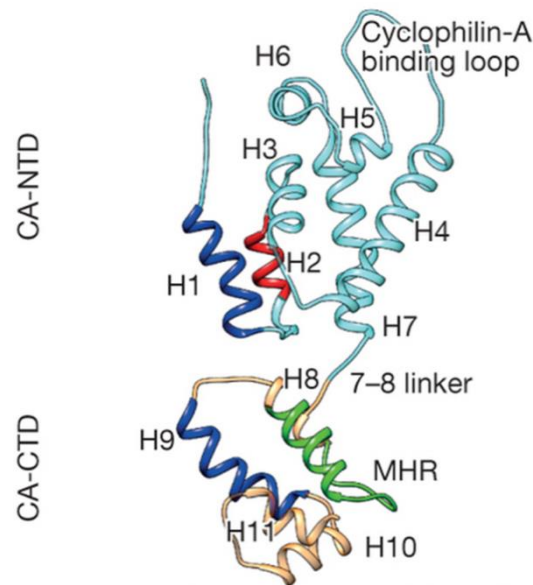


Figure 3. Structural model of the HIV-1 CA protein [42]. An annotated p24^{CA} model depicts the 7 alpha helices and the cyclophilin-A binding loop of the amino-terminal domain (NTD) connected, by a 5-residue flexible linker, to the carboxyl-terminal domain (CTD) comprising 4 alpha helices and the major homology region (MHR) in green. The helices highlighted in blue and red are involved in the intermolecular interactions which contribute to the formation of hexameric and pentameric rings, and the subsequent hexagonal lattice [42].

1.3.2 Capsid structure – capsid core

During virion budding and maturation the Gag polyprotein is cleaved through the action of the autogenous protease enzyme, and the CA monomers reassemble to form the geometric fullerene core [43]. The CA monomers are organised into hexameric (**Fig. 4B and D**) and pentameric rings (**Fig. 4C and E**), which are stabilised by interactions between the first three helices of the CA_{NTD} [36]. The capsid rings are in turn stabilised by an exterior ‘girdle’ formed by the CA_{CTD} that also forms inter-subunit contacts with adjacent CA_{NTD}. The CA_{CTD} also makes inter-ring contacts across the local two- and three-fold axes, which stabilises the

extended lattice. Larger assemblies of hexamers and pentamers are maintained by hydrophobic residues within the CA_{CTD}, which provide the structural support for the mature capsid core [44]. When assembled into the mature conical core (**Fig. 4A**) the CA_{NTD} is orientated towards the outer surface of the structure, whereas the CA_{CTD} is located within the interior of the core. The CA_{NTD} and CA_{CTD} interface forms a binding pocket between helices 3, 4, 5 and 7, which interacts with various host cellular factors intrinsic to HIV-1 infection, such as nucleoporin (Nup) Nup358 and cleavage and polyadenylation specificity factor 6 (CPSF6), and is also a target for the small molecular restriction compounds PF74 and BI-1 [45][46][47][48].

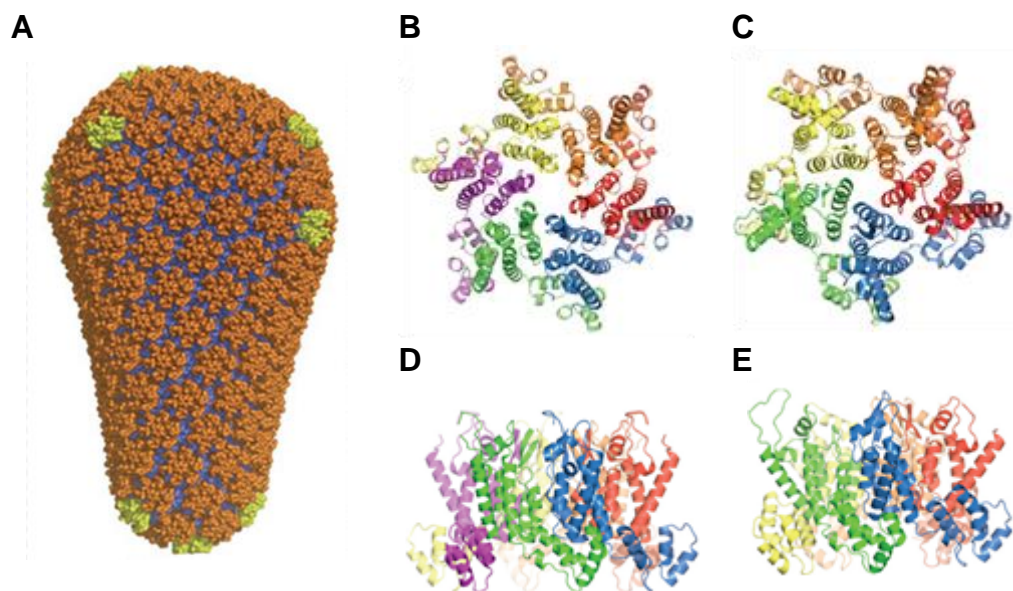


Figure 4. Model of an HIV-1 capsid core and structure of the CA hexamers and pentamers [49]. (A) 3D representation of a mature capsid core, showing the spatial configuration of the hexamers, pentamers and dimers highlighted in orange, yellow and blue, respectively. The arrangement of 12 CA pentamers at polar ends of the structure create the distinctive cone shaped appearance of the capsid core. (B and C) Top view of a CA hexamer and pentamer, respectively, with their corresponding side views depicted directly underneath (D and E). Helices are represented as ribbons, and each subunit is presented in a different colour.

1.4 Capsid – roles in the early phase of infection

Early work using biochemical methods for isolating the RTC/PICs implied that capsid only had a small role in the early phase of the HIV-1 replication cycle, delivering the viral genome and associated proteins into the cytoplasm of the target cell [15]. The viral capsid core is a relatively fragile complex, and the detergents/low salt conditions used for hypotonic lysis and removal of the viral membrane were probably stripping the core from the viral nucleoprotein, precluding its detection in immunoprecipitation assays [16][50][51][52][53]. Advances in genome-wide analysis and cellular imaging techniques, however, have enabled the detection of PIC associated CA within the nucleus, suggesting a more prominent role in HIV-1 infectivity [54][55][56][57][58].

Below is a list of some of the roles in the early phase of infection that CA/capsid has been linked with.

1.4.1 Housing of the viral ribonucleoprotein

The principle role of the capsid core is to provide an encapsulating sheath with which to contain two copies of the viral RNA genome and proteins necessary for infection, such as PR, RT, IN, NC, Nef and Vpr [17][59]. This is produced during maturation of the nascent viral particle through protease cleavage of the Gag polyprotein, and ensures the correct delivery of the viral ribonucleoprotein complex into the target cell.

1.4.2 Immune evasion

Several reports suggest a role in immune evasion for the viral core [60][61][62][63]. A recent study by Rasaiyaah and co-workers provided evidence of the innate immune sensor evasion properties of the capsid core in monocyte-derived macrophages (MDMs) [60]. HIV-1 is able to replicate in primary human macrophages without stimulating innate immunity, despite the production of cDNA, a key trigger for interferon (IFN) mediated restriction in HIV-1 infection [64]. The capsid mutants N74D and P90A, however, cannot replicate in MDMs because they trigger innate sensors leading to type 1 IFN production and an antiviral state [60]. Using the RT (D185E) or IN (D116N) mutants in combination

with the N74D capsid mutant, *IP10* expression (an IFN stimulated gene) was induced with the CA/IN double mutant but not with the CA/RT double mutant. This data indicated that viral DNA produced by reverse transcription was the pathogen-associated molecular pattern (PAMP) that triggered the innate immune response in MDMs. Depletion or pharmacological inhibition of the cofactors CPSF6 and cyclophilin A (CypA,) which interact with the CA mutants N74D and P90A, respectively, also induced wild-type HIV-1 infection to stimulate IFN secretion in MDMs. The authors propose that CPSF6/CypA recruitment to CA suppresses premature viral DNA synthesis, allowing evasion of innate immune sensors, adding weight to the importance of correctly orchestrated HIV-1 uncoating and nuclear entry [60].

1.4.3 Reverse transcription

The capsid core may also act to maintain both the viral genome and RT in a spatially enclosed environment. Numerous strand transfers are necessary for the conversion of the viral genome into double stranded DNA, and it has been suggested that the HIV-1 capsid is essential for maintaining a high stoichiometry of RT relative to the viral RNA, to offset its tendency to detach from the template during reverse transcription [65][66]. Dilution of RT in the cellular cytoplasm would substantially reduce the efficiency of reverse transcription [15]. Interestingly, several studies support a functional link between reverse transcription and uncoating [67][68], demonstrating that suppressing reverse transcription delays uncoating. Alternatively, several CA mutations altering *in vitro* core stability generated fewer reverse transcripts, indicating that it was capsid stability that affected reverse transcription [65][69][70]. One theory behind this relationship is that the double-stranded reverse-transcription product forms a more rigid structure, which could provide an outward force to destabilise the core [67]. Thus, the viral core may act as a reaction chamber containing the necessary reagents just long enough for the completion of reverse transcription. Another hypothesis holds that at least partial uncoating is required to enable entry of the cellular factors (nucleic acid binding proteins, DNA repair and splicing factors) necessary for completion of reverse transcription [54][71][72]. However, the capsid lattice is reported to be an open structure containing inner-

ring gaps of up to 10 nm which would allow, at the least, the entry of the cellular nucleotide triphosphates for reverse transcription [73].

1.4.4 Trafficking towards the nucleus

HIV-1 capsid/p24 has also been reported to play a role in transporting the viral nucleoprotein towards the nucleus through the interaction with the host cell microtubules, hijacking the cytoskeletal networks to support their movement across the cell [44][74]. Various experiments have been employed to support this role, including disrupting microtubule mediated trafficking using nocodazole, and pharmacological or small interfering RNA (siRNA) inhibition of the dynein and kinesin-1 microtubule motor complexes which interact with the virus particles [75][76][77]. *In vitro* assembled HIV-1 CA-NC complexes were shown to directly interact with the kinesin-1 adaptor protein fasciculation and elongation factor zeta 1 (FEZ1), which regulates movement towards the nucleus [76]. Fluorescently labelled capsid particles have also been visualised associating with the microtubule network, providing further evidence of a possible role in CA mediated cytoplasmic trafficking of HIV-1 particles [53][78].

1.4.5 Nuclear entry

Nuclear pore complexes (NPC) are multiprotein channels that pepper the nuclear envelope and act as a selective barrier against infection from retroviruses unable to infect non-dividing cells, such as Murine leukaemia virus (MLV) [79][80][81]. HIV-1 is able to actively transport through the NPC of non-dividing cells by hijacking the cellular transport machinery [82][83][84]. Capsid was first identified as having a role in nuclear import when an HIV-1 chimera, in which the HIV-1 CA coding sequences were replaced with MLV, lost the ability to efficiently infect non-dividing cells [79]. Several genome-wide siRNA screenings identified a number of nuclear transport factors as potential cofactors in HIV-1 infection [54][56][58], with CypA, transportin 3 (TNPO3), CPSF6, and the nucleoporins Nup358 and Nup153 seeming to have a direct interaction with CA during nuclear translocation [85][86][87]. It is difficult to determine the significance of these CA-mediated interactions as depletion of nuclear transport factors alters the structure and function of the NPC, leading to concerns that the knockdown effects were actually due to indirect consequences caused by perturbations of cellular activity

[85]. The role of CA in nuclear trafficking, however, is supported through studies using a number of CA mutants. For example, the CA mutants T45A/N57A and Q63A/Q67A exhibit cell cycle dependent infectivity responses as attested to by PCR quantification of two-long-terminal-repeat (2-LTR) circles, with cell cycle arrest leading to a decrease in infection after nuclear import with the T45A/N57A CA mutant, but before nuclear import with the Q63A/Q67A CA mutant [88][89]. Also, the N74D CA mutation was shown to be insensitive to the knockdown of TNPO3, Nup358 or Nup153 [90][91][92], and the G89V and P90A CA mutants were less sensitive than WT virus to Nup358 and Nup153 depletion [90][91][92][93].

1.4.6 Integration

Evidence is growing that CA may also play a role in post-nuclear events, including integration [94]. HIV-1 preferentially targets clusters of active genes within gene dense regions of chromosomes [95]. Although lens epithelium-derived growth factor (LEDGF/p75) is the predominant factor in directing integration within active gene bodies [96][97], knockdown studies have revealed that the nuclear factors TNPO3 and CPSF6, and the Nups 358 and 153 may have a part in targeting the gene dense regions of chromosomes [91][98][99][100][101][102]. Similar shifts in integration-site preferences have also been observed when using CA mutants, suggesting a post-nuclear entry targeting role for this protein. The HIV-1 CA cyclophilin-binding mutants G89V and P90A generally integrated in genomic regions with a higher density of transcription units compared to WT virus, whereas the N74D and N57A CA mutants, which are insensitive to Nup358 and TNPO3 depletion, favoured integration in genomic regions sparse in transcription units [91]. Inhibition of CypA-CA binding through the presence of cyclosporine A (CsA) led to integration of wild type (WT) virus in regions of higher transcription density, similar to that of the G89V and P90A binding mutants, suggesting that the CA-CypA association has a role in influencing nuclear import, and subsequently, site of integration [91]. Studies using the gyrase B targeting antibiotic Coumermcin-A1 (C-A1), which binds to hexameric CA in a binding pocket defined by two adjacent monomers, showed that C-A1 inhibits integration in a CA-dependent way, without affecting reverse transcription [103]. The N74A and A105S CA mutants negated the

restrictive capacity of CA-1, enabling normal integration. Further experiments using the tripartite motif-containing protein-cyclophilin (TRIM-Cyp)/CsA washout assay seemed to link integration-site selection with earlier CA uncoating events, influencing the cofactors the PIC associated with during nuclear translocation.

Recent studies employing the knockdown of CPSF6, or the deletion of the CA binding domain of CPSF6, revealed an obstruction of HIV-1 integration within transcriptionally active gene-dense regions, intron-rich genes, and the specific location of integration within the genes [98][99]. Capsid staining revealed a similar location of CA within the nucleus for WT virus within CPSF6 depleted cells, to that of control cells infected with a N74A CA mutant virus which prevents binding with CPSF6 [99]. A preference for proviral integration at the periphery of the nucleus was also shown for WT type virus in CPSF6 depleted cells, and the CPSF6 non-binding CA mutants N74D and A105T in control cells.

Collectively, these data indicate that TNPO3, Nups 153 and 358, and particularly CPSF6, play important roles in the regulation of sites of HIV-1 integration, and that CA is the component of the PIC most likely to interact with these proteins.

1.5 Models of capsid uncoating

Historically, capsid uncoating has been considered from a structural perspective, and is defined as the specific dissociation of the capsid shell from the viral core in the host cell cytoplasm [104]. However, based on recent demonstrations that CA influences late events including nuclear import and integration [92][98][99][100][101][102][105], and has been visualised colocalised with IN within the nucleus [55][57], it is unlikely that CA loss from the RTC is a single, discrete event. Thus, some re-evaluation of the traditional definition of uncoating is required [44].

Although there is general agreement that uncoating occurs after fusion dependent entry into the cytoplasm and before nuclear entry, the field remains divided as to the precise moment and location at which this takes place, and the extent of capsid disassembly from the viral nucleoprotein complex (VNC) before nuclear translocation. One of the defining features of HIV-1 infection is its ability

to infect non-dividing cells [79], which necessarily incurs the translocation of the PIC from the cellular cytoplasm into the nucleus through the NPC. Studies have revealed that the upper size limit for passage within the NPC to be ~39 nm, which is considerably smaller than the 50-60 nm diameter of the wide end of the capsid cone [39][106][107], affirming the model of cytoplasmic capsid uncoating.

Three main models of uncoating have been proposed (**Fig. 5**):

- i. A rapid core disassembly following cellular entry
- ii. A more gradual uncoating as the virus traverses the cytoplasm towards the nucleus
- iii. Uncoating at the nuclear pore

i) Rapid uncoating

With this model the capsid core disassembles close to the cellular membrane almost immediately following viral fusion (**Fig. 5A**). Although most of the capsid is described to disassociate from the VNC, this does not rule out the presence of a residual amount of CA remaining with the RTC/PIC after uncoating [17][108][109][110]. This model was proposed due to the absence of detectable CA when using biochemical means to study the content of the RTC [16][50]. This model, however, does not account for the cytosolic sensors that would be activated in the presence of viral cDNA PAMPs upon rapid core disassembly [60][61][63], or the loss of a closed environment to facilitate reverse transcription.

ii) Gradual/biphasic uncoating

This model proposes that the viral core remains intact for some time post-fusion, and that uncoating takes place gradually during passage towards the nucleus through interaction with cytoplasmic host cell factors and reverse transcription (**Fig. 5B**) [67][72][111]. Experiments using the intact capsid core targeting properties of TRIM-Cyp, and immunofluorescent imaging, support this model [53][67]. Loss of sensitivity to TRIM-Cyp binding was observed 3-4 h post-infection, and approximately two thirds of RTCs were observed still containing detectable amounts of CA 4 h post-infection. Some authors suggest that the CA-CA interactions that create the delicate lattice of the viral core would not tolerate

a gradual disassembly of CA and, like the rapid uncoating model, the cDNA would be exposed to cytosolic sensors [44][86]. However, cellular factors recruited to the RTC/PIC during capsid uncoating may be able to mask the nascent viral cDNA from antiviral innate immune detection [44].

iii) Uncoating at the nuclear pore

A third model proposes that the capsid core remains intact during transport towards the nucleus, and uncoating takes place at the nuclear pore (**Fig. 5C**) [86]. In this model, premature uncoating is suppressed through the interaction of CypA and CPSF6. Upon arrival at the NPC the capsid core binds to Nup358 and uncoating is triggered with the assistance of CA-associating factors (TNPO3, CypA and CPSF6), upon which the PIC is released and is translocated through the nuclear pore into the nucleus [86]. With this model the viral genome would be protected by the capsid core, thus excluding the triggering of the innate DNA sensor of cyclic GMP-AMP synthase (cGAS). This system is supported by work performed in MDMs which have been shown to be infected with WT HIV-1 without triggering an innate immune response [60]. Capsid mutations, however, and HIV-1 infection in CPSF6 and CypA-depleted macrophages, which potentially generate the premature release of cDNA, activate an antiviral state within the cell.

There is evidence based data supporting and opposing all of these models for capsid uncoating, and it may be that the real system contains aspects from each model. Uncoating may also vary depending on the cell type and the activation state of the cell at the time of infection [44]. Contemporary thinking seems to support a model of uncoating involving the initial loss of integrity of the intact core, leaving a residual amount of CA associated with the viral nucleoprotein for interaction with the host proteins [44].

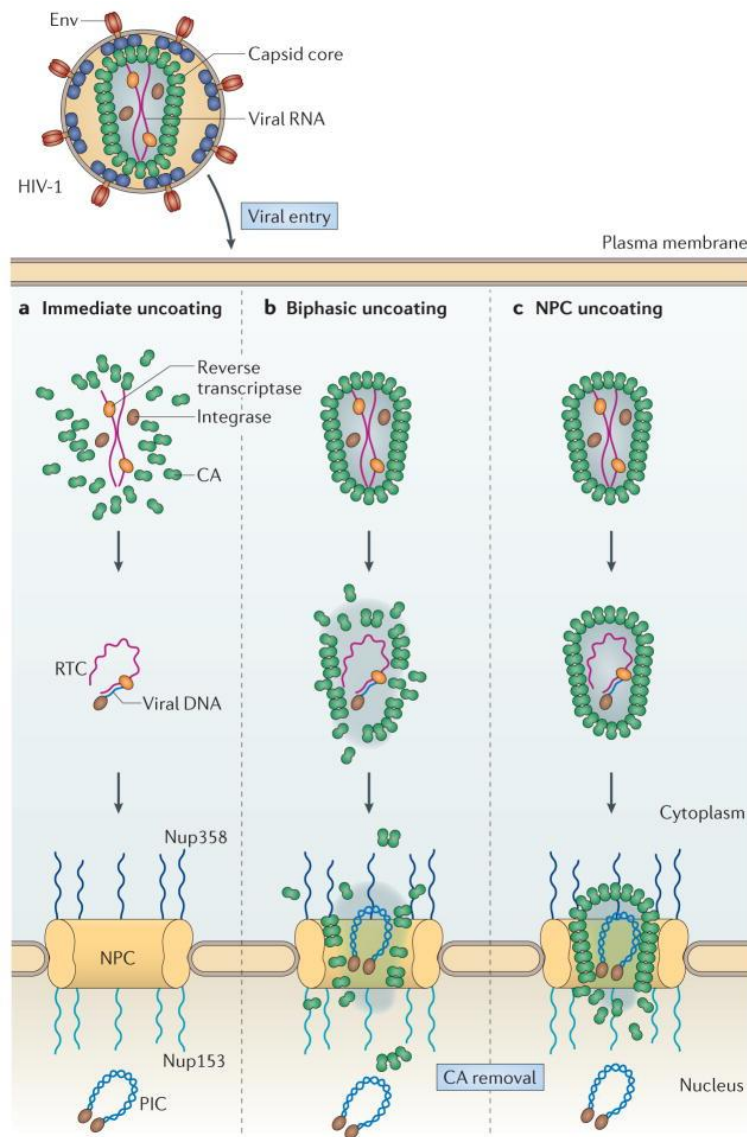


Figure 5. Illustrations depicting the principal models of HIV-1 capsid uncoating [44]. Three models of uncoating have been proposed, subjective to the methods deployed for analysis: A) Immediate uncoating of the entire capsid core directly after viral fusion with the cellular membrane; this model was supported by early biochemical studies [16][44]; B) Gradual/biphasic uncoating, in which a measurable amount of capsid disassembly occurs as the VNC traffics through the cytoplasm, with a portion of the capsid remaining to mediate nuclear docking and translocation. This model is supported by several imaging-based assays and the CsA washout assay [67][111]; (C) Uncoating at the NPC, in which the capsid core remains intact up until mooring at the nuclear pore, whereby uncoating is facilitated through interaction with Nups. With this model the viral dsDNA is shielded from cellular cytosolic sensors [60][63].

1.6 Capsid uncoating – why study?

Experiments studying CA mutations that affect the stability of the capsid core have shown a direct link with the timing of capsid uncoating and the subsequent infectivity of the virus [65][67][112]. This unique characteristic, along with the distinctive structure and nature of the individual CA proteins, makes the process of capsid uncoating a promising target for pharmaceutical intervention. The gregarious nature of CA, which associates with many cellular host factors during the early phase of HIV-1 infection, indicates that there are a large number of processes at which intervention can take place, and binding sites within the CA protein for small molecular compound interaction. The CA CypA-binding loop and a binding domain formed through the molecular interaction of helices 1, 2, 4 and 7 of the CA_{NTD}, which have been shown to bind to host factors such as CypA, TNPO3, CPSF6, and Nups 358 and 153, have already been targeted by a number of small-molecule inhibitors [48].

CA is one of the most conserved proteins within HIV-1, with the MHR in the NTD and the zinger-finger motif in NC being the only sequences in Gag that show significant amino acid identity between divergent retrovirus genera [9]. The assembled HIV-1 capsids also exhibit remarkable structural homology between those of other retroviruses, despite an overall lack of sequence homology between these proteins [113][114]. This suggests that CA molecules between the genera have evolved to capacitate the delicate balance of functional burdens placed upon them. As such, they are likely to be stretched to the limit by the pressure to produce functional cores of optimal stability, which are still able to interact with the numerous host factors necessary for infection [44]. Thus, CA is unlikely to have the genetic flexibility employed by other HIV-1 proteins, such as RT and protease, for evolving resistance to restrictive compounds.

The fragility of the CA core, as attested to by the numerous CA mutations affecting core stability [65][112], makes it an attractive target for therapeutic intervention at the early stage of infection, whereby it would be possible to activate intrinsic host defence pathways that induce production of type-1 interferons and the 'antiviral state' [60]. This would enable manipulation of pathways that restrict or alter the sites of productive integration, and the

stimulation of an innate immunity that would both reduce viral infectivity and induce an antiviral immune response that would obstruct subsequent infection cycles [44]. Put together, the conserved structural nature of the capsid core, the large number of host factors with which CA interacts, and the tight relationship between infectivity and the kinetics of capsid disassembly, make the process of capsid uncoating an attractive target for antiviral drug action.

1.7 Systems for studying uncoating

Several *in vivo* and *in vitro* methods of studying uncoating have been employed over the years with varying levels of success. The highly conserved nature of the p24^{CA} monomers, and fragility of the capsid core, make it very difficult to detect in pull-down assays, and to label without affecting the maturation and quaternary structure of the core. Many of the assays measure core stability and uncoating events in bulk viral samples and therefore would not exclude the analysis of defective particles. In the field of CA uncoating, the main techniques employed for studying this process can be grouped into four basic approaches [44]:

1.7.1 *In vitro* core-stability and disassembly assay

This method involves the isolation of HIV-1 cores from the viral supernatant by ultracentrifugation through a detergent layer (removing the viral membrane) into a sucrose gradient [65][115][116]. Pelleted capsid cores containing the viral RNA and associated proteins, but lacking the envelope proteins, can then be removed from the appropriate sucrose fraction. Disassociation of p24^{CA} from the purified cores can then be measured by incubation at 37°C and further ultracentrifugation. This technique has provided valuable information regarding the stability and infectivity of capsid cores plus/minus mutations or following pharmacological treatment. However, the assay measures bulk core samples of which only a proportion may be infectious, and core stability *in vitro* does not necessarily reflect *in vivo* uncoating events [44].

1.7.2 Fate of capsid assay

In this system, lysates from infected cells are centrifuged through a sucrose cushion enabling the fractionation of intact capsid cores from soluble CA proteins and vesiculated virions [44]. Thus, the relative amounts of intact capsid cores over time following infection can be determined, through which an estimation of uncoating events can be calculated. This method has been used to measure the capsid core destabilisation and stabilisation properties of the restriction factors TRIM5 α [117] and myxovirus-resistance 2 (Mx2) [118], respectively, and the effects of reverse transcription [68][119] and microtubule trafficking on capsid uncoating [75][120]. As with the *in vitro* core-stability assay, this method focuses on bulk populations of cores, of which only a small percentage may be infectious [44], and the stability of the core can be effected during processing.

1.7.3 Cyclosporine A washout assay

This assay takes advantage of the HIV-1 restriction properties of a TRIM-cyclophilin A (TRIM-CypA) protein first described in Owl monkeys [121]. TRIM-CypA binds intact capsid cores prior to the onset of uncoating and, by some as yet identified process, affects restriction leading to premature uncoating [122][123]. Binding of TRIM-CypA to the viral capsid can be blocked by the addition of CsA, allowing the core to go through the normal process of uncoating and infection. At various time points post-infection, CsA is washed from the cells allowing TRIM-CypA to resume restriction. Because TRIM-CypA binds to intact capsid cores, insensitivity to restriction is a good indicator for initiation of uncoating. The half-life of uncoating can be calculated by the time post-infection of CsA washout. Using GFP labelled viruses, infection can be measured by flow cytometry. Unlike the previous assays that measure the uncoating of bulk sample viruses, many of which may not be infective, this system measures the uncoating of infective viruses that have escaped TRIM-CypA restriction [44]. However, because uncoating is being indirectly measured by a capsid-binding restriction factor, it is possible that host factors may be competing with TRIM-CypA for a limited number of capsid binding sites [86].

1.7.4 Imaging assays

Many imaging-based techniques have been employed for the direct visualisation of uncoating through the use of fluorescently tagged capsid core components. The systems generally involve the fluorescent labelling of a cellular or viral component within the capsid core, such as Vpr, IN, an APOBEC3 protein or the viral genome itself, and the level of associated CA can be comparatively analysed by immunofluorescence using capsid-specific antibodies [53][57][67][111][124][125][126][127]. Microscopically based techniques enable the visualisation and analysis of individual virus particles within the spatial context of the cell, and various approaches have been used to track virions live over time. The labelling of p24^{CA} protein can, however, disrupt the proteolytic processing and proper assembly of the viral cores, and the insertion of fluorophores into the Gag polyprotein can give rise to fluorescently labelled vesicles which are difficult to distinguish from true viral particles [127].

Despite the complications associated with studying capsid uncoating using imaging based assays, we turned to these techniques for our investigation of the process. This was because of the additional information that can be obtained through use of visual examination, which is often not possible when using other techniques, such as the dynamics of uncoating within the spatial-temporal localisation of the cell.

The methods described above are a general outline of the main approaches used for studying capsid uncoating, and many novel adaptations have been employed with these methods, some of which will be described later [**section 1.9**]. One of the main questions these assays attempt to answer is the precise timing of capsid uncoating, from which it may be possible to determine the specific factors (viral and cellular) that are involved in this process.

1.8 Factors affecting the kinetics of uncoating

As described earlier [section 1.6], timely capsid uncoating is thought to be crucial for the productive infection of HIV-1 and therefore many factors affecting the kinetics of uncoating have been investigated, both for the better understanding of this process and for the establishment of new therapeutic strategies. These factors, in turn, have proved useful as controls for validating new assays for measuring uncoating. The main approaches used in the uncoating assays for influencing the kinetics of capsid disassembly include the use of CA mutations in the viruses used for transduction, restriction compounds, and the knockdown of host cell proteins; all of which either directly or indirectly effect the stability of the capsid core.

1.8.1 Capsid mutations

Many studies have been performed involving mutations in p24^{CA}, as these have been found to have a knock-on effect on the stability of the viral core [65]. This, in turn, has been found to influence events in the early phase of the HIV-1 life cycle, including uncoating, the initiation or completion of reverse transcription, and viral infectivity [65][128]. CA mutations have also revealed insights into the interaction of the capsid core with specific cellular host factors, and have been shown to influence the pathway with which the PIC enters the nucleus and integrates [91][103]. Some of the CA mutations that have a significant effect on the dynamics of capsid uncoating are described below [65][112].

1.8.1.1 Mutations that effect the stability of the capsid core

Many experiments conducted *in vitro* and *in vivo* have shown a pronounced effect of CA mutations on the stability of the viral core. *In vitro*, the CA mutations Q63A/67A caused the viral core to disassemble more rapidly than WT capsid, whilst the mutations E45A and R128A/R132A caused the capsid core to disassemble more slowly [65]. Similar uncoating kinetics have been observed *in vivo*, with the CA mutations E45A, T54A/N57A, N74D, E128A/R132A, E45A/R132A and 5Mut reported to delay uncoating, whereas the mutations A92E and K203A induced premature uncoating [67][89][103][111][124][129]. All the viruses containing mutations that altered the stability of the capsid core *in vivo* and *in vitro* exhibited a decrease in relative infectivity from 0 to 20% of that

compared to viruses containing WT cores [65][112]. Interestingly, the viruses containing CA mutant cores that disassembled with similar kinetics to the WT cores *in vitro* (Q4A, G116A, T119A, N139A and P207A) exhibited similar infectivity as the WT virus. These observations support a functional correlation between capsid uncoating and infectivity. The reason why a change in the stability of the capsid core should affect infectivity has not yet been established, but may be due to subsequent effects on reverse transcription, cellular trafficking along the microtubules, interactions with nuclear pore proteins, or even integration events.

1.8.2 Restriction compounds

Many studies have employed the use of restriction compounds to investigate the kinetics of HIV-1 uncoating. The CA protein is a popular choice for targeting with restriction compounds because it is the more conserved of the Gag-Pol proteins, the structural fragility of the core making it less likely that resistant forms will evolve. The cyclophilin-binding domain also provides a convenient pocket with which many of the small molecule inhibitors bind. The binding of these small molecules often brings about structural changes within the viral core, thereby increasing or decreasing its stability, which in turn effects its uncoating kinetics.

1.8.2.1 Pfizer-3450074 (PF74)

PF-3450074 was originally identified in a high-throughput screening assay as a small-molecule inhibitor of HIV-1 that targets the CA protein [47]. Structural analysis indicates that PF74 binds in a preformed pocket encompassing the NTD-CTD interface, binding with a higher affinity to intact CA hexamers than to the monomeric form [130]. Recent studies suggest that it has a multi-modal action for HIV-1 inhibition, interacting with host proteins CPSF6 and NUP153 at low doses (<5 μM) and CypA at high doses ($\geq 5 \mu\text{M}$) [131]. High concentrations of PF74 have been reported to destabilise the capsid core [111][115][130].

1.8.2.2 Ebselen

Ebselen, an organoselenium compound, was identified as an inhibitor of CA dimerization in a high-throughput screening method based on time-resolved fluorescence energy transfer, using the CTD of HIV-1 [132]. Electrospray

ionisation mass spectrometry analysis revealed that ebselen covalently bound to the CTD of capsid, most likely through a selenylsulfide linkage with Cys198 and Cys218. A fate of capsid assay revealed an increase in pelletable capsid in the presence of ebselen [20 μ M], suggesting a stabilisation of the capsid core and inhibition of capsid uncoating [132].

1.8.2.3 Boehringer-Ingelheim compounds 1 and 2 (BI-1/BI-2)

BI-1/BI-2 are examples of a novel class of pyrrolopyrazolone HIV-1 inhibitors, identified in a phenotypic cell-based viral replication screening assay [45]. The compounds were demonstrated to directly bind within an 'inhibitor binding pocket' between CA helices 4, 5, and 7 on the surface of the CA^{NTD}, an area corresponding to the binding site for the host factors CPSF6 and Nup358. The compounds were shown to modestly stabilise purified HIV-1 cores *in vitro*, but BI-2 did not alter the uncoating kinetics of HIV-1 in a CsA washout assay [55]. Further experiments suggest that BI-2 may exert its effect during the nuclear import of the PIC, by binding to residual CA particles still present after uncoating.

1.8.2.4 Coumermycin-A1

Coumermycin-A1 (C-A1) is an antibiotic that is predicted to bind to an extended binding pocket delineated by two adjacent capsid monomers within the capsid hexamer of a viral core [103]. A CsA washout assay in the presence of C-A1 significantly reduced the period for which the capsid cores were sensitive to TRIM-CypA restriction, indicative of premature uncoating.

1.8.2.5 Nevirapine

Nevirapine is a non-nucleoside reverse transcriptase inhibitor (NNRTI) of HIV-1, which binds allosterically to the enzyme and blocks the RNA and DNA-dependent DNA polymerase activities by disruption of the enzyme's catalytic site [133]. It was discovered by Hargrave and co-workers at Boehringer Ingelheim Pharmaceuticals, Inc [134]. Binding of nevirapine leads to opening of the NNRTI-binding pocket, which causes the 3'-end of the DNA primer to shift by ~ 5.5 Å from its polymerase active site position [133]. As a result, the interactions between DNA and the polymerase domain are reduced, the dNTP-binding site is deformed, and the RNase H active site is shifted with respect to the site of

polymerase activity. The inhibition of reverse transcription has been found to delay HIV-1 uncoating [55][67][135]. The relationship between reverse transcription and uncoating is unsure, but it is thought the transformation of the more flexible compact viral RNA genome into the more rigid double-stranded DNA extended structure may provide an outward force that destabilises the capsid core [67].

1.8.3 Protein knockdowns – CA interaction with host proteins

Protein knockdown studies through the use of short interfering (siRNA) or short hairpin RNA (shRNA) have provided important information on the specific host cell proteins that interact with p24^{CA} [54][56][58]. Using these approaches it has been possible to identify the effects of these proteins on the stability of the capsid core, and the knock-on effect of the timing of capsid uncoating on reverse transcription, nuclear entry and integration, and ultimately HIV-1 infectivity [87]. A few of the key host factors that have been reported to interact with CA, and therefore have a potential role in capsid uncoating, are listed below.

1.8.3.1 Microtubules

Microtubules are comprised of α/β -tubulin heteropolymers that form polarised filaments within the cellular cytoplasm, with the ‘minus-ends’ attached to the centrosome, the perinuclear microtubule-organising centre (MTOC) of the cell, and the ‘plus-ends’ extending towards the plasma membrane [136]. Specialised motor complexes bind the protein cargoes and traffic their movement along the microtubules, with the minus-end (retrograde) movement predominantly directed by dynein, whilst the plus-end (anterograde) motion is directed by kinesins [137]. Viruses have evolved a number of approaches for hijacking the cytoskeletal networks to support their movement across the cell [74]. HIV-1 RTCs have been shown to interact with both actin and the microtubule cytoskeleton, using the actin microfilaments for short-range transport towards the plasma membrane, and microtubule motors for more extensive intracellular movement [53][138][139][140][141][53]. Various studies have substantiated the movement of HIV-1 in a dynein-dependent manner along the microtubules to the nucleus, during which uncoating and reverse transcription take place [53][78][142]. *In vitro* assembled HIV-1 CA-NC complexes were also shown to interact with the

kinesin-1 adaptor protein FEZ1, which regulates HIV-1 movement towards the nucleus [76]. This study reported that both dynein and kinesin-1 were needed for viral transfer to the nucleus. Two studies have reported that microtubule disruption and knockdown of microtubule motors delays HIV-1 uncoating [75][120]. These observations have led to the suggestion that capsid uncoating may be mediated through the interaction between the opposing motor proteins dynein and kinesin-1, creating a 'tug-of-war' type effect [44].

1.8.3.2 Cyclophilin A

Cyclophilin A (CypA) is a peptidyl prolyl isomerase that catalyses the cis-trans isomerisation of proline peptide (xaa-pro) bonds [143]. X-ray crystallography revealed that CypA binds via an extended loop (the cyclophilin-binding loop) which encompasses residues 85-93 within helices 4 and 5 of the NTD of CA [144]. CypA is packaged into HIV-1 virions during the late phase of infection through interactions with the CA domain of Gag, but its main role in HIV-1 infection is recorded to be in target cells, and the previously packaged molecules do not appear to play a role in this [145][146][147]. In the mature capsid core the CypA-binding loop is exposed towards the external surface of the viral core enabling interaction with target cell CypA proteins. Cyclophilin A has been reported to catalyse the isomerisation of the Gly89-Pro90 peptide bond of CA, inducing conformational changes in the CA_{NTD} remote from the CypA-binding loop [148]. It has been speculated that this change may provide the mechanical force for the disassembly of the capsid core, but experimental data supporting this has been contradictory [44][149][150]. Through cryoEM structural elucidation of CypA in complex with the assembled HIV-1 capsid, a non-canonical, second CypA binding site was revealed, bridging two CA monomers from adjacent hexamers, thereby strengthening the lattice [151]. It was shown that sub-stoichiometric amounts of CypA stabilise the capsid assembly, whereas high levels of CypA reduced capsid stability and promoted capsid disassembly [151]. These apparently contradictory observations can be explained by the steric hindrance induced between two CypA molecules when simultaneously binding to neighbouring CA hexamers at high concentrations, weakening the dimer assembly interface of an intact capsid core. This interaction may explain the

variations in uncoating times observed between different cell types that express different levels of CypA [147][152][153].

Cyclophilin A interaction with CA may also play a role in the pathway with which the PIC transverses the nuclear membrane, and the subsequent host genomic integration site, through interplay with Nups 358 and 153 [91]. Inhibition of CypA-CA binding with CsA or the CA cyclophilin-binding domain mutants G89V and P90A [145][154][155], impairs subsequent PIC interactions with Nup358 and Nup153, resulting in proviral integration in areas with a high density of transcription units (less productive).

1.8.3.3 Myxovirus-resistance B

Myxovirus-resistance B (MxB/Mx2) is an IFN-inducible myxovirus resistance (Mx) protein belonging to the dynamin-like family of GTPases. Recently, MxB has been implicated in having potent inhibitory activity against HIV-1 infection [156][157][158][159]. HIV-1 viruses containing the capsid mutations P90A, G89V and N57S escaped MxB restriction, suggesting that capsid was the principle factor in MxB mediated interactions [157][158][159]. Myxovirus-resistance B was subsequently shown to interact with *in vitro* assembled CA-NC complexes [118]. Further investigation using a benzimidazole-based capsid-binding compound and domain mapping experiments, identified an MxB binding domain next to the base of the cyclophilin binding loop of CA [118]. The binding of MxB with the HIV-1 core has been shown to inhibit capsid uncoating [118]. The function of MxB appears to be linked to CypA, as CypA depletion or disruption of CypA/CA interaction prevents MxB mediated restriction [159]. As yet the exact mechanism of HIV-1 inhibition by MxB is still under investigation, and may occur through restriction of uncoating, inhibition of nuclear import, or through perturbatory effects on proviral stability or integration [118][160].

1.8.3.4 Transportin3/transportin-SR2

Transportin 3 (TNPO3) is a member of the karyopherin β superfamily of proteins, which bind serine/arginine (SR) rich proteins and governs their nuclear localisation [87][161][162]. It was first identified as a potential HIV-1 infection co-factor in a number of genome-wide RNA interference screens [54][56][58], and

the subsequent depletion of TNPO3 in HIV-1 infected cells showed a reduction of infectivity [91][93]. A decrease in infectivity was not observed, however, when CA mutant viruses (N74D, E45A or Q63A/Q67A) were used to infect TNPO3 depleted cells, providing the first link between CA and TNPO3 [90][150][163]. A study analysing viral DNA concentrations within the cytoplasmic and nuclear fractions of TNPO3 depleted cells, revealed an accumulation of HIV-1 DNA within the nucleus [150]. This, in line with various other experiments, provided evidence that TNPO3 was not required for HIV-1 entry into the nucleus [164][165], and therefore, the TNPO3-depleted restriction of infection occurred somewhere between nuclear entry and integration [150]. Wild type capsid (but not the N74D mutant capsid) was also shown to accumulate in the nuclei of TNPO3 depleted cells, indicating that TNPO3 may contribute to the removal of capsid from the nucleus [163]. TNPO3 has also been linked to HIV-1 capsid uncoating. The addition of recombinant TNPO3 to purified capsid cores *in vitro* has been shown to accelerate their disassembly [150]. Conversely, the N74D CA mutant reduced the effect of TNPO3 on HIV-1 uncoating. Cyclophilin A stabilised HIV-1 cores, however, seemed to antagonise this TNPO3-mediated uncoating effect. Taken together, this gave rise to the speculation that TNPO3 and CypA may interact in the coordinated control of HIV-1 uncoating [150].

Depletion of TNPO3 and/or infection with the TNPO3-independent capsid mutant viruses (E45A and N74D), has also been shown to alter the integration site of HIV-1 [90][93][101][150]. Recent models suggest that TNPO3 participates in the nuclear translocation and maturation of the PIC in a RanGTP dependent system, in which TNPO3 coordinates a series of steps where different host factors bind to and are released from the PIC in a regulated manner, until host genomic integration [44][87][94].

1.8.3.5 Cleavage and polyadenylation specificity factor 6

Cleavage and polyadenylation specificity factor 6 (CPSF6) is an mRNA-processing protein that dynamically shuttles between the cytoplasm and the nucleus [166]. Although active both within the nucleus and cytoplasm, a serine/arginine (SR)-rich nuclear localisation signal (NLS) on its C-terminus retains its predominantly nuclear localisation [44][57][167]. This protein has been

shown to attach to the binding-pocket formed through intermolecular interactions between the CA_{NTD} and CA_{CTD} of adjacent CA monomers [130][167][168]. An interaction between CPSF6 and CA has been reinforced by additional studies, which showed that cytoplasmic CPSF6 stabilised CA-NC tubes *in vitro* and viral cores *in vivo* [93][149]. Further evidence of CA interaction was supplied with a truncated murine form of CPSF6 lacking the SR-rich C-terminal domain (CPSF6₁₋₃₅₈), rendering it predominantly cytoplasmic in its localisation [90]. This mutant construct potently inhibited HIV-1 infection, but a N74D mutation in the CA rescued the virus from restriction. The C-terminally truncated form of CPSF6 has also been reported to interact at a stage before reverse transcription, delaying both reverse transcription and uncoating [93][169][170].

It has also been proposed that CPSF6 binding to HIV-1 CA facilitates its use of nuclear import factors such as TNPO3, and this was backed up by studies showing that TNPO3-dependence of HIV-1 infection is correlated with the ability of CPSF6 to bind to CA [93][167][170]. Thus, it seems likely that the binding of CA with full length CPSF6 has a role in mediating the nuclear import of the RTC [44]. Two recent studies have revealed that CPSF6 may also play a role in HIV-1 integration [98][99]. Knockdown of CPSF6 or deletion of the CA binding domain of CPSF6 led to proviral integration in less gene dense and transcriptionally active regions of the chromosome, towards the periphery of the nucleus. Infection of control cells with the CPSF6 non-binding CA mutants N74D and A105T revealed a similar predilection in the location of proviral integration, and a matching CA orientation was revealed by immunostaining; thus suggesting that CPSF6 mediated PIC navigation was implemented by CA binding.

1.8.3.6 Nucleoporins

Genome-wide RNA interference screening identified a number of nucleoporins as potential nuclear transport factors for HIV-1 infection [54][56][58]. Of these, Nup358 and Nup153 have been the most extensively investigated in relation to HIV-1 nuclear translocation. The CA binding motifs of these Nups have led to the speculation that these proteins may also play a role in late phase capsid uncoating at the nuclear pore [86][91].

Nucleoporin 358 is a large 3224 aa protein that forms cytoplasmic filaments extending from the NPC into the cellular cytoplasm. These filaments possess phenylalanine/glycine repeat motifs that actively regulate the traffic of molecules ~40 kDa through the nuclear pore [171][172]. A CypA homology domain is located at the C-terminus of Nup358, which binds to the NTD domain of CA, with a slightly weaker affinity than CypA [173][174][175], although NMRZZ-exchange spectroscopy indicates that Nup358 catalyses a more rapid cis/trans isomerisation of the G89-P90 bond than CypA [160][175]. This has led to the speculation that Nup358 may have a role in CA uncoating [86][91]. Nup358 depletion reduced HIV-1 infectivity three to eightfold [91][176][177]. Contrastingly, the CA mutants N57A, N74D, P90A and G89V have been shown to infect host cells independently of Nup358, and have been shown to retarget integration within different gene dense regions of the chromosome, suggesting a role for Nup358 in the CA associated guiding of proviral integration [91][101][178].

Nucleoporin 153 is 1475 aa protein which is found anchored to the rim of the nuclear side of NPC by its N-terminal domain [179]. Its highly flexible CTD consists of Phe/Gly (FG)-repeats which can traverse the nuclear basket towards the cytoplasmic side of the NPC, where it plays a large role in nucleocytoplasmic transport [180][181][182]. Nup153 has been shown to bind directly with CA within a site that overlaps the region at which PF74 and BI-2 bind [105]. This protein has been shown to interact with WT CA and the N74D CA mutant, although the CA binding mutants G89V, P90A and N74D are less sensitive to Nup153 knockdown compared to WT CA [91][90][92][93][100][105]. Depletion of Nup153, also significantly reduced viral cDNA integration within gene dense regions of chromatin [102].

The large number of CA mutations, restriction compounds, host cell (and viral) proteins that have been shown to affect the stability of the capsid core, and in turn modulate the timing and thus cellular location of capsid uncoating, attests to the complexity of this process. Collectively, these accounts suggest a specific and structured interplay between the CA/capsid and viral/host cell proteins which is crucial for the productive infection of HIV-1. The capsid binding properties of the host factors localised within different regions of the cell, also suggests that

CA is involved in many parts of the early phase of HIV-1 infection, such as reverse transcription, nuclear entry, and viral integration. This raises important questions to our understanding of the definition of capsid uncoating, and suggests that at least a portion of capsid proteins remain with the RTC/PIC for interaction with host factors within the nucleus.

1.9 The role of imaging methods in studying uncoating

Much attention has been paid to the studying of capsid uncoating, and many methods employed for studying this process, but this particular area of the HIV-1 life cycle still remains an enigma. This may be, in part, due to the many different and novel techniques that have been used for investigating this process, which may focus on distinct aspects of capsid uncoating. With many of the biochemical methods for analysing the RTC/PIC failing to detect CA proteins associated with these complexes, we decided to focus more on the imaging based systems for investigating uncoating. As such, it is worth exploring these systems in further detail, with particular reference to some of the more innovative approaches that have expounded our knowledge of this process.

1.9.1 Imaging within living cells – Vpr-GFP

The observation of HIV-1 in living cells was first made possible by hijacking one of its accessory proteins for incorporation of a fluorescently labelled protein within a budding virion [53]. A GFP fluorophore was fused to the NH₂-terminus of Viral protein r (Vpr), which is incorporated into newly assembling viruses through interaction with the p6 region of Gag [183][184]. Approximately, 100 to 200 Vpr molecules are incorporated into each virus during conventional viral assembly, and even more so when Vpr is overexpressed during DNA transfection [185][186]. Using this system, it was possible to visualise GFP-labelled viral particles accumulating around the nucleus in close proximity with the microtubule-organising centre [53]. Virus particles were also observed associating and trafficking along microtubules in a dynein dependent manner. Lastly, the Vpr-GFP labelled viruses were observed colocalised with significant amounts of immunostained CA particles, providing the first evidence of CA associating with a reverse transcribing complex. Although the direct fusion of

fluorophores to Vpr still remains a valuable system for studying HIV-1 intracellular interactions, there is speculation as to whether some of these particles are non-specifically endocytosed particles rather than productively fused viruses [187].

1.9.2 Fluorescently labelled integrase

One of the issues perceived with fluorescently labelled Vpr was that it could not be observed within the nucleus, thereby limiting the portion of the HIV-1 life cycle that can be observed with this system [187]. However, the period for intra-cellular viral visualisation was extended to include post-nuclear entry steps by using various techniques for labelling the HIV-1 IN protein. One system involved the insertion of a small tetracysteine tag within IN, which could be visualised through the addition of the fluorescein arsenical hairpin (FlasH) [78]. Fluorescein arsenical hairpin is a non-fluorescent compound when complexed with ethanedithiol (EDT), but becomes fluorescent upon binding to tetracysteine motifs [188][189][190]. This, along with the small size of the tetracysteine tag making it less prone to disrupting the structure and function of the protein into which it is inserted, made it an attractive candidate for intra-cellular imaging. This system enabled the observation of viral kinetics during trafficking towards the nucleus, including a decreased mobility attributed to peri-nuclear docking, and the more restrained diffuse movements within the nucleus itself [78]. However, this system was complicated with non-specific binding to endogenous cysteine-rich proteins, and low sensitivity within the nucleus, possibly due to the fixed analysis time required for its functioning [125].

An alternative system for tracking the VNC up to and including nuclear translocation employed the use of a fluorescently labelled IN protein [125]. An Enhanced GFP (EGFP) fluorophore was fused to the C-terminus of codon optimised IN, and the resultant IN-EGFP fusion protein subsequently fused to the C-terminus of Vpr for trans-incorporation into assembling viral particles via interaction with Gag p6. An HIV-1 sensitive proteolytic site was introduced between Vpr and IN-EGFP, to enable separation of the proteins during viral maturation, so that the IN-EGFP molecule could effectively catalyse integration. By exploiting the Vpr/p6 interaction for incorporation of labelled IN, this system

effectively avoided the reduced infectivity levels usually observed with the introduction of a large fluorescent tag within the viral genome [125]. Using this construct in conjunction with nuclear lamina staining, it was possible to establish the time point for peak PIC association within the nucleus (6 h post-infection), and the preferential distribution of PICs at the periphery of the nucleus within actively transcribed genes in the decondensed areas of chromatin. The Vpr-IN system of incorporating a moiety within the capsid core was used in all three of the systems we developed for studying capsid uncoating.

1.9.3 Cyclosporine A washout and internalised GFP (iGFP)

As described above (**section 1.7.3**), the CsA washout assay uses the CA specific restricting properties of TRIM-CypA, along with a GFP labelled HIV-1 proviral clone (R7 Δ envGFP) [67]. This clone contains a GFP-coding sequence in place of the Nef-coding sequences, providing a fluorescent marker for quantitation of viral infection [191]. By blocking the TRIM-CypA mediated restriction of intact capsid cores using CsA, Hulme and co-workers determined a 50% uncoating time for HIV-1 of approximately 39 min post-infection [67]. In the presence of nevirapine, the half-time of uncoating time was increased to 112 min post-infection. The same group concurrently performed experiments using Vpr-GFP and immunostaining for p24^{CA} as an alternative method for measuring uncoating. A 50% uncoating time between 1 and 2 h was recorded with a non-capsid mutated virus, and earlier and delayed uncoating was observed with less stable (K203A) and more stable (E128A/R132A) capsid mutants, respectively [65][67]. The use of a fluorescently labelled membrane targeting protein, S15-mCherry, enabled the differentiation between productively entered and endocytosed viral particles [192].

Interestingly, a difference in the half-time of uncoating time was also detected in this study when pseudotyping with different viral envelopes [67]. An average 50% uncoating time of ~39 min and ~74 min was observed when pseudotyping with vesicular stomatitis virus G (VSV-G) protein or with WT HIV-1 envelope, respectively. Using fusion inhibitors, a half-time of ~16 min was determined for VSV-G and ~48 min for HIV-envelope mediated fusion, suggesting that the differences in uncoating times could be attributed to viral fusion pathways.

Hulme and co-workers also used a fluorescent based system for determining capsid integrity [55]. This consisted of a GFP molecule flanked by proteolytic cleavage sites, cloned between the MA and CA sequences of Gag – designated internalised GFP (iGFP). Upon viral maturation, GFP is cleaved out of Gag, and a subset is retained within the capsid core, which can be used as a marker of capsid integrity. A CsA washout assay determined that HIV-1 remained susceptible to the action of two capsid binding drugs (PF74 and BI2) for hours after initial uncoating, suggesting that a residual amount of CA remained with the VNC after the loss of the capsid core [55]. However, addition of these compounds had no effect on capsid integrity as determined by iGFP, suggesting that PF74 and BI2 do not effect uncoating, but a CA associated step at a later step in viral replication.

1.9.4 Evidence of a biphasic model of capsid uncoating

Xu and co-workers employed the use of ‘click labelling’ for the tracking of viral RNA and monitoring of the associative capsid uncoating events [111]. This system involved the incorporation of the modified nucleoside, 5-ethynyl uridine (EU), into viral RNA during virus production, and the subsequent detection through microinjection of an azide-containing fluorescent dye. Uncoating was determined by when the fluorescent dye could enter the core and bind to the EU labelled RNA, allowing detection by confocal microscopy. This study showed an initial increase in fluorescently labelled viral RNA 15 to 45 minutes post-infection, suggestive of an early uncoating phase soon after viral fusion. This was followed by a steady, reproducible loss of viral RNA detection consistent with uncoating and the instability of RNA within the cellular cytosol. The kinetics could be altered through the introduction of PF74, and CA mutants known to affect the stability of the capsid core. Interestingly, the inhibition of reverse transcription did not affect the early events of HIV-1 capsid uncoating. Also, studies using the E45A CA mutation (creating a more stable capsid core in biochemical assays [65]) showed an initial early uncoating phase, followed by an independent more gradual disassociation of CA from the VNC. In conjunction with findings from the biochemical assay [65], this lead to the hypothesis that capsid uncoating was a biphasic process: an early uncoating step allowing entry of cellular factors

necessary for reverse transcription, and a subsequent more gradual disassembly to prevent disassociation of key components from the RTC.

1.9.5 Live imaging of HIV-1 uncoating

Recently, a group has managed to track the uncoating of individual HIV-1 particles over time using live microscopy [127]. This was accomplished through the labelling of a known capsid-targeting cellular protein, CypA, with a tetrameric DsRed fluorescent protein. The oligomerisation properties of the DsRed protein, in turn drove the oligomerisation of CypA, enabling its high affinity binding to the capsid core. Various experiments determined that the loss of the CypA-DsRed fusion protein from superfolder GFP (sfGFP) labelled IN was concomitant with that of capsid, suggesting it to be an effective tool for studying live uncoating events. Using this system, the group was able to determine that the majority of cores uncoated relatively early after fusion (~23 min post-infection), but a small proportion of VNCs retained their capsid cores for a few hours after infection. Analysis of the CypA-DsRed capsid labelling system in the presence of nevirapine and BI-2, and with the K203A CA destabilising mutant, revealed uncoating kinetics similar to that reported by Hulme and co-workers [67]. Interestingly, the E45A CA mutation reported to stabilise the capsid core *in vitro* [65], had little effect on the uncoating dynamics *in vivo*. However, a moderate affect in capsid uncoating was detected with the addition of PF74.

1.9.6 Capsid within the nucleus

Two groups have recently reported the visualisation of CA colocalised with IN PIC within the nucleus of infected cells [55][57]. As described above (**section 1.9.3**), the effects of the CA binding compounds PF74 and BI-2 on later stages of viral infectivity led Hulme and co-workers to suspect that a residual amount of CA remained with the VNC after 'uncoating' [55]. CA associated PICs were subsequently identified within the nucleus via high-resolution structured illumination microscopy (SIM), using GFP labelled IN viral complexes stained for p24^{CA}. An average ~6-fold lower level of CA intensity was detected in viral complexes localising within the nucleus compared with those present at the peri-nuclear membrane or cytoplasm, indicating a measure of CA loss during nuclear import [55]. Peng and co-workers also managed to detect CA colocalised PICs in

the nuclei of primary MDMs, again using GFP labelled IN stained with p24^{CA}, and super-resolution microscopy [57]. Almost all (97%) of PICs were positive for CA in MDMs, however, CA was absent from all but one nuclear PIC in a HeLa derived (TZM-bl) cell line. This contrasts with their observations preceding nuclear translocation, where almost all the VNCs associated with CA in the TZM-bl cells and less than half associated with CA in the MDMs. The authors speculate that the CA negative viral complexes within the cytoplasm of MDMs represent dead end products, which possibly contribute to the strong antiviral state reported with HIV-1 infected MDMs [60]; and that capsid or a capsid-derived structure remains associated with the VNC during reverse transcription and nuclear import, at least in the case of MDMs. The lack of CA associated PICs in the nucleus of TZM-bl cells may indicate a more rapid loss of CA prior to or after nuclear import with these cells compared to MDMs [57], although it may also be due to lack of sensitivity of the CA staining method employed in this study [55].

The above studies (**section 1.9**) seem to suggest an uncoating model which includes an initial uncoating phase, or the uncoating of a large fraction of the capsid cores, early after (10-45 min) fusion with the cellular membrane with VSV-G pseudotyped viral particles. This is then followed by a more gradual disassembly phase, with a portion of the capsid core remaining with the VNC up to and including nuclear translocation. To assist in the further elucidation of this process of capsid uncoating, we employed the use of a few recently developed novel labelling strategies, which will be examined in further detail below.

1.10 Novel labelling systems

Many systems have been developed over the years to enhance the labelling and studying of host cell interactions *in situ*, which have recently led to the long-term imaging of single proteins within living cells [193]. Some of the latest developments, which have been employed in this study, will be described below.

1.10.1 Intra-capsid core labelling using APOBEC3F and G

Recent work by Burdick and co-workers 2013, describes how they managed to label HIV-1 PICs using apolipoprotein B mRNA editing enzyme, catalytic polypeptide-like (APOBEC) proteins APOBEC3F (A3F) and APOBEC3G (A3G) fused to yellow fluorescent protein (YFP) [124]. These catalytic proteins belong to a family of DNA cytidine deaminases, inhibiting viral replication in Vif protein deficient HIV-1 by inducing G-to-A hypermutation, blocking viral DNA synthesis and impeding viral DNA integration [194]. The incorporation of A3F and A3G into the capsid of Vif-deficient virions is reported to occur through the non-discriminate binding of RNA during viral assembly [195]. Minus-strand DNA is the target for both A3F and A3G-mediated cytidine deamination, although A3G obstructs the removal of the tRNA primer forming an aberrant viral DNA end, whereas A3F specifically inhibits the 3' processing reaction catalysed by IN [196]. As such, both A3F and A3G are likely to remain associated with the PIC during DNA synthesis, although the dsDNA targeting properties of A3F suggest a longer affiliation [124]. Although a fivefold reduction of viral infectivity was recorded with A3F and a cytidine deficient E25Q A3G mutant (A3G*), approximately 60-84% of the virions produced were labelled with these proteins, and A3F, and to a lesser extent A3G*, were observed associated with the PIC up to and including nuclear entry. Using this system in combination with fluorescence *in situ* hybridization (FISH), a reverse transcriptase mutant (D110E) and the addition of nevirapine, the authors could detect A3F-YFP signals colocalised with HIV-1 RNA within the nucleus of infected cells, showing that inhibition of RT had no impact on the nuclear import of HIV-1 PICs. Previous studies have suggested a link between RT and capsid uncoating [67], but these findings indicate that the viral uncoating that is associated with RT is not required for nuclear import. Two mutations that render the capsid core less (K203A) or more (E128A/R132A) stable were tested with this system. Although only a

twofold decrease in cytoplasmic A3F-YFP particles was recorded after 6 h compared to WT virus (non-mutated CA), a 54- and 13-fold decrease in nuclear PICs were observed with the K203A and E128A/R132A capsid mutants, respectively.

1.10.2 SuperNova Tagging (SunTag)

Recently, a novel protein tagging system has been developed enabling amplification of a signal to the extent by which single protein molecules can be observed within living cells [193]. This method utilises single-chain variable fragment (scFv) antibodies, in which the light and heavy chains of the epitope-binding regions of the antibody are fused to form a single polypeptide, allowing successful expression in soluble form within cells. This is used in conjunction with a short peptide epitope, EELLSKNYHLENEVARLKK, derived from the transcription activator GCN4 (endogenously expressed in the budding yeast *Saccharomyces cerevisiae*) with which the scFv binds tightly [197]. Superfolder GFP was used as the reporter fused to the scFv antibody (scFv-sfGFP), as a reduced amount of protein aggregation was observed with this compared to when using other fluorophores [198]. The addition of a small solubility tag (GB1) to the C-terminal domain of sfGFP, effectively eliminated protein aggregation, even at high expression levels [193][199]. The addition of short flexible linkers (GGSGG) between repeat peptide epitopes enabled saturation of the epitopes without steric hindrance from competing antibodies. Using this system, it was possible to design a scaffold containing up to 24 repeats of the GCN4 epitope allowing full occupancy of the scFv-sfGFP fused antibodies (**Fig. 6**). Because of the brightness of a fully saturated peptide scaffold, the tagging system was named SuperNova (SunTag) after the extremely bright stellar explosions. The authors managed to successfully use this system for single molecule imaging and tracking, and for measuring the movements of cytoskeletal motors *in vivo*.

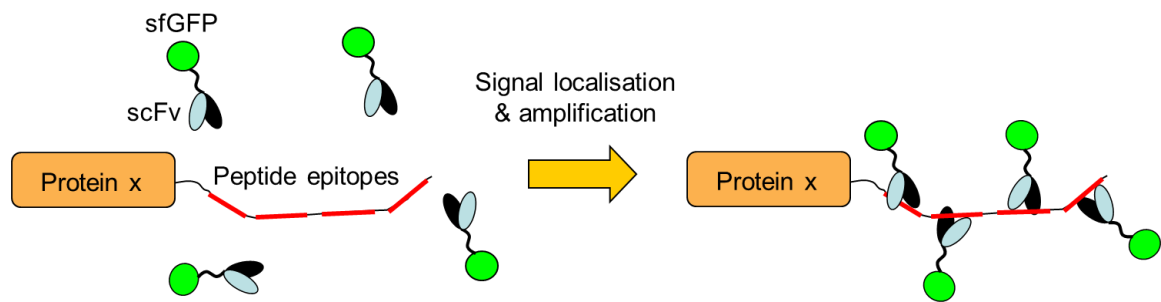


Figure 6. SuperNova SunTag system of signal amplification. Peptide epitopes flanked by short flexible linkers are fused together to form a 'scaffold', comprising up to 24 of these peptide epitopes, which can be fused to a target protein. Each epitope can be sterically bound by fluorescently labelled single chain variable fragment (scFv) antibodies, facilitating extensive signal amplification and *in situ* single molecule tracking [193].

There are many positive features associated with this labelling system. The brightness of the SunTag enables visualisation of single molecules with low expression levels, and imaging of organelles and molecules with lower laser intensities, reducing the phototoxicity and bleaching effects associated with longer-term imaging. Another advantage of indirect labelling compared to traditional methods (i.e. fusing the peptide epitope, instead of a fluorophore, directly to the target protein) is that signal intensity can be increased without the addition of extra fluorophores, which can affect the tertiary structure of the resultant protein. However, the large size of a fully saturated 24x repeat array (~1.4 mDa) gives rise to a slower diffusion kinetic through the plasma membrane ($0.76 \mu\text{m}^2/\text{s}$) compared to an averaged sized protein labelled with a single GFP ($\sim 20 \mu\text{m}^2/\text{s}$) [193].

1.10.3 NanoBit

Protein-fragment complementation assays are commonly used for investigating the complex interactions that occur within the cellular microenvironment. These systems consist of a split reporter molecule, whereby the individual fragments display little reporter activity separately, but regain activity when re-assembled through the interaction of the molecules to which they are fused. Assays using split luciferases are often favoured over fluorescent based systems for cellular investigation, due to their sensitivity, simplicity and the instantaneous reporter activity generated with addition of substrate to the growth medium. NanoLuc is a

small (19 kDa), stable engineered luciferase obtained from the deep sea shrimp *Oplophorus gracilirostris*, which is capable of producing bright and sustained luminescence within intracellular systems [200]. Circularly permuted variants were created in a method to identify the optimal dissection point within NanoLuc for the production of a split reporter, resulting in an 18 kDa polypeptide (Large BiT) and 1.3 kDa (11 aa) peptide (Small BiT) with luminescence properties similar to that of NanoLuc (**Fig. 7**) [201]. The system was further enhanced through the structural optimisation of the individual fragments. Further analysis ascertaining the interaction affinities and kinetics of the fragments for effective use in protein complementation assays determined an intrinsic affinity (equilibrium and dissociation constant - K_D) of 190 μM , and association constants of $500 \text{ M}^{-1} \text{ s}^{-1}$ K_{on} , and 0.2 s^{-1} K_{off} ; outside the range for protein interaction [201].

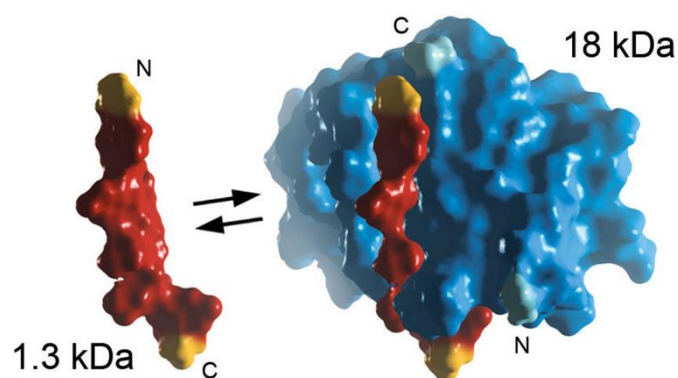


Figure 7. Model of the two subunit NanoBiT split luciferase enzyme. The NanoBiT is a structurally engineered luciferase, derived from the deep-sea shrimp, capable of bright and sustained luminescence within intracellular systems. Further engineering led to the production of an 11 aa peptide with an affinity (K_D) for the large fragment of 700 pM, making it ideal for use in determining primary uncoating stages.

Further modifications on the small bit peptide resulted in its increased affinity for the large bit polypeptide, subsequently termed the HiBiT (Promega). The small size (11 aa) of the peptide and the spontaneous bright luminescence achieved through fragment complementation, make it an attractive tool for use as a molecular marker of intracellular events; although as it has only recently been developed the effectiveness of this system has yet to be evaluated.

We employed the use of the SUpErNova tagging (SunTag) and protein-fragment complementation (NanoBiT) systems, in conjunction with Vpr-IN and APOBEC3F/G* capsid trans-incorporation, in the development of two novel assays for studying HIV-1 capsid uncoating.

1.11 Summary

The above account suggests that CA, and the structure of the capsid core, have an intrinsic role in many parts of the early phase of the HIV-1 replication cycle, and it is an area that still requires a lot of investigation for the clarification of these roles. The large number of systems and methods that have been deployed for studying capsid uncoating attest to both the importance with which this process is held, and the difficulties associated in the investigation of this event. The link between the actual process of uncoating and effective viral genomic integration seems to play a key part in HIV-1 infection, and therefore the development of authentic systems for the elucidation of this relationship is essential. Understanding this process could lead to the development of new therapeutic approaches for targeting this infection which, due to the conserved nature of the assembled capsid structure, would be less subject to the development of resistant mutants.

METHODS

2.1 Cell lines

HeLa P4 cells stably expressing CD4 were a kind gift from Dr. Zeger Debyser, (University of Leuven). HEK293T and U-2 OS cells were purchased from the American type culture collection ATCC. TZM-bl cells were a kind gift from (Dr. Massimo Pizzato (CIBIO, University of Trento). All cell lines were maintained at 37°C and 5% CO₂ and were cultured in Dulbecco's Modified Eagle medium (DMEM) (GIBCO, Thermo Fisher Scientific) supplemented with 10% Fetal Bovine Serum (GIBCO, Thermo Fisher Scientific), 2% Glutamine (GIBCO, Thermo Fisher Scientific) and 100 units penicillin/streptomycin (GIBCO, Thermo Fisher Scientific), henceforth termed as DMEM complete.

2.1.1 Stable cell lines:

2.1.2 ScFv-sfGFP:

Stable clones expressing the single-chain variable fragment antibody fused to superfolder GFP (scFv-sfGFP) ± a nuclear localisation signal (NLS) were prepared to use in conjunction with the GCN4 SunTag peptide. The scFv-sfGFP fluorescent antibody was digested from the pHR-scFv-GCN4-sfGFP-GB1-±NLS plasmid (Addgene) using NheI and NotI and ligated into the XbaI and NotI restriction sites of the puromycin resistant pAIP transfer vector, and viruses prepared by pseudotyping with VSV-G (10 µg: 3.5 µg). HEK293T, HeLa P4 (including TZM-bl 126/322 stable clones) and U-2 OS cell lines were transduced with 1 to 4 reverse transcription units (RTU) of pAIP-scFv-sfGFP + VSV-G. Stable clones were produced by limiting dilution, puromycin selection (1 µg/ml in 293T, U-2 OS cells and HeLa P4 cells, the TZM-bl 126/322 cells were already puromycin resistant) and visual selection of scFv-sfGFP production under a fluorescent microscope. Cells expressing a lower intensity of sfGFP in the nucleus or cytoplasm were selected as too much background made it difficult to distinguish the scFv-sfGFP antibody bound to the GCN4 peptide repeat arrays.

2.1.3 LgBiT

The LgBiT was PCR amplified from the pBiT1.1-C [TK/LgBiT] vector (Promega) with BamHI and EcoRI restriction sites to enable ligation into the blasticidin resistant proviral vector pAIB (pAIB-LgBiT):

(BamHI)LgBiT fwd: 5'-ATTAGGATCCACCATGGTCTTCACACTCGAAGATTTTCG-3'
(EcoRI)LgBiT rev: 5'-TAATGAATTCTTAGCTGTTGATGGTTACTCGG-3'

HeLa P4 cells were transduced with 1 to 4 RTU of pAIB-LgBiT and selected using 6 µg/mL Blasticidin. Stable clones were produced by limiting dilution.

2.1.4 TRIM-CypA

TZM-bl cells stably expressing TRIM-CypA (TZM-bl 322) or a mutated inactivated form (TZM-bl 126) were kindly supplied by Massimo Pizzato (CIBIO, University of Trento), and kept under selection using DMEM complete supplemented with 2 µg/mL puromycin (GIBCO, Thermo Fisher Scientific).

2.2 Virus production

Vectors were produced using the viral protein R (Vpr) and envelope (Env) mutated molecular clone pNL4-3.Luc.R⁻E⁻ (pNL4-3) [10 µg] and either the vesicular stomatitis virus envelope glycoprotein (VSV-G) [3.5 µg] or the WT HXB2 envelope [4 µg] (NIH AIDS Research and Reference Reagent program).

Transfection was performed using polyethylenimine (PEI) reagent (Sigma). Briefly, 10-cm-diameter culture dishes were seeded with 3.5×10^6 HEK293T cells and grown to approximately 90% confluency. Plasmid DNA was added to 1 mL DMEM (minus supplements) and 45 µL PEI, vortexed briefly, and incubated at RT for 10 min. Culture media on the HEK293T cells was replaced with 5 mL Opti-MEM Reduced Serum Media (GIBCO, Thermo Fisher Scientific) and the DNA/PEI mixture added drop-wise. Plates were incubated for a minimum of 7 h before the media was replaced with 10 mL DMEM plus supplements and the plates re-incubated. Virus containing supernatant was collected at ≥ 36 h post media change, centrifuged at 500 x g for 5 min to remove cellular debris, passed

through 0.45 µM pore size syringe filters (Sarstedt), aliquoted into 1 mL microfuge tubes and stored at -80°C.

2.3 Virus quantification

Quantification of HIV-1 was achieved through measurement of reverse transcriptase activity by real-time PCR or through antibody detection of the p24^{CA} protein.

Measurement of reverse transcription activity was performed using the SYBR Green (SG) I qPCR-based product-enhanced RT (PERT) assay (SG-PERT) [202][203]. Briefly, 5 µL of cell-free virus was mixed with 5 µL of 2x concentrated lysis buffer (0.25% Triton X-100, 50 mM KCl, 100 mM Tris-HCl pH7.4, 40% glycerol) centrifuged at 10,000 x g for 10 min at RT and diluted up to 1 mL with 1x core buffer (50 mM (NH₄)₂SO₄, 20 mM KCL, 20 mM Tris-HCL pH 8.3). Ten microlitres of PERT master mix (5 mM (NH₄)₂SO₄, 200 mM KCL, 200 mM Tris-HCL pH 8.3, 10 mM MgCl₂, 0.2 mg/ml BSA, 1/10,000 SYBR Green I, 400 µM dNTPs, 1 µM each of forward 5'-TCCTGCTCAACTTCCTGTC-GAG-3' and reverse 5'-CACAGGTCAAACCTCCTAGGAATG-3' primer, 7 pM/ml MS2 RNA) was aliquoted into a 96-well PCR plates along with 10 µL of the sample and centrifuged briefly. PCR amplification was performed using a Bio-RAD C1000 Thermo Cycler using the following parameters:

Temp (°C)	Time (min)	Cycles	
42	20:00		Reverse transcription
95	2:00		Hot-start Taq activation
95	0:05		Denaturation
55	0:05	x39	Annealing
72	0:15		Extension
82	0:05		Acquisition
65	0:05		
to			Melting analysis
95			

Fluorescence acquisition was recorded at the end annealing phase. Cycles of quantification (C_q) were analysed using Bio-Rad CFX Manager 3.0 software and RTU values extrapolated from a standard curve of MS2 bacteriophage RNA (Sigma-Aldrich).

Capsid protein quantification was achieved using the Immunodeficiency Virus type-1 p24^{CA} protein (high sensitivity) AlphaLISA detection kit per the manufacturers standard protocol (PerkinElmer).

2.4 Infectivity assay

HEK 293T cells were seeded at 6.0×10^4 cells/well in 24-well cell culture plates (Eppendorf) and incubated at 37°C for 24 h. Culture media was replaced with 1 mL of 1 RTU/mL viral supernatant and spinoculated (1400 x g, 90 min, 16°C). Four hours post spinoculation the supernatant was replaced with fresh media and the cells re-incubated for 36-48 h. The cells were then washed 2x with PBS, trypsinised with 200 µL 0.25% trypsin for 4 min, resuspended in 1 mL of DMEM complete and centrifuged at 1500 x g for 5 min. The cells were rinsed in 1 mL PBS, centrifuged (1500 x g/5 min) and the PBS aspirated. The cells were resuspended in 100 µL RT Glo Lysis buffer (Promega) and lysed for 5 min. Thirty microliters of sample was added to 30 µL of Bright-Glo Assay Reagent (Promega) in a 96-well plate, mixed briefly and the relative luminescence units (RLU) measured using an Infinite M200 multimode reader (TECAN). Fluorescence intensity was normalised to protein concentration using the Bradford assay (Sigma-Aldrich) according to the manufacturer's protocol.

2.5 Immunostaining

Viral particle immunostaining was performed by adsorbing viral supernatants on microscope slides (Superfrost Plus, Thermo Scientific) for 2 h at 37°C with 10 µg/ml of polybrene (Sigma-Aldrich), followed by rinsing with phosphate-buffered saline (PBS) and fixation with 4% paraformaldehyde (PFA) in PBS for 10 min at RT. Intracellular immunostaining was performed in cells grown on coverslips. Coverslips were fixed with 4% PFA in PBS for 10 min at RT followed by permeabilisation with 0.1% Triton X-100 in PBS for 5 min. After treatment in blocking buffer (0.1% Tween and 1% BSA in PBS) for 30 min, primary antibodies were incubated for 1 h at 37°C in blocking buffer followed by incubation for 1 h at 37°C with secondary antibodies. Coverslips were mounted with VECTASHIELD Antifade Mounting Medium (Vector Laboratories Inc.) before microscopy analysis. Primary and secondary antibodies used include:

Primary antibodies used: HIV-1 p24^{CA} mouse monoclonal antibody (AG3.0) (NIH AIDS Research and Reference Reagent program); Lamin B goat polyclonal antibody (M-20): sc-6217 (Santa Cruz Biotechnology); HIV-1 Integrase Antibody (IN-2) mouse monoclonal: sc-69721 (Santa Cruz Biotechnology); and GFP (FL) rabbit polyclonal antibody: sc-8334 (Santa Cruz Biotechnology).

Secondary antibodies used: Alexa Fluor 633 goat anti-rabbit (Thermo Fisher Scientific); Alexa Fluor 633 rabbit anti-mouse (Thermo Fisher Scientific); Alexa Fluor 488 donkey anti-mouse secondary antibody (Thermo Fisher Scientific); and DyLight 633 rabbit anti-goat IgG (Thermo Fisher Scientific).

2.6 Restriction compounds

All HIV-1 restriction compounds used in this project were resuspended in DMSO and were used at the following concentrations: Nevirapine (NIH AIDS Research and Reference Reagent Program) at 5 to 20 μ M; Ebselen (Merck Millipore) at 20 μ M and PF-3450074 (Sigma-Aldrich) at 10 to 20 μ M.

2.7 Preparation of capsid mutants

Viruses containing the p24^{CA} point mutations E45A (delayed uncoating), E128A/R132A (delayed uncoating) and K203A (premature uncoating) were created in pNL4-3, pNL4-3-IN-HiBiT, pcDNA3 MA-CA-GFP, and Δ 8.91/psPAX2 packaging vectors using site-directed mutagenesis and phusion high-fidelity DNA polymerase (Thermo Fisher Scientific). Forward and reverse complimentary primers were used to create mutations:

In pcDNA3 MA-CA-GFP, Δ 8.91 and psPAX2:

E128A/R132A: 5'-CCTATCCCAGTAGGAG**CG**ATCTACAAG**GC**GTGGATAATCCTGGG-3'

K203A: 5'-GTAAGACCATCCTG**GC**GGCTCTCGGCCAGCG-3';

In pNL4-3.Luc.R'E:

E45A: 5'-GTTTTTCAGCATTATCAG**C**AGGAGCCACCCACAAG-3'

E128A/R132A: 5'-CTATCCCAGTAGGAG**CA**ATCTATAAA**GC**ATGGATAATCCTGGG-3'

K203A: 5'-GATTGTAAGACTATTTTA**GC**AGCATTGGGACCAGG-3'

2.8 Capsid uncoating assays:

2.8.1 Dual-labelled system:

2.8.1.1 Matrix-Capsid-EGFP (MA-CA-GFP):

The Matrix and Capsid sequences, were PCR amplified from pNL4-3.Luc.R-E- and ligated into pcDNA3-EGFP using the KpnI and BamHI restriction sites, to give pcDNA3-Matrix-Capsid-EGFP (pcDNA3-MACA-EGFP):

(KpnI)MACA fwd: 5'-ATTAGGTACCATGGGTGCGAGAGCGTCCGTATTAAGC-3'
(BamHI)MACA rev: 5'-TAATGGATCCCAAACCTCTTGCTTTATGGCC-3'

The fluorescent protein mRuby2 (pmRuby2-C1), and those from the mKusabira Orange family mKO, mKO2 and mKOk (pmKO-N1, pmKO2-N1, pChicken Mermaid S188, respectively, addgene) were also PCR amplified from their respective host plasmids and cloned into pcDNA3-MACA-EGFP, in place of EGFP, using the restriction enzymes BamHI and NotI:

(BamHI)mRuby2 fwd: 5'-TAATGGATCCGTGTCTAAGGGCGAAGAGCTG-3'
(NotI)mRuby2 rev: 5'-TAATGCGGCCGCTTACTTGTACAGCTCGTCCATCC-3'
(BamHI)mKO/mKO2/mKOk fwd: 5'-TAATGGATCCGTGAGTGTGATTAACCAG-3'
(NotI)mKO/mKOk rev: 5'-TAATGCGGCCGCTTAGGAATGAGCTACTGCATC-3'
(NotI)mKO2 rev: 5'-TAATGCGGCCGCTTAGCTATGAGCTACTGCATC-3'

2.8.1.2 Vpr-IN-mCherry (VINC):

pVpr-IN-mCherry was assembled using a construct previously prepared within the Molecular Virology group [125]. Briefly, pVpr-IN-ECFP was constructed by cloning PCR amplified Vpr (pNL4-3) in frame with codon optimized IN into the pECFP-N1 vector (Clontech Laboratories, Inc., Saint-Germain-en-Laye, France). An HIV-1 protease cleavage site (IRKVL), flanked at both C- and N- termini by a flexible linker (KRIQST), was introduced between Vpr and IN. ECFP was removed from the C-terminal of pVpr-IN-ECFP and replaced with an mCherry fluorophore.

Trans-incorporated virions were produced by transfection of HEK293T cells with 16 µg of pNL4-3, 4 µg of MA-CA-GFP, 6 µg of VINC and pseudotyped with 4 µg of either VSV-G or HXB2 (WT) envelope. Control viruses were prepared as above minus either MA-CA-GFP, Vpr-IN-mCherry or both plasmids.

2.8.1.3 Time course:

Fifteen-millimetre cover-slips (Thermo Fisher Scientific) were placed into 24-well cell culture plates (Eppendorf), treated for >30 min with 0.01% poly-L-lysine (Sigma-Aldrich), rinsed 2x with phosphate-buffered saline (PBS) and dried for 2 h under a class II biological safety cabinet. Wells were seeded with 1.2×10^5 or 6.0×10^4 HeLa P4 cells for confocal or infectivity assays, respectively. Twenty-four hours post-seeding media was aspirated from the cells and replaced with 1 mL of virus at 1 RTU/mL and infection synchronised by spinoculation at 1400 x g/16°C for 90 min. After spinoculation the plates were incubated at 37°C for 30 min (VSV-G pseudotyped) or 50 min (HXB2 Env pseudotyped), the media aspirated and the cells washed 2x with PBS. The cells were then treated with 250 µL of 0.05 % trypsin (GIBCO, Thermo Fisher Scientific) for 1 min/37°C to remove non-fused virions and the media replaced with 0.5 mL DMEM. Plates were re-incubated and fixed with 4% paraformaldehyde (PFA) (Sigma-Aldrich) for 10 min at 15, 30 or 60 min intervals post-trypsinisation, and stored in PBS at 4°C until mounting.

The fixed samples were either stained with immuno-fluorescent antibodies or the coverslips mounted directly on to microscope slides (Superfrost Plus, Thermo Scientific) using 8 µL VECTASHIELD Antifade Mounting Medium (Vector Laboratories) and sealed using nail varnish. The cells were then visualised using confocal microscopy.

2.8.2 SunTag – capsid-Tag

The SunTag peptide was inserted into various regions of the cyclophilin-A binding loop of p24^{CA} through site directed mutagenesis. The matrix and capsid genes from pCMVdeltaR8.91 were primarily inserted into the cloning vector pUC-21 using SpeI to facilitate mutagenesis. Two systems were employed:

Firstly, region 87 to 97 (11 aa) of the CypA binding loop was exchanged with the 19 amino acid SunTag (CA-Tag v2.1) as this region was predicted to have a minimal effect on the structure of the protein using LOOPP protein folding recognition software (<http://cbsu.tc.cornell.edu/software/loopp/>).

CA-Tag v2.1 fwd and rev complimentary primers:

5'-GAATGGGATAGAGTGCATCCAGTGGGAAGAATTATTAAGTAAGAATTATCATTAGAAAATG
AAGTAGCAAGATTAAAGAAAGAACCAAGGGGAAGTGACATAGCAG-3'

Secondly, region 79 to 94 (16 aa) of the CypA binding loop was exchanged for the 19 amino acid sequence of the SunTag peptide (CA-Tag v1) due to a slight complementarity (2 aa) between the two sequences.

CA-Tag v1 fwd and rev complimentary primers:

5'-GAATGGGATAGAGTGCATCCAGTGGGAAGAATTATTAAGTAAGAATTATCATTAGAAAATG
AAGTAGCAAGATTAAAGAAAGAACCAAGGGGAAGTGACATAGCAG-3'

The CA-Tag v2.1 construct was used as a template for these primers and the resultant PCR product was used as a primer to insert the CA-Tag v1 into pNL4-3 and pUC21- Δ 8.91 (through a pCDNA3 intermediate containing the matrix and capsid genes). All mutations were verified by sequencing.

Vectors were produced in HEK293T cells (both in cells expressing or not-expressing scFv-sfGFP) using a self-inactivating lentivirus vector (SIN-Luc), VSV-G envelope, and different ratios of Δ 8.91-CA-CypA v2.1 to WT Δ 8.91 to see the effects of the CA-Tag on viral infectivity (measured via PERT, luciferase assay and western blot). Vectors were also prepared using increasing ratios of the NL4.3-CypTagV1 vector with WT NL4-3.

2.8.3 SunTag – repeat peptide array

The 10x and 24x GCN4 (SunTag) peptide repeats were PCR amplified from the transfer vectors pHRdSV40-dCas9-10xGCN4_v4-P2A-BFP and HRdSV40-NLS-dCas9-24xGCN4_v4-NLS-P2A-BFP-dWPRE (Addgene), respectively:

(AheI)10x/24xSunTag fwd: 5'-ATTAACCGGTGGCAGCGGCAGCGGCGAAGAAGACTTTTGA
GCAAGAATTAT-3'
(EcoRI/XhoI)10xSunTag rev: 5'-TAATCTCGAGAATTCTCACTTTTTGAGCCTAGCAACTTC-3'
(Sall)24xSunTag rev: 5'-TAATGTCGACTCACTTTTTAAGTCGGGCTACTTC-3'

The resultant bands were then digested and ligated onto the C-terminus of HIV-1 integrase in either a Δ 8.9 packaging vector (Δ 8.9-IN-10xSunTag) or an expression vector (pcDNA3) containing HIV-1 Vpr-IN for trans-incorporation into virions (pcDNA3-Vpr-IN-10x/24xSunTag).

Vectors were produced using 10 μ g of the transfer vectors pNL4-3 (for pcDNA3-Vpr-IN-nxST) and SIN-Luc for (Δ 8.9-IN-10xSunTag), and were pseudotyped with 3.5 or 4 μ g of VSV-G or HXB2 derived envelope, respectively. A titration study was then performed to determine the effects of increasing concentrations of Δ 8.9-IN-10xSunTag versus Δ 8.9 packaging vector, and pcDNA3-Vpr-IN-10x/24xSunTag trans-incorporation on virus production (measured using PERT assay) or infectivity (measured through luciferase activity). The viruses were then analysed using confocal and Operetta high-content imaging.

2.8.3.1 APOBEC SunTag

The apolipoprotein B mRNA editing enzyme, catalytic polypeptide-like (APOBEC) 3G and 3F (A3F and A3G) genes were incorporated into the pcDNA3-Vpr-IN-24xSunTag plasmid through PCR amplification of the pBTe2-A3F/G*-HiBiT vector (**section 2.8.4**), using a forward primer (containing a KpnI restriction site) complementary to the 5' end of both A3F and A3G*, and a reverse primer (containing an AgeI restriction site) complementary to the 3' end of the V5 tag:

(KpnI)A3FG* fwd: 5'-ATTAGGTACCGCCACCATGAAGCCTCACTTCAGAAACACAG-3'
(AgeI)A3FG* rev: 5'-TAATACCGGTCCCCGTAGAATCGAGACCG-3'

The A3F/G* PCR fragments were ligated into the pcDNA3-Vpr-IN-24xSunTag plasmid in place of Vpr-IN. Viruses were prepared as with the A3F/G* HiBIT (**section 2.8.4**), but with a SIN-Luc transfer vector (in place of SIN-GFP) which does not express Vif or GFP: SIN-Luc (10 µg), Δ8.91/psPAX2 (6.5 µg), A3F/G* (5 µg) and VSV-G (3.5 µg) or HXB2 Env (4 µg).

2.8.4 NanoBiT

The sequences for the Large Bit (LgBiT) and High Bit (HiBiT) of the two-subunit based system were obtained from pBiT1.1-C [TK/LgBiT] and pBTe2(CtermHiBiT), respectively (NanoBiT PPI MCS Starter System, Promega).

The A3F and A3G genes were PCR amplified from cDNA derived from HEK293T cells using reverse primers containing the sequence for a V5-tag on the C-terminal of the APOBEC genes. NheI (forward), and EcoRI/SalI (reverse) restriction sites were incorporated into the primers for ligation of the A3F/G genes into pBTe2(CtermHiBiT), subsequently named pBTe2-A3F/G-HiBiT:

(NheI)A3F/G fwd: 5'-ATTAGCTAGCGCCACCATGAAGCCTCACTTCAGAAACACAG-3'
 (SalI)A3F rev: 5'-TAATGTCGACCCCGTAGAATCGAGACCGAGGAGAGGGTTAGGG
 ATAGGCTTACCCTCGAGAATCTCCTGCAGCTTG-3'
 (EcoRI)A3G rev: 5'-TAATGAATTCCCGTAGAATCGAGACCGAGGAGAGGGTTAGGGA
 TAGGCTTACCGTTTTCTGATTCTGGAGAATGG-3'

Site-directed mutagenesis was used to incorporate a glutamic acid to glutamine mutation at point 259 of A3G to create a cytidine deaminase deficient mutant (pBTe2-A3G*-HiBiT). Forward and reverse complimentary primers:

pBTe2-A3G* fwd: 5'-GAAGGCCGCCATGCACAGCTGTGCTTCCTGG-3'

The HiBiT was also cloned into pNL4-3 (pNL4-3-HiBiT) using a method described by Petit and co-workers whilst cloning hemagglutinin (HA) and flag epitopes into an HIV-1 BRU infectious molecular clone [204]. Briefly, two sets of primer pairs were used. For the 1st set a forward primer (AgeI pre-IN forward) was designed overlapping an AgeI restriction site upstream from the IN gene and

was used in conjunction with a reverse primer (BspEI HiBiT reverse) complementary to the C-terminal sequence of IN and containing part of the 5' sequence of the HiBiT epitope including a BspEI restriction site. For the 2nd set the forward primer (BspEI HiBiT forward) contained the remaining part of the HiBiT epitope, including the BspEI restriction site, and a portion complementary to the sequence downstream of IN, and a reverse primer (PflMI post-IN reverse) overlapping a PflMI restriction site further downstream. After PCR amplification and digestion, equimolar concentrations of the two PCR products were ligated forming a template for further PCR amplification using the AgeI pre-IN forward and PflMI post-IN reverse primers. The resultant PCR product was digested with AgeI and PflMI and ligated into pNL4-3. The sequences for the primers were as follows:

(AgeI)pre-IN fwd: 5'-GATTCTAAAAGAACCGGTACAT-G-3'
 (BspEI)HiBiT rev: 5'-CGCCATCCGGACACATCCTCATCCTGTCTACT-TGC-3'
 (BspEI)HiBiT fwd: 5'-ATGTGTCCGGATGGCGGCTGTTCAAGAAGATTAGCTAACACATG
 GAAAAGATTAGTAAAACAC-3'
 (PflMI)post-IN rev: 5'- TTCCTCCATTCTATGGAGACTC-3'.

Viruses were prepared using the self-inactivating vector pHR.SIN.CSBgallGW-GFP (10 µg), which does not express the Vif or luciferase proteins, the packaging vectors Δ8.91/psPAX2 (6.5 µg), APOBEC 3F/G* (5 µg), and were pseudotyped with either VSV-G (3.5 µg) or HXB2 (4 µg) envelope.

2.8.4.1 NanoBiT assay

HeLa P4 pAIB-LgBiT stable clone and HeLa P4 WT cells were seeded at 1.5×10^4 cells/well into 96-well tissue culture plates (PerkinElmer). Twenty four hours later the control cells were transfected with 50-100 ng of pNL4-3-HiBiT or pBTe2-A3F/G*-HiBiT plasmid DNA using Lipofectamine 3000 Reagent (Thermo Fisher Scientific) and re-incubated for 20-24 h. The following day the cells were infected with 200 µL of virus plus associated restrictive compounds and spinoculated for 90 min at 1400 x g/16°C. During spinoculation a stock of NanoGlo Live Cell Reagent was prepared according to the NanoBiT PPI Luminescence protocol (Promega). After spinoculation the virus was replaced with 100 µL pre-warmed (37°C) DMEM complete plus HEPES (plus associated

restrictive compounds) and 25 μL of Nano-Glo Live Cell Reagent per well, and analysed using an Infinite M200 multimode reader (TECAN). The plate reader was pre-warmed to 37°C before use, and upon insertion mixed the plate with an orbital motion at 500 rpm for 15 seconds. Luminescent readings were acquired every 5 min for 150 min, using an integration time of 2 s.

2.9 Operetta High-Content screening

Ninety six-well cell carrier plates (PerkinElmer) were treated with poly-L-lysine and then seeded with 1.5×10^4 HeLa P4 scFv-sfGFP stable clone cells per well. Twenty-four hours later the cell culture media was replaced with 200 μL of virus containing the Vpr-IN/APOBEC-24xSunTag constructs and spinoculated for 90 min at 1400 x g/16°C. The virus was replaced with pre-warmed 200 μL fluoroBrite (Thermo Fisher Scientific) supplemented with HEPES (GIBCO, Thermo Fisher Scientific) and imaged directly in the live cell chamber (5% CO₂/37°C) of the Operetta high-content imaging system (PerkinElmer). Images were acquired every 5 min over a 150 min time frame and analysed using the Harmony High-Content Imaging and Analysis Software.

2.9.1 Harmony High-Content Imaging and Analysis Software

Input Images were selected and a flat-field correction using the 'Advanced' method was applied to correct uneven illumination in the field of view. To facilitate the segmentation of cells in the images, the signal to background window was enhanced using the 'Calculate Images' building block, and an arbitrary formula was applied to keep only the pixels with a green fluorescence intensity greater than 150, with the rest reset to zero. Cells were segmented using the 'M' method of the 'Find Cells' building block, with the cell lower limit diameter set at 40 μM , the splitting coefficient at 0.45, and a common threshold (the lower level of pixel intensity for the whole image that may belong to cells) of 0.15 (**Fig. 8A**). Since applying a common threshold resulted in a reduced area of segmentation in these image conditions, the cells were then resized by 10 pixels to ensure the inclusion of the cell border (**Fig. 8B**).

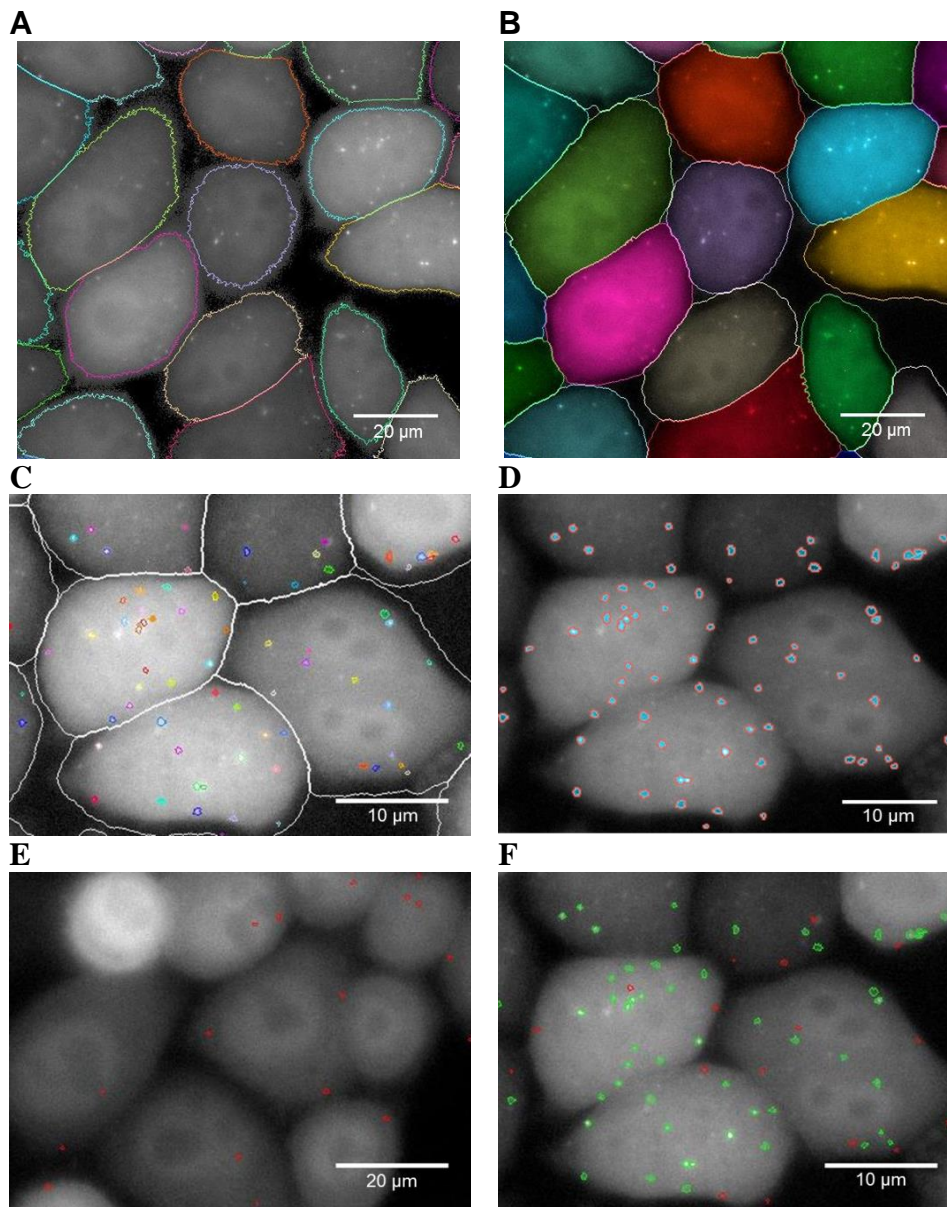


Figure 8. Segmentation and counting of cells and spots using the Harmony high-content imaging and analysis software. (A) Cells were primarily segmented using the ‘Find cells’ building block. (B) Cells were resized by 10 pixels to include the cell borders. (C) Spots were segmented using the ‘Find spots’ building block (total spot count). (D) Spots were resized to define a ring region that include the background of the area immediately surrounding the spot to determine the S-B of the spots. (E-F) A threshold was set based on the value of S-B in the negative control cells (E) to remove aspecific segmentation (red) and identify true spots (green) representing the ‘spot selected’ population.

Spots were detected using method ‘A’, which detects the local intensity maxima, and the relative intensity of the spot peak to background was set at >0.020 , with a splitting coefficient of 1.0 (**Fig. 8C**). The spot region was resized by -0.5 pixels of ‘Inner Border’ and -1.5 pixels of ‘Outer Border’ to select a ring region in which

the background value immediately surrounding the spot was determined (**Fig. 8D**), and the signal minus background (S-B) value calculated. A threshold was set based on the value of S-B in the negative control cells (infected with NL4-3 + VSV-G minus the epitope peptide array) to be able to distinguish a true spot from segmentation artefacts (red spots) (**Fig. 8E**). This selection was applied to derive the 'spot selected' population (green minus red spots) (**Fig. 8F**) displayed in the results.

2.10 Confocal Microscopy

Images were acquired using a Leica TCS SP5 laser-scanning confocal microscope and the Leica Application Suite Advanced Fluorescence (LAS AF) user interface. High resolution images were obtained using the 63x/1.4 NA HCX PL APO oil immersion objective. An argon (Ar) and Helium Neon (HeNe) laser was used for excitation of EGFP/sfGFP ($\lambda = 488$ nm), mKO/mCherry ($\lambda = 543$ nm), and Alexa-633/680 ($\lambda = 633$ nm). Unless otherwise stated the Ar laser was set at 29% power and 15% intensity, and the HeNe laser at 30% intensity. The fluorescence emission spectra were collected in the ranges of 493-510 (sfGFP), 493-550 (EGFP), 550-700 (mKO), 560-630 (mCherry) and 645-795 nm (Alexa-633/680). A pinhole of 1.5 and 1.0 airy units (AU) was used when acquiring the CA-GFP/IN-mCherry and CA-mKO/IN-sfGFP images, respectively. A pinhole of 1.0 AU is the standard setting for confocal acquisition, producing images with high contrast and low background in the presence of sufficient fluorescence, as with the CA-mKO and IN-sfGFP labelling. However, due to the reduced signal obtained with the mCherry fluorophore, a pinhole of 1.5 AU was employed which enabled greater exposure of mCherry-labelled particles without significantly affecting resolution from out of focus light. Sequential imaging was used for two and three-colour acquisition to reduce the crosstalk between the signals. Unless otherwise stated, A zoom 6x was used in the time courses, and cells were selected (~4 cells per field) using the bright-field illumination to reduce bias in cell selection.

A z-step (axial resolution) of 300 nm was used for acquisition of the images in the time courses, determined from the numerical aperture of the objective using the following formula:

$$r_{axial} = \frac{1.4\lambda \cdot \eta}{NA^2}$$

Where λ is the emission wavelength (543 nm), η is the index of refraction (1.5) and NA is the numerical aperture (1.4); thus giving a r_{axial} of 582 nm. According to the Nyquist criterion the optimal sampling rate is half that of the axial resolution, approximately 300 nm. The CA-GFP/IN-mCherry images were acquired using a frame/line average of 1 and 3, and the CA-mKO/IN-sfGFP signal was captured using frame/line averages of 2 and 5.

2.10.1 Semi-automatic colocalisation

The first set of images (up until the capsid was tagged with the mKO fluorophore) were analysed in a semi-automated approach using the open source image processing package ImageJ. A macroinstruction (Macros) was developed using the 'Record...' function plugin detailing a sequential set of tasks for segmenting and determining colocalisation between the fluorescently labelled CA and integrase proteins. After acquisition the images were imported into ImageJ and the channels were split. The channel containing the images of the IN fluorescence were processed using the Gaussian Blur 3D function, a filter that uses convolution with a Gaussian function for smoothing (using an X, Y and Z sigma of 1.0) to reduce the background signal and enable segmentation. Segmentation was performed using the '3D Objects Counter' function and a threshold that was manually determined for each time course. This resulted in a map of 'objects', with the number of voxels (volume picture elements) constituent for each object. The objects map was imported into the '3D Manager' plugin (Add Image) followed by the channel containing the images of CA fluorescence (Select All). Colocalisation was performed using the 'Quantif 3D' function of 3D Manager and derived from the maximum 'Max' colocalising voxels readout. Colocalisation was calculated as the number of CA objects colocalising with IN objects (over various thresholds) divided by the total number of integrase objects and was presented as a percentage.

2.10.2 Bleed-through

In the calculation of the percentage of colocalised vs. uncoated PICs, the number of colocalised CA-GFP and IN-mCherry particles was determined using the 3D Manager plug-in (ImageJ) and then divided by the total number of IN-mCherry particles counted within that time point. A readout was displayed listing the IN-mCherry segmented objects and the highest CA-GFP signal colocalised within that object. Because of the closeness between the excitation and emission spectra a small amount of bleed-through was transferring from the GFP into the mCherry channel (GFP excites at $\sim 2.12\%$ with the HeNe laser ($\lambda = 543 \text{ nm}$), which meant a certain amount of 'mCherry' signal was colocalising with itself (**Fig. S1**), giving artificially high percentages at low colocalisation thresholds (**Fig. 9**). Although some of the localisation at low thresholds would be true data, to limit bias from false spots a colocalisation threshold from 10 to 20 of the gray level range was chosen.

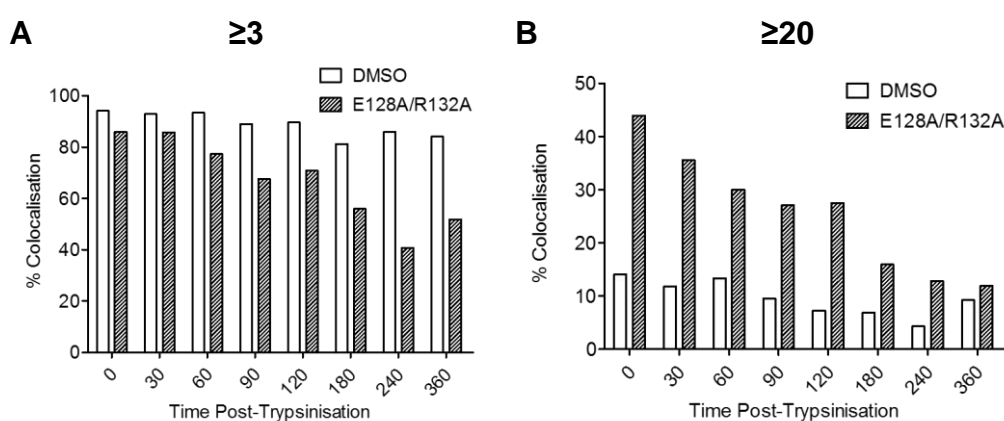


Figure 9. Percentage of colocalisation between CA-GFP and IN-mCherry depending on the threshold for colocalisation selected. Colocalisation was determined by segmenting the IN-mCherry puncta using the 3D Object Counter (ImageJ) and establishing the maximum CA-GFP signal within the segmented object using the 3D Manager plug-in (ImageJ); percent colocalisation was then calculated by dividing the number of colocalised objects by the total number of segmented IN-mCherry objects. (A and B) Examples of colocalisation when the threshold (determining colocalisation of CA with IN) in the green channel (CA) was set at ≥ 3 or ≥ 20 gray level units.

2.10.3 DeconvolutionLab

To reduce the time it took to analyse colocalisation between the capsid (EGFP/mKO) and integrase (mCherry/sfGFP) proteins a pipeline was developed to automate the process, in collaboration with the Predictive Models for Biomedicine & Environment (MPBA) and the Molecular Imaging groups in Fondazione Bruno Kessler (FBK). Using DeconvolutionLab open source software and Python scripting the pipeline used a series of algorithms to improve the contrast and resolution of the image. Deconvolution was performed using an experimental point spread function (PSF) and a Tikhonov-Miller algorithm, which consisted of 30 iterations and a regularisation factor of 0.01 (determined experimentally). The deconvolution was comparable to that performed with (Huygens Remote Manager), but the former was used as it was compatible with DeconvolutionLab open software.

The images were then segmented, a process of partitioning a digital image into multiple quantifiable segments through image thresholding and connectivity analysis to locate the objects or 'spots' to be colocalised and the boundaries of the image. The individual spots were detected using ImageJ based on the local maxima of the fluorescence intensity, each pixel being marked as a 'spot' if its intensity was maximum within its surrounding region. Colocalisation was determined if a fluorescent spot denoting a CA particle fell within 5 pixels distance of the centroid (central pixel) of a fluorescent spot signifying an IN particle.

RESULTS

3.1 A dual-fluorescent virus for studying uncoating

The ultimate system for studying capsid uncoating would be to visualise single capsid cores and their associated viral nucleoprotein in real time. This would make it possible to determine exactly when, where and how the capsid cores disassemble in relation to the nucleoproteins, within the 3D spatial context of the target cell. This requires labelling of both the p24^{CA} protein and a component of the RTC/PIC. Albanese and co-workers developed a system for labelling the RTC without impairing the genome processing capacity of the provirus by cloning Vpr in frame with codon optimised IN into a pEGFP-N1 vector [125]. During viral assembly and budding Vpr-IN-EGFP is incorporated into the viral particle through interaction with the p6 domain of Gag without significantly impairing infectivity. Using this system, it was possible to track the virus from fusion with the target cell membrane until integration with the host genome.

We developed a p24^{CA} labelling system that could be used in conjunction with fluorescently labelled Vpr-IN, to allow visualisation of capsid disassembly (uncoating) from the RTC/PIC. The MA and CA proteins from an envelope and Vpr deficient provirus, pNL4-3.Luc.R⁻E⁻ (pNL4-3), were cloned into pcDNA3 and an enhanced green fluorescent protein (EGFP) was fused to the C-terminus of the CTD of capsid (MA-CA-GFP). During viral maturation the matrix protein would be cleaved from the NTD of capsid leaving the CA-GFP fusion protein. Similarly, the mCherry fluorophore was fused to the CTD of Vpr-IN (Vpr-IN-mCherry) as it had good brightness and bleaching profiles, and its fluorescent spectra was compatible with the EGFP fused to capsid. As the insertion of exogenous coding sequences into the Gag gene can lead to loss of viral infectivity [205], we tested this by producing virions with the pNL4-3 provirus and the WT HXB2 envelope, and different concentrations [μ g] of the MA-CA-GFP, Vpr-IN-mCherry and pcDNA3 (control) vectors. HeLa P4 cells were transduced with 1 RTU of the subsequent vectors and infectivity was measured through luciferase activity 48 h post infection (**Fig. 10**). A loss of infectivity compared to the WT control (pNL4-3 + HXB2) was observed with all the trans-incorporated viruses. An infectivity of 28% and 18% with respect to WT was observed with

trans-incorporation of 2 μg or 4 μg of MA-CA-GFP with 6 μg of Vpr-IN-mCherry, respectively. However, the latter combination was chosen for use in the future experiments to increase the probability of CA-GFP incorporation into the viral core.

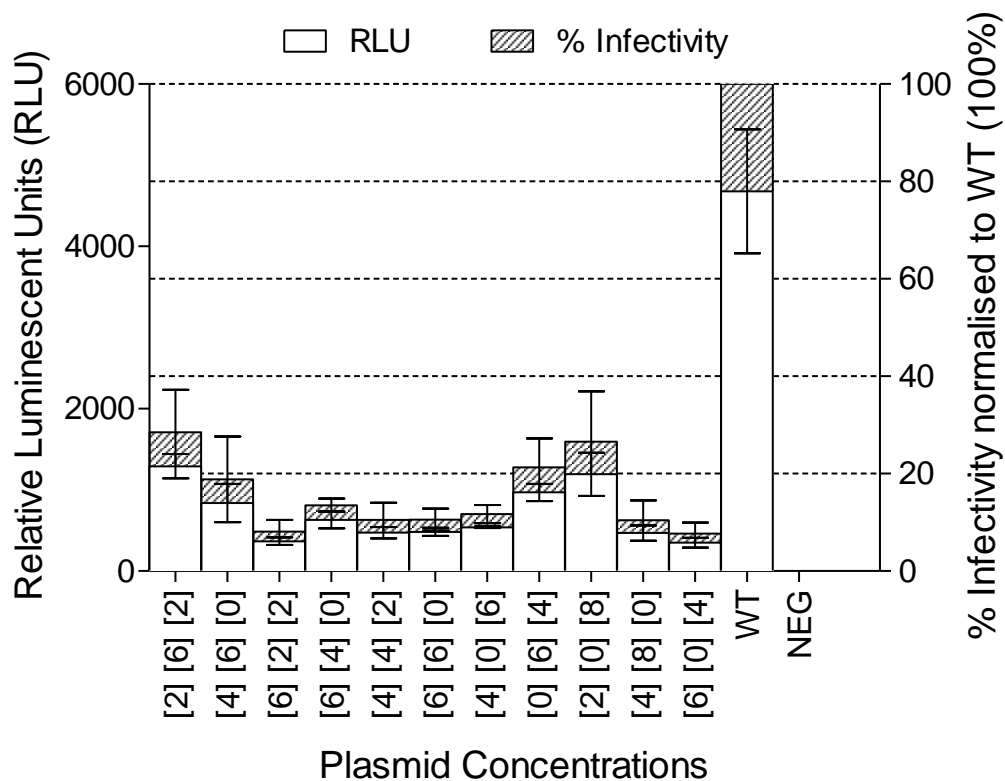


Figure 10. Infectivity of viruses transfected with increasing concentrations of MA-CA-GFP and Vpr-IN-mCherry vectors. HeLa P4 cells were transduced with viruses prepared with pNL4-3 and HXB2 envelope, and varying concentrations [μg] of the MA-CA-GFP, Vpr-IN-mCherry and pcDNA3 (plasmid control) vectors. Infectivity was measured 48 h later through luciferase activity against a standard WT (non trans-incorporated) virus. Graph showing SEM of $n = 3$ technical repeats, with the left vertical access displaying the RLU and the right vertical access showing the percentage of infection normalised to the WT control (100%). Labels on the x axis = [MA-CA-GFP] [Vpr-IN-mCherry] [pcDNA3].

The insertion and/or deletion of sequences from the Gag gene can also have an effect on the protease cleavage of the precursor Gag polyprotein during maturation of the virus [206][207], influencing the rate of cleavage and, subsequently, the proper assembly of virions. As the SP1, NC, spacer peptide 2 (SP2), and p6 sequences were absent from the MA-CA-GFP vector, we wanted to assess the effect this would have on the assembly of the trans-incorporated virus and, specifically, the cleavage of capsid from the matrix protein. Virions were produced with increasing concentrations of the MA-CA-GFP vector and

pelleted through ultracentrifugation. Western blot was performed on the concentrated virus, and lysate from the producer cells, using antibodies specific for CA (24 kDa), EGFP (27 kDa) and IN (32 kDa). Bands corresponding to the expected cleavage products were observed, confirming that protease cleavage at the expected sites was occurring, including CA-GFP (~51 kDa) (**Fig. 11**). A large proportion of the matrix, however, remained attached to CA-GFP (MA-CA-GFP ~68 kDa). Apart from this, bands of similar intensity were observed to that of the NL4-3 control, including: Gag (~55 kDa), MA-CA-SP1-NC (~48 kDa), MA-CA (~41 kDa) and CA (~24 kDa). The intensity of the band corresponding to CA-GFP, however, was substantially lower to that of p24^{CA}.

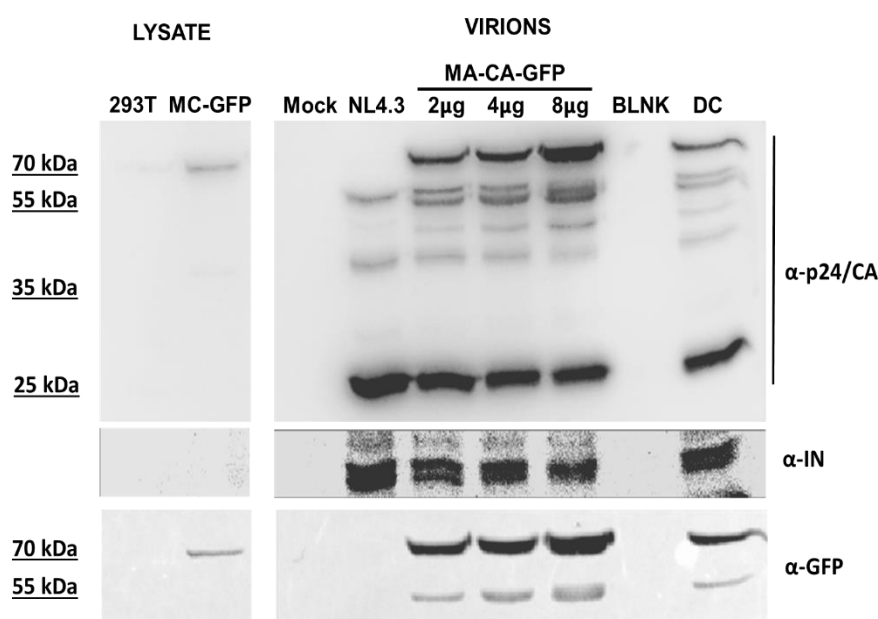


Figure 11. Protease cleavage of CA-GFP. Viruses were prepared with pNL4-3, HXB2 envelope and increasing concentrations of MA-CA-GFP and pelleted by ultra-centrifugation through a 20% sucrose cushion. Samples were analysed by western blot using antibodies targeting p24^{CA}, integrase and GFP. DC = dual colour (MA-CA-GFP + Vpr-IN-mCherry).

3.1.1 Colocalisation of CA-GFP with IN-mCherry in CD4⁺ cells

Because of the relatively low cleavage product obtained with CA-GFP compared to p24^{CA}, we wanted to see if enough CA-GFP molecules were present to observe colocalisation with IN-mCherry. Vectors were prepared using the pNL4-3 provirus [16 μg], MA-CA-GFP [4 μg], Vpr-IN-mCherry [6 μg] and the WT HXB2 envelope [4 μg] and used for transducing HeLa P4 cells containing the CD4 receptor as well as HeLa WT cells lacking the CD4 receptor. These cell lines

were used to distinguish between productive HIV-1 entry (HeLa P4) and endocytosis (HeLa WT). The cells were fixed and mounted on microscope slides for confocal acquisition. Images were acquired using the argon ($\lambda=488$ nm) and Helium Neon ($\lambda=543$ nm) lasers, and fluorescent emission collected at 500-550 and 560-700 nm, respectively (**Fig. 12**). For HeLa WT cells (**Fig. 12A**), fluorescent puncta were only observed surrounding the cell, in accordance with the HXB2 enveloped viruses being unable to productively fuse to the cell. The high intensity profiles of the GFP spots also demonstrated that the capsid-EGFP proteins were being incorporated sufficiently into the virus to enable confocal visualisation.

Fluorescent puncta were, however, observed within HeLa P4 CD4 expressing cells (**Fig. 12B**), indicating the productive entry of HXB2 enveloped viruses. Measurement of the fluorescence profiles of these puncta established the overlapping of EGFP and mCherry fluorophores within the same pixels. This colocalisation of fluorescence confirmed that MA-CA-GFP and Vpr-IN-mCherry were being incorporated into the viruses.

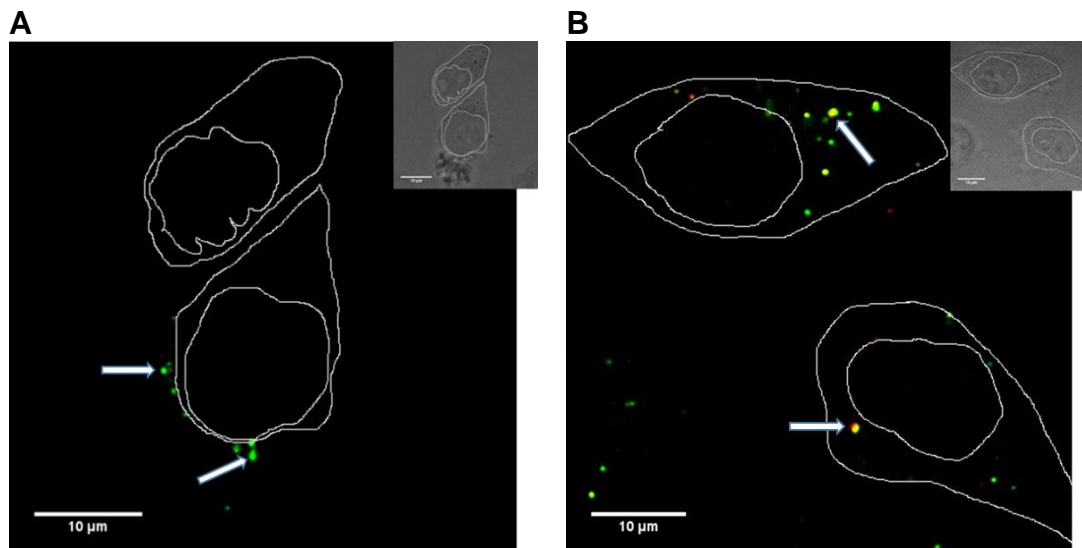


Figure 12. Colocalisation of CA-GFP and IN-mCherry can be observed within HeLa P4 cells. (A) HeLa WT cells (not expressing the CD4 receptor) were transduced with HXB2 enveloped viruses produced with the MA-CA-GFP fluorescent protein. Fluorescent puncta were only observed on the outside of the cells (white arrows). (B) HeLa P4 cells stably expressing the CD4 receptor were transduced with HXB2 enveloped viruses produced with both the MA-CA-GFP and Vpr-IN-mCherry fluorescent proteins. EGFP and mCherry colocalised puncta were observed within the cells (white arrows). Colocalisation was confirmed using the 'Plot Profile' plugin (ImageJ).

3.1.2 Development of a time course for studying uncoating

An assay was designed to see if the dual-labelled virus could be used to study the process of uncoating. Briefly, HeLa P4 cells were seeded on coverslips treated with poly-L-lysine in 24-well plates. The following day the media was replaced with 1 RTU of the dual labelled virus and the plates spinoculated at 1400 x g for 90 min at 16°C, to synchronise infection [208]. The plates were then incubated at 37°C for 30 min or 50 min, for VSV-G and HXB2 enveloped viruses, respectively, to allow fusion with the cellular membrane [67]. The cells were then trypsinised, briefly, to remove non-bound viruses, acting as a '0 min' time point at which the maximum number of viruses with intact capsid cores would be present. The cells were then re-incubated, fixed at regular intervals after trypsinisation and mounted on to microscope slides for confocal acquisition. Images were acquired with the standard excitation and emission parameters (**section 2.10**), together with: zoom (x4), line average (x4) and a z-step of 0.3 µm (**Fig. 13**). In the preliminary images the IN-mCherry spots were appreciably dimmer than those of the CA-GFP and so the pinhole was increased to 1.5 AU to be able to capture the less intense IN-mCherry spots. Although this interfered with the resolution of the image, particularly on the XZ axis, and is not the recommended setting for confocal acquisition, the enhanced signal-to-noise ratio (SNR) enabled the discernment of more spots. Since the viral particles are smaller than the PSF, and the actual position of the particle is defined by the xyz position of the centroid, there was no real loss of 3D resolution.

Large numbers of yellow (CA-GFP (green) and IN-mCherry (red)) puncta were observed both intra- and extracellularly (**Fig. 13A**), and subsequent plot profiles confirmed a high level of colocalisation. A brief trypsinisation removed most of the particles that remained outside of the cells (**Fig. 13B**). Although high numbers of green spots could be observed at this stage (**Fig. 13A and B**), plot profiles revealed the presence of colocalised IN-mCherry. A steady increase in the number of IN-mCherry puncta compared to CA-GFP/colocalised spots could be observed 60 min after trypsinisation, indicating the disassembly of CA-GFP from IN-mCherry (**Fig. 13C**). Finally, only a small number of spots remained 360 min post-trypsinisation (**Fig. 13D**). These preliminary, qualitative, examinations of

the data, encouraged the further analysis of the images using more quantitative means of establishing colocalisation.

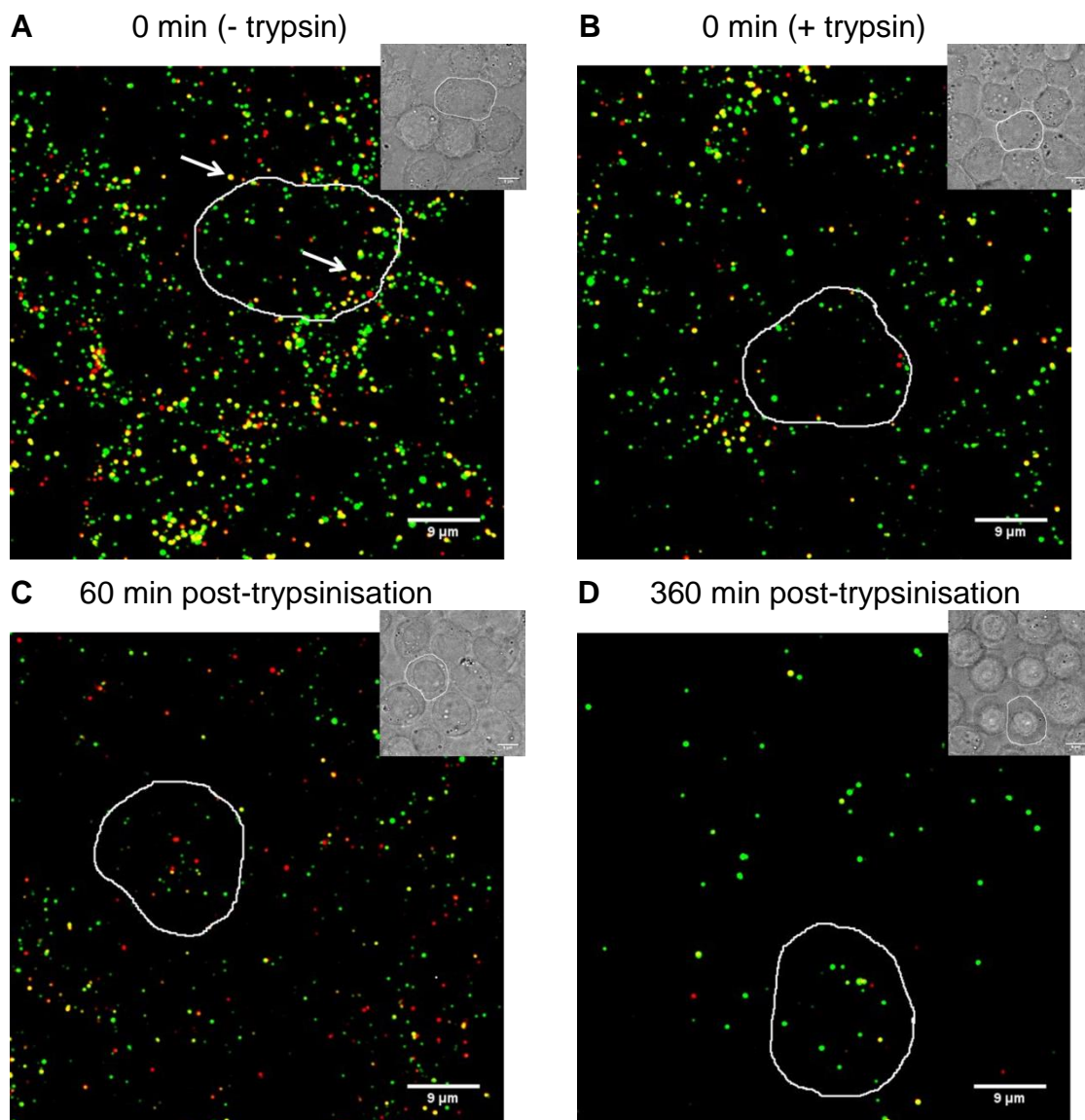


Figure 13. Example images from a representative time course used in the measuring of capsid uncoating. HeLa P4 cells were transduced with viruses trans-incorporated with MA-CA-GFP + Vpr-IN-mCherry. The cells were then incubated for 50 min (HXB2 envelope), and either directly fixed (A), or trypsinised for 1 min to remove non-bound viruses and fixed at 0 min (B), 60 min (C) or 360 min post-trypsinisation (D). Images were acquired using confocal microscopy. Green spots represent CA-GFP, red spots IN-mCherry, and yellow spots are indicative of colocalisation.

3.1.3 Effects of restriction compounds and capsid mutants

Capsid uncoating was determined by the loss of colocalisation between CA-GFP and IN-mCherry over time. To determine the amount of colocalisation between CA-GFP and IN-mCherry, a semi-automated system was developed to segment and count the fluorescent puncta and establish colocalisation, using the 3D Objects Counter and 3D Manager plugin (ImageJ), respectively (**section 2.10.1**). Capsid uncoating was calculated by dividing the total number of colocalised CA-GFP and IN-mCherry puncta by the total number of IN-mCherry spots per Z-stack.

To assess whether the fluorescently labelled virus was behaving like WT virus, HIV-1 restriction compounds and viruses prepared with capsid mutations known to alter the kinetics of capsid uncoating were tested in the time course assay (**Fig. 14**). The restrictive compounds nevirapine, a non-nucleoside reverse transcriptase inhibitor, and PF74, a molecule that binds to the NTD of capsid, were tested due to their reported capsid destabilisation properties [131][115]. TZM-bl cell lines stably expressing the TRIM5-CypA fusion protein were also tested, as this protein has been reported to target intact capsid cores for premature disassembly [209][126]. Two mutations, which have been shown to effect the stability of the viral core both *in vitro* and *in vivo*, were introduced into the capsids of both pcDNA3-MA-CA-GFP and the pNL4-3 provirus - a lysine to alanine mutation (K203A) and a glutamic acid/arginine to alanine double mutation (E128A/R132A), which have been reported to decrease and increase core stability, respectively [67][65].

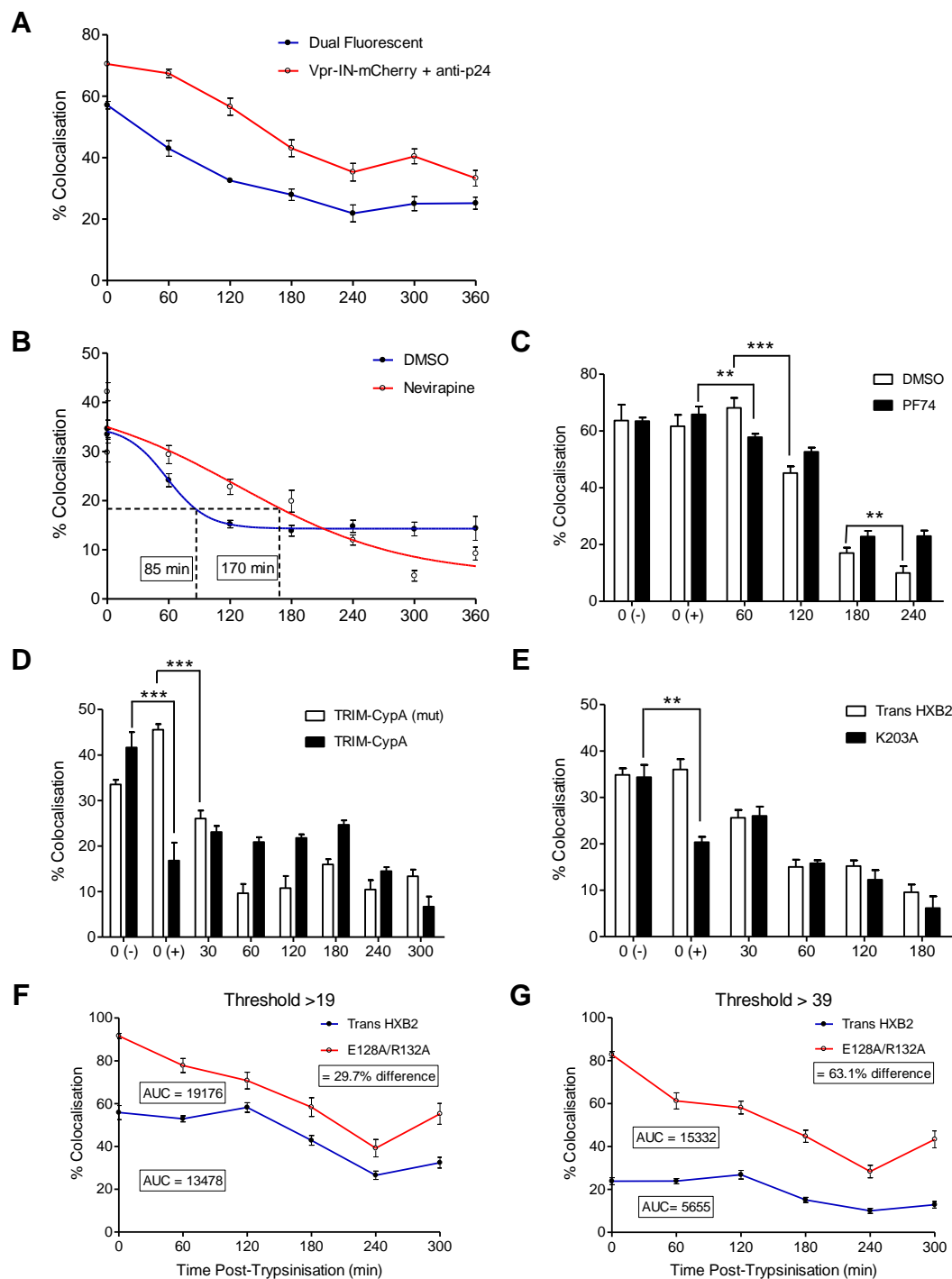


Figure 14. Effects of restrictive compounds/proteins and capsid mutations on the uncoating kinetics of the dual-labelled virus. HeLa P4 cells were transduced with dual-labelled viruses and fixed at regular intervals post-trypsinisation. Images were acquired using confocal microscopy, segmented, and colocalisation between CA-GFP and IN-mCherry determined using the 3D Manager plug-in (ImageJ). (A-G) Colocalisation of the dual labelled virus over time: (A) compared to an IN-mCherry only trans-incorporated virus immunostained with an p24^{CA} antibody, (B-C) ± the restriction compounds nevirapine and PF74, (D) in TZM-bl cell lines stably expressing a TRIM-CypA fusion protein or a non-restrictive mutant, (E) compared to viruses containing the less stable (K203A) and (F-G) more stable (E128A/R132A) capsid mutations. Graphs show the SEM from n = 5 technical repeats.

Generally, an initial peak of colocalisation was observed at the zero-minute time point (plus/minus trypsinisation), followed by a steady loss of colocalisation over time (CA uncoating); but colocalised puncta were always detected at the end of the time course (up to 360 min post-trypsinisation) (**Fig. 14A-F**). A half-time of uncoating (the time by which 50% of the particles had uncoated compared to the '0 hr' time point) was recorded from 60 to 240 min post-trypsinisation with the regular dual-labelled virus without the addition of restriction compounds. A similar kinetic of uncoating was observed with the dual-labelled virus compared to the IN-mCherry only trans-incorporated virus stained with an anti-p24^{CA} antibody (**Fig. 14A**). A 50% uncoating time of 175 min post-trypsinisation was recorded with the dual-labelled virus, and 240 min with immunostaining, but visibly larger puncta when staining may have exaggerated colocalisation. The addition of nevirapine delayed the 50% uncoating time from 85 to 170 minutes compared to the DMSO control (**Fig. 14B**). The addition of PF74 resulted in a slight premature uncoating event compared to the DMSO control (**Fig. 14C**), in line with the capsid destabilising properties reported with this small molecule compound [111][115][130]. A 50% half-time of uncoating was recorded at the 180 min time point \pm PF74, with a subsequent stabilisation of uncoating in the presence of PF74 compared to the DMSO control. A sharp decrease in colocalisation was observed in both TZM-bl cell lines infected with the dual-labelled virus (**Fig. 14D**). A 50% half-time of uncoating was recorded at the 0 min 'plus' trypsin time point with the TRIM-CypA producing cell line, and at 60 min post-trypsinisation with the cell line producing a mutated non-restrictive form of TRIM-CypA. The former result can be explained by the presence of a large amount of colocalised (coated) particles external to the cellular membrane in the directly fixed 0 min timepoint, whereas the 0 min 'plus' trypsin time point would contain only fused and internalised particles; most of the internalised particles in this case having already uncoated. A similar drop in colocalisation at the 0 min 'plus' trypsin time point was also observed with the dual-fluorescent virus containing the less stable (K203A) capsid mutation (**Fig. 14E**). A slightly delayed 50% half-time of uncoating was observed when the dual-labelled virus was assayed in parallel with the more stable (E128A/R132A) capsid mutant. However, a higher percentage of colocalisation was observed throughout the time course with the E128A/R132A CA mutant (**Fig. 14F**). When the threshold determining capsid

colocalisation with IN was increased (**Fig. 14G**), a substantial drop in the area under the curve (AUC) was observed with the non-mutated capsid compared to the more stable mutant. This suggests that increased uncoating was occurring with the virus without the CA mutation, but a certain amount of capsid was remaining with the IN to enable colocalisation at lower thresholds. A small increase in colocalisation was also observed at the end of the time point (300 min post-trypsinisation) with both the WT and more stable capsid mutant (**Fig. 14F and G**).

These results suggest that labelling of both the CA and the IN is an effective system for tracking uncoating, but biological replicates are needed to further evaluate this.

3.1.4 High-throughput analysis of uncoating

To improve the method for analysing capsid uncoating, we exchanged the fluorophores used for labelling the proteins with ones more suitable for the lasers on the confocal microscope. The IN-mCherry fluorophore was exchanged for superfolder GFP (sfGFP). As CA-EGFP was no longer compatible with IN-sfGFP, we tested four different fluorophores for their suitability in labelling capsid based on their excitation and emission profiles, brightness and photostability (**Table 1**) - monomeric Kusabira Orange (mKO), mKO2, mKOk and mRuby [210][211].

Table 1: Values for the excitation, emission, brightness and photostability of the fluorophores used for labelling the capsid and integrase proteins [210].

Fluorophore	λ ex (nm)	λ em (nm)	Brightness	Photostability*
EGFP	488	507	33.6	174
sfGFP	485	510	54.1	157
mKO	548	559	31.0	122
mKO2	551	565	39.6	228
mKOk	551	563	64.0	?
mRuby2	559	600	43.0	123†
mCherry	587	610	15.8	96

† (Bajar et al. 2016)

* Time for bleaching from an initial emission rate of 1,000 photons/s down to 500 photons/s; data are not indicative of photostability under focused laser illumination

The fluorophores were exchanged for EGFP on the CTD of capsid, viruses prepared with the pNL4-3 provirus and VSV-G envelope, and HeLa P4 cells transduced by spinoculation. Images were acquired under confocal microscopy using the HeNe laser excitation λ 543 nm (50% intensity), an acquisition window of 550-700 nm, a pinhole of 1 AU, and a frame and line average of 2 and 4, respectively. The signal to noise ratio was determined using 'Plot Profile' analysis from ImageJ (**Fig. 15**), the average of >10 plot profiles for each image can be seen in the table (**Fig. 15F**).

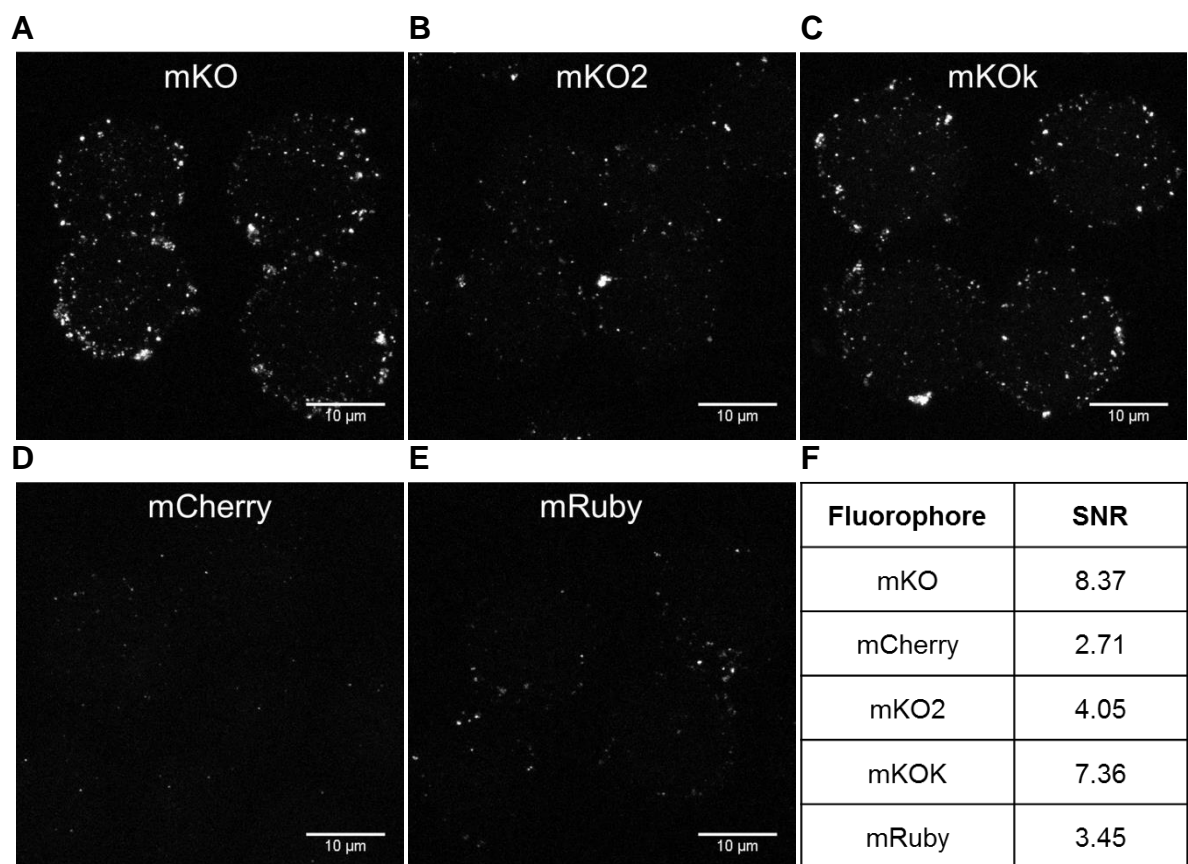


Figure 15. Signal to noise ratios of mKO, mKO2, mKOk, mCherry and mRuby fluorophores in HeLa P4 cells. HeLa P4 cells were transduced with viruses trans-incorporated with the following fluorescent fluorophores fused to the CTD of capsid: (A) mKO, (B) mKO2, (C) mKOk, (D) mCherry and (E) mRuby, and images acquired with the confocal microscope. Signal-to-noise ratios (SNR) were determined using 'Plot Profile' (ImageJ).

The highest SNR in HeLa P4 cells were achieved using the mKO, mKO2 and mKOk fluorophores (SNR of 8.37, 4.05 and 7.36, respectively), therefore, further analysis of their spectral and fluorescent intensity profiles was conducted to establish the fluorophore most suitable for the time course. Maximum emission

was observed at 570 nm for all fluorophores (**Fig. 16A**). A rapid loss of fluorescent intensity (bleaching) was observed, compared to when using arc-lamp illumination (**Table 1**), in a semi-quantitative comparison of the intensity profiles (**Fig. 16B**). The fluorescent intensity profiles were indicative of a double exponential, as opposed to the single exponential line plot usually observed with bleaching kinetics, suggesting that the fluorescent molecule may exist in two distinct populations, with one population having a more delayed bleaching profile than the other. However, a slight delay in the bleaching kinetics was observed with mKO compared to mKO1 and mKOk. As mKO also had the highest SNR in our experiments, we used this to label capsid, along with IN-sfGFP in all future experiments.

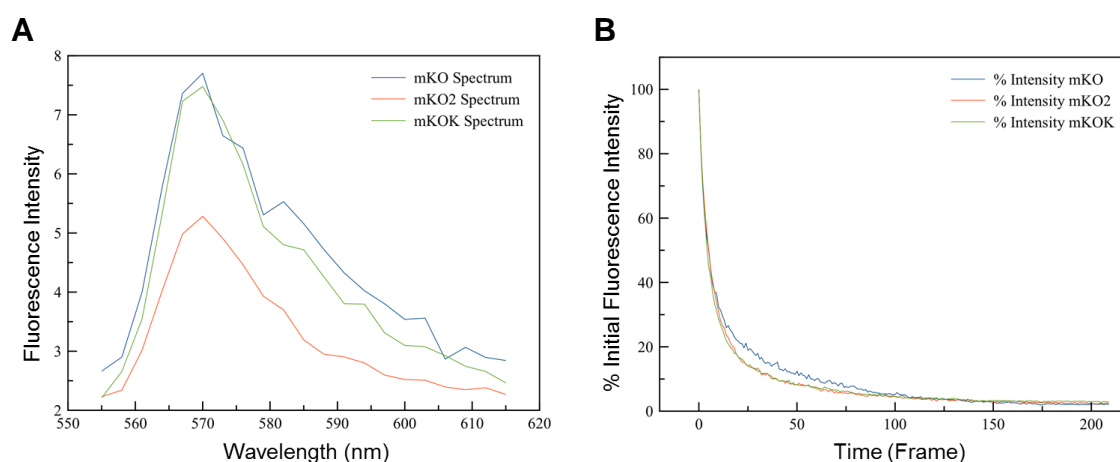


Figure 16. Fluorescent spectra and intensity profiles of mKO, mKO2 and mKOk. HeLa P4 cells were transduced with viruses trans-incorporated with MA-CA-mKO, MA-CA-mKO2 or MA-CA-mKOk and imaged using confocal microscopy. (A) Graph showing the fluorescent spectra obtained for mKO, mKO2 and mKOk. (B) Graph showing the fluorescent intensity profiles of mKO, mKO2 and mKOk. The fluorescent spectra and intensity profiles were acquired using the HeNe ($\lambda=543$ nm) laser set at 60% and 40% intensity, respectively, with a detection bandwidth of 550 to 615 nm.

To increase the speed and reduce the bias in image analysis we devised a pipeline for the high-throughput deconvolution, segmentation, counting and colocalisation of the images. The deconvolution pipeline was designed using Python scripting and the DeconvolutionLab open source software package (ImageJ), and consisted of a chain of three processing elements – deconvolution, segmentation and object counting, and colocalisation (**Fig. 17**).

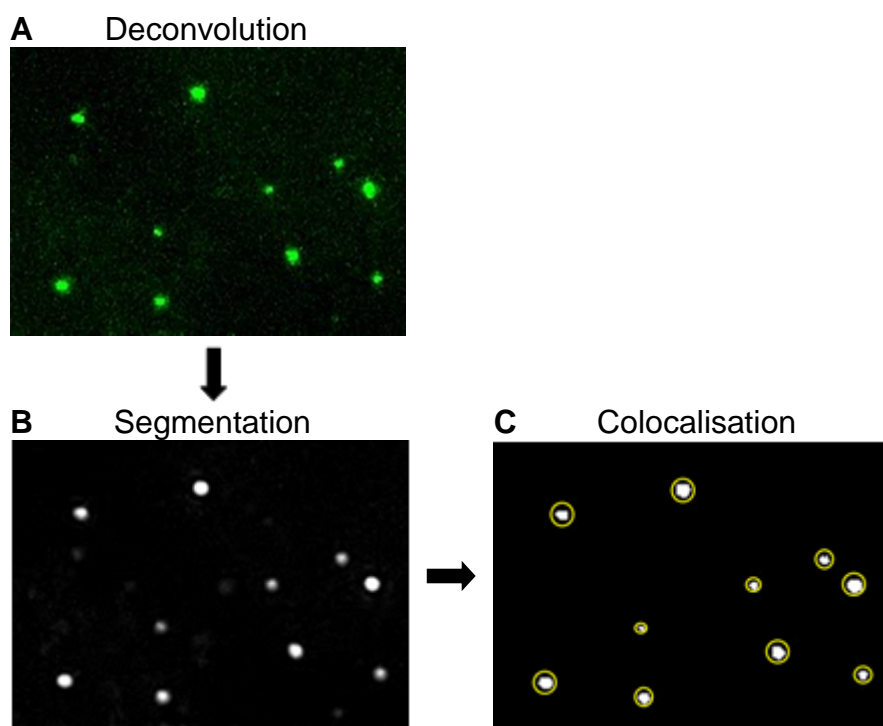


Figure 17. Deconvolution, segmentation, object counting and colocalisation of CA-mKO and IN-sfGFP. A pipeline was designed using Python scripting and ImageJ DeconvolutionLab open source software. (A) Confocal images were primarily deconvolved using an experimental PSF and the Tikhonov-Miller Algorithm. (B) Images were then segmented and the resultant objects counted using an empirically derived background threshold and the Image 3D Objects counter. (C) Colocalisation was established if two objects (CA-mKO and IN-sfGFP) from the two separate channels fell within five pixels' distance of the central pixel (centroid) of each object.

The images were deconvolved to increase the SNR, as a significant amount of noise was still detected in the mKO channel, despite increasing the frame and line averages in the image acquisition. It was reasoned that the background noise may lead to false spot identification in the semi-automated analysis pipeline. Deconvolution was performed using an experimental point spread function (PSF) and the Tikhonov-Miller Algorithm with a regularisation factor of 0.01 and 30 iterations (**Fig. 17A**). The deconvolved images were then segmented using a background threshold derived from the extreme planes of z-stacks, all pixels with an intensity above this threshold being considered as object's pixels, and the number of spots determined using the 3D Object counter plug-in (ImageJ) (**Fig. 17B and C**). Colocalisation was established if two objects (CA-mKO and IN-sfGFP) from the two separate channels fell within five pixels' distance of the central pixel (centroid) of each object. The sensitivity and accuracy of the system was verified by comparison with deconvolution through

Huygens Remote Manager (Scientific Volume Imaging B.V.) using an experimental PSF, and manual object counting and colocalisation using ROI Manager (ImageJ).

As there was a slight variation in the SNR between time courses, the optimal segmentation thresholds for both mKO and sfGFP needed to be re-evaluated within each data set (from 5 to 40 intensity graduations in an 8-bit image). Example segmentation threshold boxplots (from data set 7, DMSO control) can be seen in **Fig. 18**.

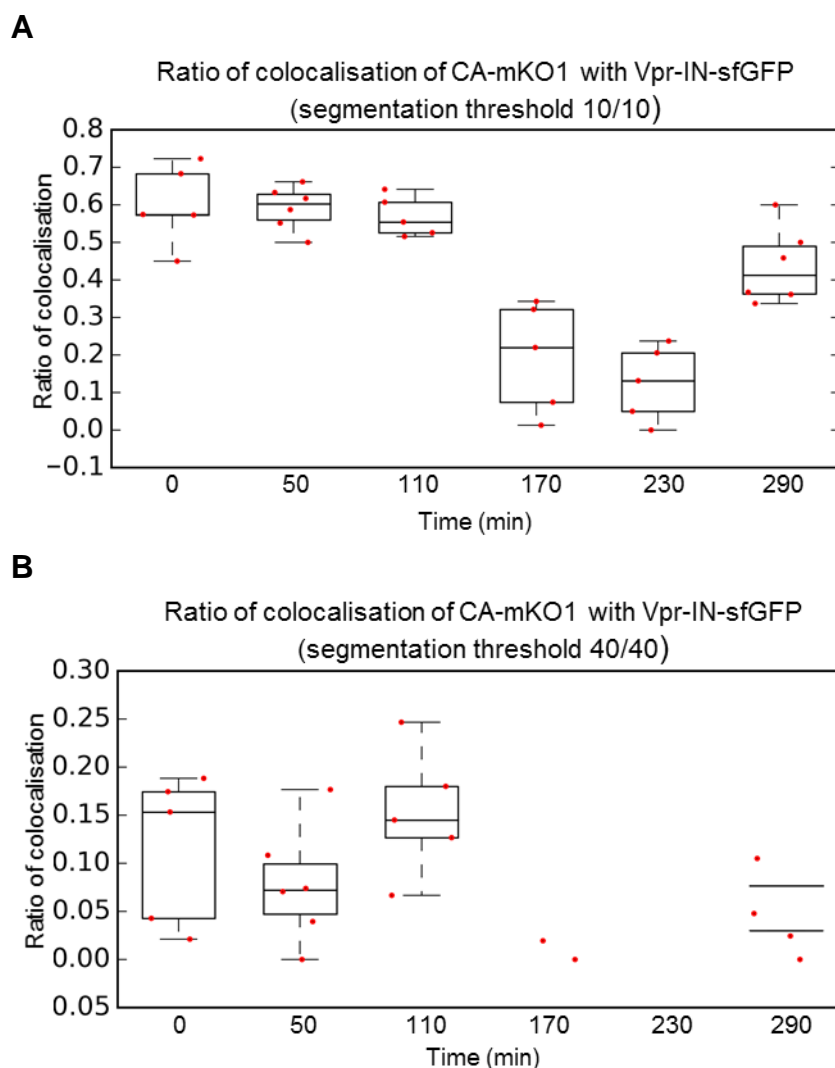


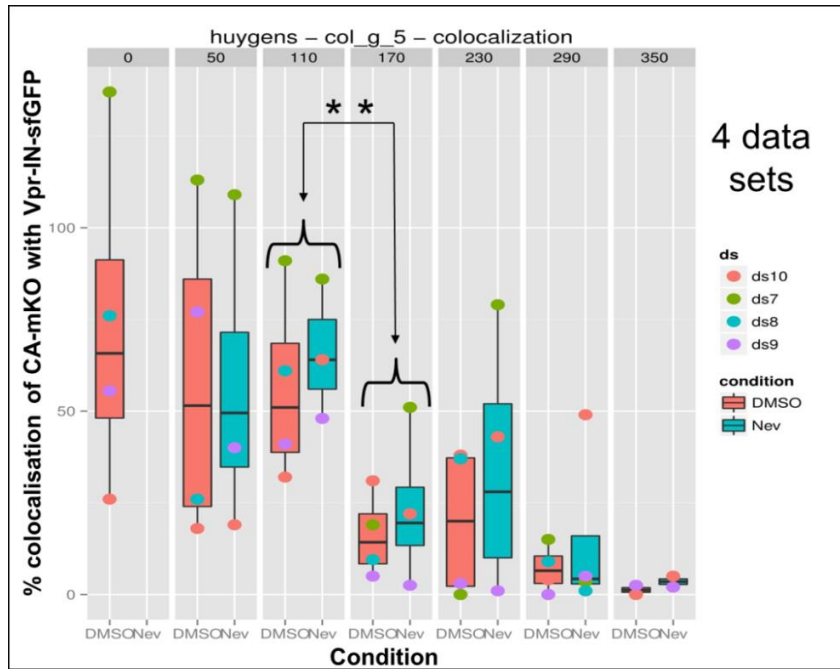
Figure 18. Segmentation thresholding of CA-mKO and IN-sfGFP. Example graphs (from dataset 7, DMSO control) showing the difference in the ratio of colocalisation between CA-mKO and IN-sfGFP, after processing with DeconvolutionLab, depending on the segmentation threshold employed. Segmentation thresholds for CA-mKO/IN-sfGFP of 10/10 (top) and 40/40 (bottom), led to median ratios of colocalisation at the 50 min time point of ~0.58 and ~0.07, respectively, and the loss of data points from 110 to 290 min in graph B.

A lower segmentation threshold (≤ 10 in both channels) led to more colocalised spots being detected over time (**Fig. 18A**), but increased the chance of false positives being detected. A higher segmentation threshold (≥ 40) reduced the number of false positives being detected due to background noise, but also diminished the detection of true signal leading to a loss of genuine positive spots recorded. This led to the loss of data points from 170 to 290 min in **Fig. 18B**. This added an element of operator bias to the system, but the optimal thresholds were typically ≤ 10 intensity graduations.

The time course was repeated, as described earlier, with HeLa P4 cells transduced with the dual-labelled virus pseudotyped with a HXB2 envelope. Nevirapine was used to validate the system because it had been shown to inhibit capsid uncoating in a previous study [67], and meant that the same viral preparation could be used in both the control and the challenge samples, to ensure that any effects observed were due to the action of the compound and not through differences in viral preparation. The images were acquired using confocal microscopy and then processed, and colocalisation between CA-mKO and IN-sfGFP determined using the DeconvolutionLab pipeline. Three readouts were produced: the absolute number of CA-mKO and IN-sfGFP colocalised spots over time (**Fig. 19A**), and the number of CA-mKO and IN-sfGFP spots colocalising over time divided by the total number of CA-mKO or IN-sfGFP spots, i.e. the ratio of colocalisation (**Fig. 19B**).

For the absolute number of CA-mKO and IN-sfGFP colocalised spots (**Fig. 19A**) a compilation of four datasets showed a significant drop in colocalisation (increased uncoating) 170 min post-trypsinisation ($P \leq 0.01$) with both nevirapine (blue) and the DMSO control (red). When assessing the ratio of colocalisation (number of colocalised spots divided by the total number of CA-mKO spots) (**Fig. 19B**), a similar increase in uncoating was observed between 110 and 170 min post-trypsinisation. However, a significant delay in uncoating was also determined in the presence of nevirapine from 170 to 230 min post-trypsinisation compared to the DMSO control.

A



B

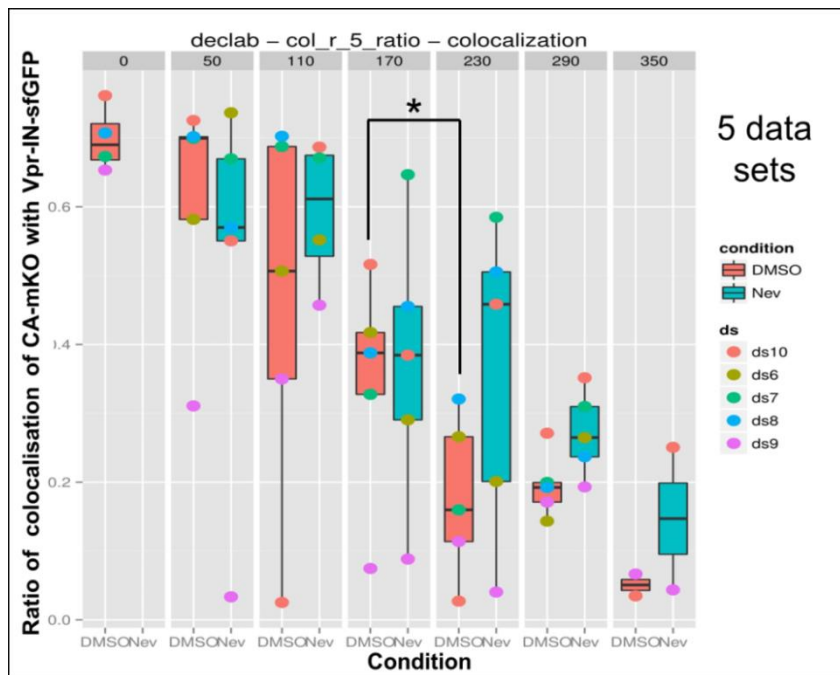


Figure 19. Effects of nevirapine on the uncoating kinetics of the dual-labelled virus over time. HeLa P4 cells were transduced with the dual-labelled virus \pm nevirapine [10 μ M] (blue) or DMSO control (red), and fixed at regular intervals post-spinoculation. Images were acquired using confocal microscopy and the fluorescent puncta counted, and colocalisation determined, using the DeconvolutionLab pipeline. (A) Boxplot showing the absolute number of colocalising spots over time (min) \pm nevirapine as a percentage of the total number of spots, with the IN-sfGFP (g) segmentation threshold set at 5. **SEM** of n = 4 datasets (ds). (B) Boxplot of the ratio of the CA-mKO spots colocalising with IN-sfGFP spots over time, with the CA-mKO (r) threshold set at 5. **SEM** of n = 5 datasets.

3.1.6 Colocalisation of capsid with integrase within the nucleus

Recent studies have reported the presence of immunostained capsid proteins colocalised with integrase-GFP within the nucleus of infected cells using super resolution microscopy [55][57]. To ascertain whether we could observe colocalised particles within the nucleus using CA-mKO, HeLa P4 cells were transduced with the dual-labelled virus pseudotyped with VSV-G and fixed at 4 to 6 hr post-spinoculation (p.s.) - the period when most PICs complexes are likely to be observed within the nucleus [125]. Nuclei were immunostained with anti-Lamin B polyclonal antibody. Z-stacks of the cells were acquired with a zoom 8 and a 0.1 μM z-plane, and the images deconvolved using Huygens Remote Manager.

Colocalised CA-mKO with IN-sfGFP puncta were observed within the nucleus of HeLa P4 cells at 6 h p.s. (**Fig. 20**), another indicator that the dual-labelled fluorescent virus was behaving like WT HIV-1 virus. The plot profile was generated along the y axis of the spot in this example, to reduce the offset which can be observed between the two channels (**Fig. 20B**). This offset may have been due to under-corrected extra-axial chromatic aberration due to the wavelengths converging at different positions along the focal plane. This offset could also have influenced the colocalisation analysis in the DeconvolutionLab pipeline. To avoid this, individual spots were detected by the local maxima of the fluorescence intensity, and colocalisation was determined if the centroid from the separate channels fell within 5 pixels distance from each other.

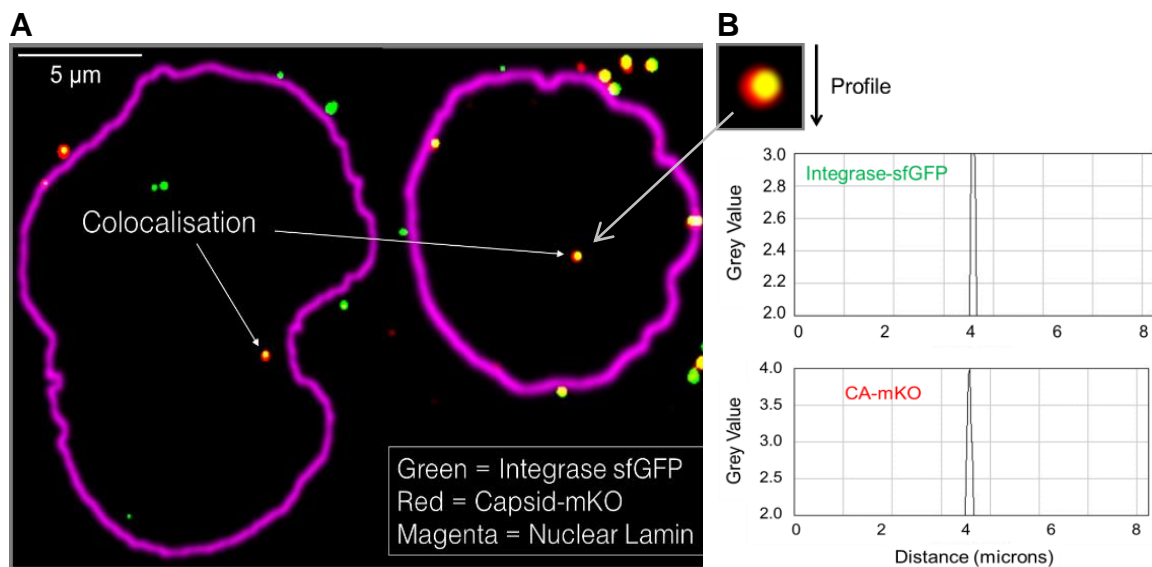


Figure 20. Colocalisation of CA-mKO with IN-sfGFP within the nucleus of HeLa P4 cells. (A) The dual-labelled virus was pseudotyped with VSV-G and used to transduce HeLa P4 cells through spinoculation. Cells were fixed 4-6 hr p.s. and immunostained with anti-Lamin B antibody. A Z-stack (0.1 μ M) of the nuclei was acquired and images deconvolved using Huygens Remote Manager and an experimentally derived PSF. Puncta containing both the CA-mKO and IN-sfGFP are marked with white arrows. (B) Plot profiles of the colocalising spot – CA-mKO (top), IN-24xST (bottom).

The CA-mKO and IN-sfGFP dual labelled virus behaved similarly to that of WT virus in regards to the decrease in colocalisation observed over time, responses to the various CA mutations and restriction compounds, and the detection of colocalised spots within the nucleus (**Fig. 14, 19 and 20**). However, even with the introduction of DeconvolutionLab analysis, the confocal acquisition of fixed cell time points was still a very labour intensive process. There was also a large disparity in the number of spots observed per cell, and colocalisation between biological repeats, as attested to by the large standard deviations between the data sets (**Fig. 19**). Part of this was likely due to variations inherent to recording uncoating events within distinct cell populations at different time points. But there were also concerns that fusing a fluorescent molecule on to the CTD of CA may affect the assembly of the capsid core [207][212][213].

3.2 SunTag capsid-tag (CA-SunTag)

Since there were concerns that fusing a 26.9 kDa fluorescent protein on to the CTD of capsid might be effecting the maturation and structure of the viral core, we tested the SunTag system (SUpErNova tagging) as an alternative method for labelling capsid proteins [193][70]. This method utilises single-chain variable fragment (scFv) antibodies fused to a fluorescent reporter (sfGFP), which can bind a short peptide inserted into the target protein (**section 1.10.2**). Because the antibody can be expressed in soluble form within cells, this system can be used for live particle tracking.

The cyclophilin-binding loop in the NTD of capsid was selected as a suitable site for the insertion of the 19 aa SunTag as it interacts with various host proteins during the early phase of infection and therefore would be accessible to the scFv-antibody [167]. There were also no reports in the literature of mutations at this site affecting capsid uncoating [70][214][215]. Using LOOPP protein folding recognition software (<http://cbsu.tc.cornell.edu/software/loopp/>), it was possible to predict the structural effects the insertion of this peptide within the loop would have on the capsid protein.

Two sites on the p24^{CA} binding loop were chosen for exchange with the GCN4 peptide: region 87 to 97 (11 aa) (CA Tag v2.1) (**Fig. 21**) and region 79 to 94 (16 aa) (CA Tag v1). The epitopes were cloned into both the pNL4-3 proviral vector and the Δ 8.91 packaging vector and viruses prepared incorporating increasing ratios of the CA-SunTag mutant compared to the original vector, to ascertain the effects of these mutants on viral infectivity (**Fig. 22A**). As the cyclophilin-binding loop is known to be important in the interaction with host proteins, we wanted a certain proportion of WT capsid monomers to be present within the core to allow for this association [154].

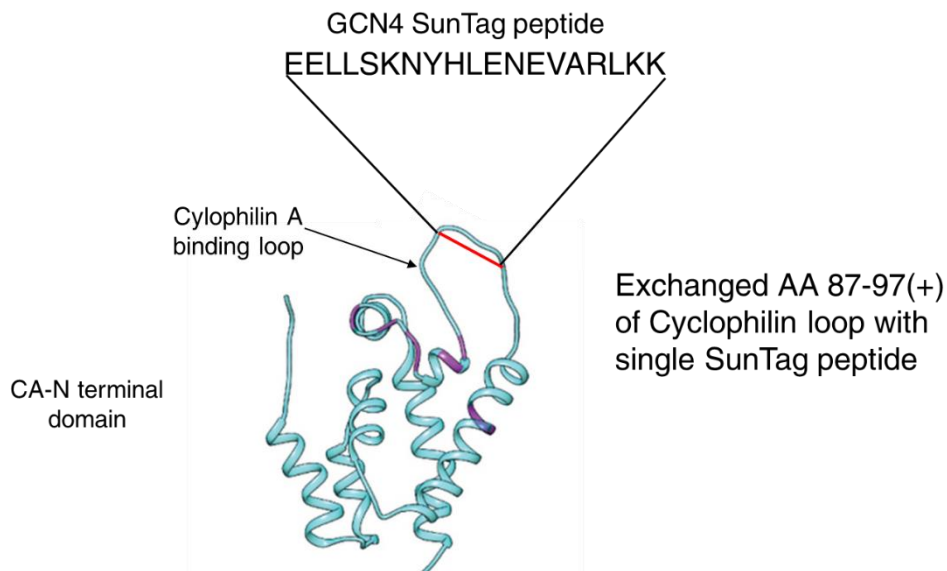


Figure 21. Schematic of the NTD of p24^{CA} showing the insertion site of the GCN4 peptide tag (v2.1) within the cyclophilin A binding loop. Adapted from a figure derived from Schur et al., 2015 [42].

For confocal imaging, viral vectors were produced in both standard 293T cells or those stably expressing the scFv-sfGFP fusion antibody, the latter to enable the antibody to bind to the capsid tag during viral assembly. Viruses were then transduced into HeLa P4 cells \pm the scFv-sfGFP fusion antibody and fixed at various time points prior to and after viral fusion. Cells were then stained for p24^{CA}.

The RTU for viruses prepared with increasing concentrations of Δ 8.91-CA-SunTag were similar to that of viruses containing Δ 8.91 alone, but a steady decrease in infectivity was observed (**Fig. 22A**). Initial experiments, transducing HeLa P4 cells stably producing the scFv-sfGFP antibody with the Δ 8.91-CA-SunTag v2.1 virus, revealed very few green spots within the cells, and of these fewer still colocalised when stained for p24^{CA}. More colocalised spots were observed with the transduction of 10 RTU of HXB2 enveloped virus (1/5 Δ 8.91-CA-SunTag v2.1 to 4/5 WT Δ 8.91) (**Fig. 22B**), but the concentration was considered too high for use in further experiments. As the infectivity with the incorporation of 1/5 Δ 8.91-CA-SunTag v2.1 was just under half that of the WT virus (**Fig. 22A**), we reasoned more spots should be visible with this system. We therefore tried producing the viruses in 293T cells stably expressing the scFv-

sfGFP, and also tested the CA-SunTag v1 mutant, inserted into regions 79 to 94 of the p24^{CA} cyclophilin binding loop. Many more green fluorescent puncta were observed in WT HeLa P4 cells transduced with CA-SunTag v1 when produced in scFv-sfGFP expressing 293T cells (**Fig. 22C**). A high proportion of these were also observed to colocalise with p24^{CA} stain, suggesting that the two antibody sites were not mutually exclusive. No green fluorescent puncta were observed in the HeLa P4 cells transduced with wild-type virus produced in scFv-sfGFP expressing 293T cells (**Fig. 22D**), suggesting the incorporation of the intrabody was epitope specific.

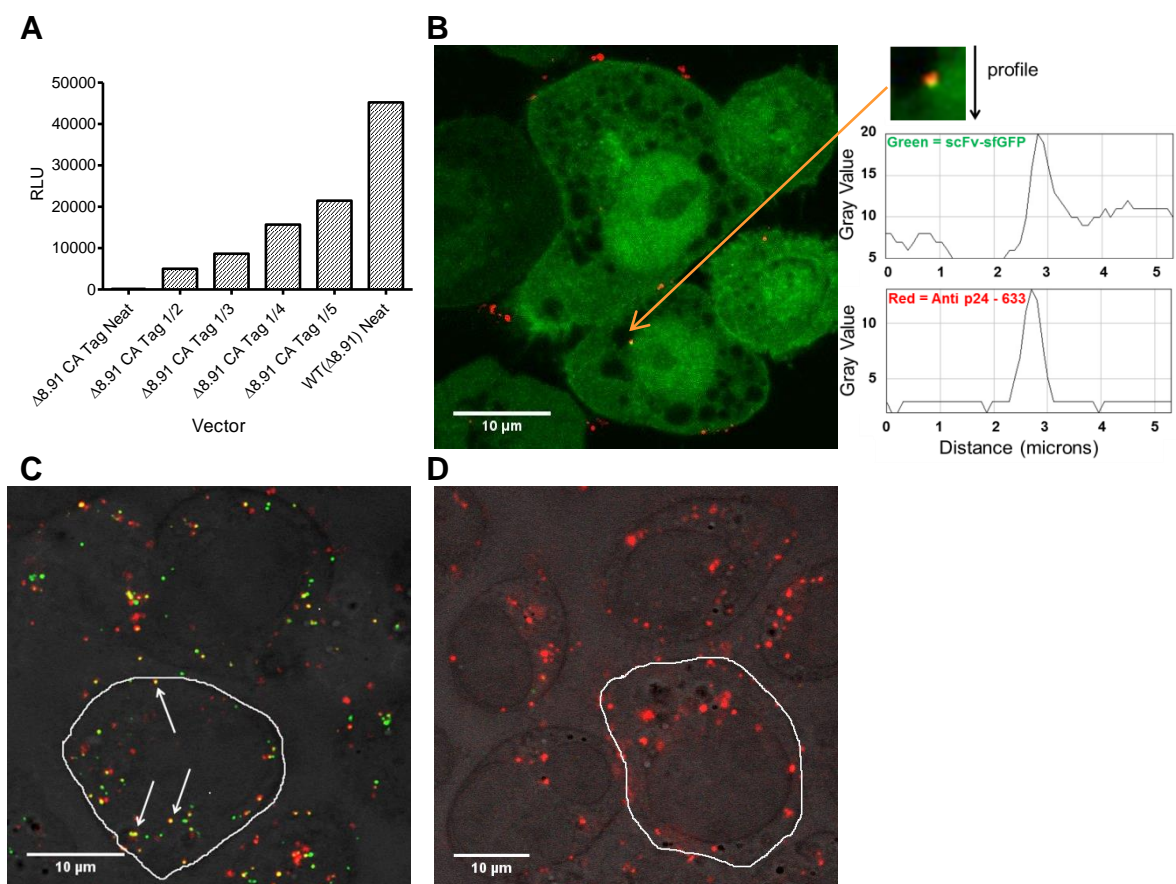


Figure 22. Infectivity and colocalisation of CA-SunTag v2.1. (A) Infectivity (RLU) of VSV-G pseudotyped virus with increasing ratios of the Δ8.91-CA-SunTag v2.1 vs. WT Δ8.91 packaging vector. (B) Colocalisation of Δ8.91-CA-SunTag v1 (green) (1/5 Δ8.91-CA-SunTag v2.1 + 4/5 WT Δ8.91) with p24^{CA} stain (red) in HeLa P4 cells stably expressing scFv-sfGFP [10 RTU]. A colocalised spot, along with the respective plot profiles, is shown. (C) Colocalisation of Δ8.91-CA-SunTag v1 (1/4 Δ8.91-CA-SunTag v1 + 3/4 WT Δ8.91) with p24^{CA} stain in WT HeLa P4 cells, with virus produced in 293T cells stably expressing scFv-sfGFP. (D) WT Δ8.91 with p24^{CA} stain (red) in WT HeLa P4 cells, with virus produced in 293T cells stably expressing scFv-sfGFP.

To test whether the incorporation of the CA-SunTag was influencing the maturation of the virus, a western blot was performed on HXB2 pseudotyped viral preparations containing decreasing ratios of pNL4-3-CA-SunTag v1 with respect to WT pNL4-3 (**Fig. 23**). Immunostaining for p24^{CA} revealed bands at ~55 kDa, ~48 kDa, ~41 kDa and ~24 kDa for the control virus (NL4-3 Full) representing all the products associated with normal HIV-1 cleavage. Smaller bands for MA-CA protein (41 ~kDa) in respect to CA (24 ~kDa) were observed in viruses containing ½ and ¼ CA-SunTag compared to the WT virus. For the virus containing full CA-SunTag, no bands were observed at 48 kDa or 41 kDa, and only a very small band was observed for p24^{CA}. This suggested that normal protease cleavage was not occurring in the presence of the CA-SunTag, and that the appropriate bands in the viruses prepared with ½ and ¼ CA-SunTag were probably derived from WT pNL4-3 that was incorporated with them.

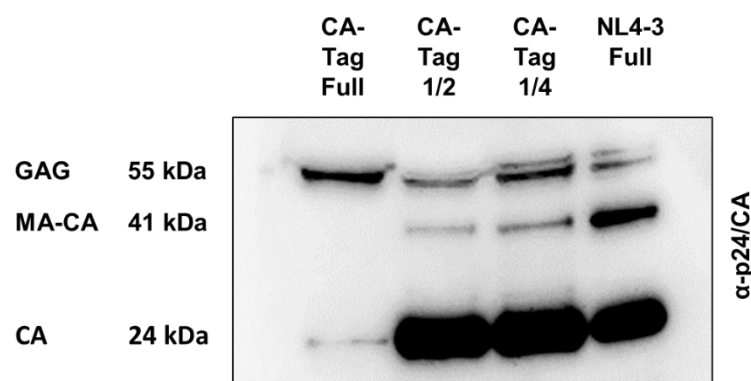


Figure 23. Western blot of virus containing decreasing ratios of pNL4-3-CA-SunTag v1. Viruses were prepared with decreasing ratios of pNL4-3-CA-SunTag v1 with respect to the pNL4-3 provirus and pseudotyped with HXB2 envelope. Viral supernatant was collected, pelleted and analysed using western blot and anti-p24^{CA} antibody.

3.3 Studying capsid uncoating with Vpr-IN-24xSunTag

Because we could not be sure whether the viruses produced when inserting the SunTag in the capsid were being correctly cleaved, we decided to try an alternative approach that would have less impact on viral maturation. Amplification of the signal derived from the scFv-sfGFP antibody could be achieved by joining repeat GCN4 peptide epitopes with a short flexible linker (GGSGG) [193]. Tests with up to 24 of these epitope arrays have been successfully implemented which, when bound by the scFv-sfGFP antibody, have produced enough signal amplification to enable live tracking of individual particles. We decided to test this system by fusing the repeat GCN4 peptide array onto the C-terminus of integrase. Instead of following individually labelled capsid particles detaching from a fluorescently labelled PIC, uncoating could be measured through the internalisation and binding of the cytoplasmic scFv-sfGFP antibodies onto the SunTag array upon disassembly of the capsid core.

The 24x SunTag (24xST) array was cloned onto the C-terminus of Vpr-IN (IN-24xST) and trans-incorporated IN-24xST viruses produced using the pNL4-3 transfer vector pseudotyped with VSV-G. The viruses were used to transduce HeLa P4 cells stably expressing the scFv-sfGFP fusion antibody, and the cells fixed and stained for p24^{CA} at regular intervals p.s. Confocal images of the cells revealed very few IN-24xST bound scFv-sfGFP spots at 0 min p.s. with both the trans-incorporated vector and the WT control, although the capsid stain revealed the presence of the virus on the surface of the cells (**Fig. 24A and C**). However, a high number of IN-24xST (green) spots were observed colocalised with the capsid stain (red) at 60 min p.s. with the trans-incorporated vector (**Fig. 24D**). Few green and no colocalised spots were observed with the WT control 60 min p.s (**Fig. 24B**). The green spots observed with the WT control were less localised and intense compared to the IN-24xST spots seen with the trans-incorporated vector, and were most likely due to aggregations of the scFv-sfGFP and autofluorescence. Fewer IN-24xST, capsid and colocalised spots were observed at 180 and 240 min p.s. (images not shown).

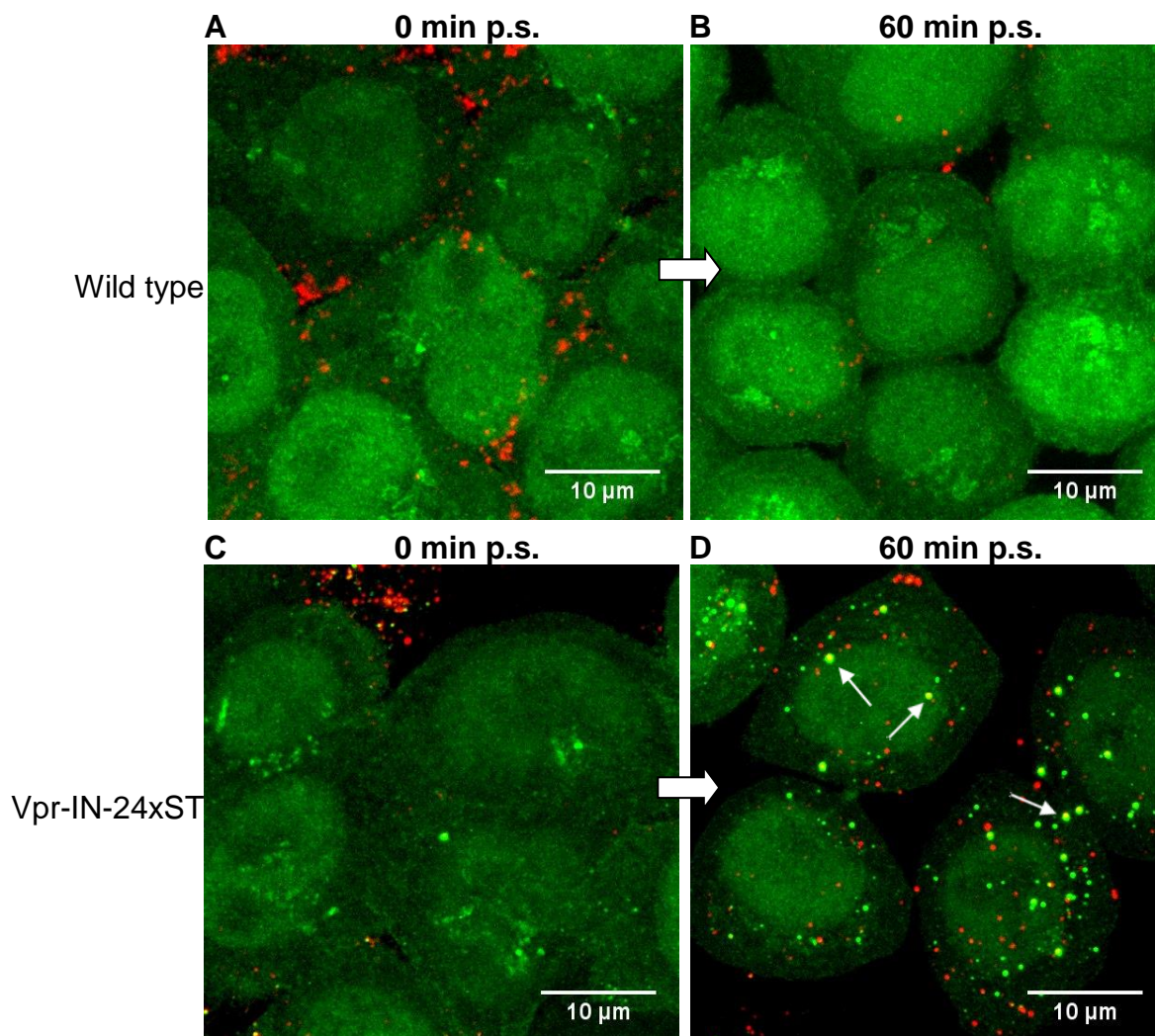


Figure 24. Vpr-IN-24xST construct vs. wild type control at 0 and 60 min post-spinoculation. HeLa P4 cells stably expressing scFv-sfGFP were transduced with VSV-G pseudotyped viruses containing the pNL4-3 proviral vector alone (WT control) or trans-incorporated with Vpr-IN-24xST, fixed at 0 and 60 min p.s., and immunostained with the anti-p24^{CA} antibody (red). (A and B) The capsid stain reveals plenty of viruses on the surface of the cells at 0 min p.s with the WT control, but few scFv-sfGFP spots (green) at 0 or 60 min p.s. (C and D) Few green spots at 0 min p.s., but many green, red and colocalised (white arrows) spots present 60 min p.s. with the IN-24xSunTag trans-incorporated virus.

To evaluate whether the appearance of green spots corresponded to capsid uncoating events, and whether the IN-24xST containing viruses were functioning like WT viruses, time courses were repeated +/- the addition of nevirapine (**Fig. 25**).

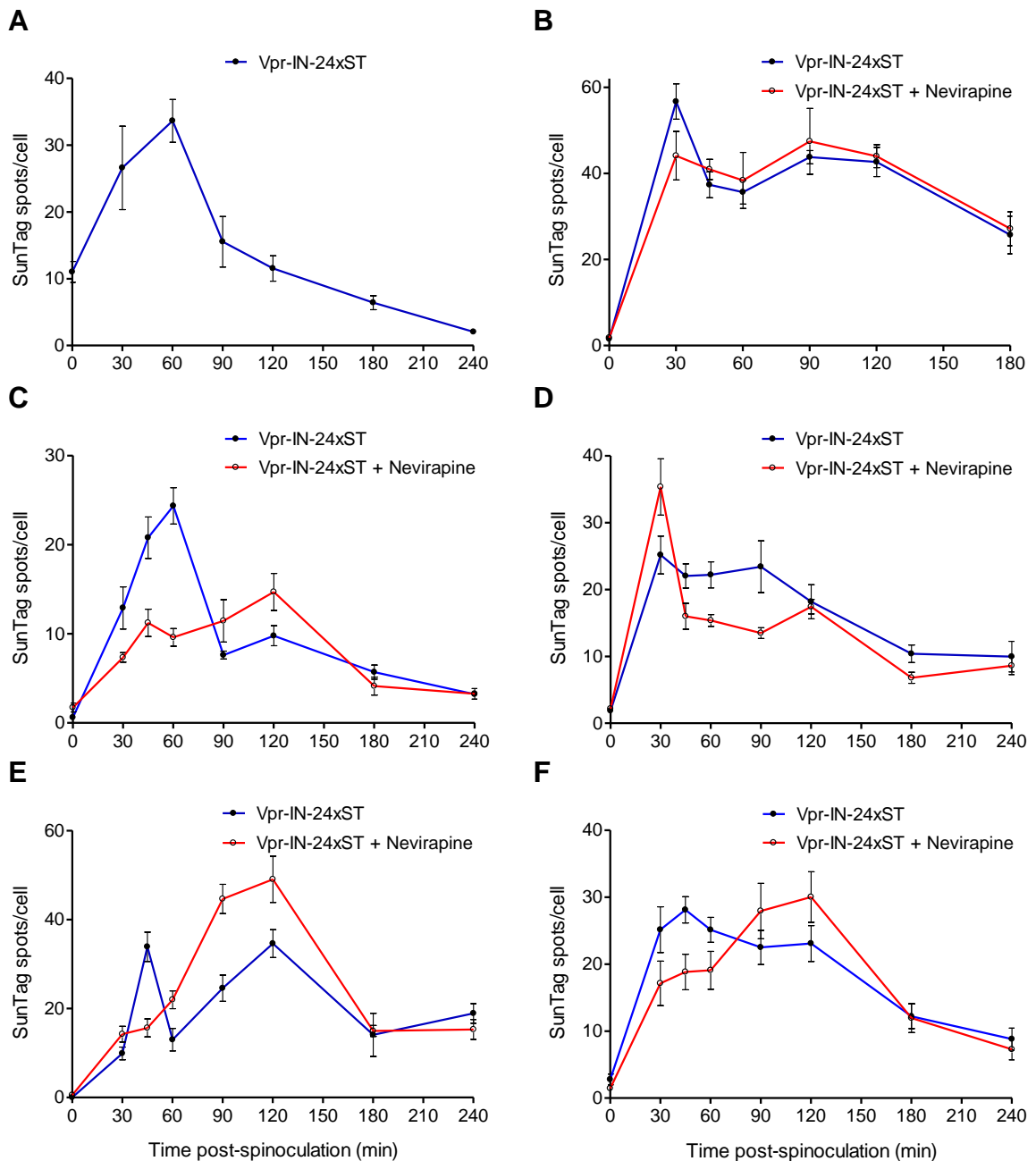


Figure 25. SunTag spots per cell over time. HeLa P4 cells stably expressing scFv-sfGFP were transduced with IN-24xST trans-incorporated viruses, fixed at regular intervals p.s., and images acquired using confocal microscopy. The number of green spots per time point was calculated using 3D Object Counter (ImageJ), threshold 6. (A-E) Graphs showing the number of spots per cell over time in individual experiments – SEM of 5 technical repeats. (F) Graph showing the number of spots per cell when graphs A-E are assembled (SEM).

In contrast to the dual-labelled system for measuring capsid uncoating (**sections 3.13 and 3.14**) which measured the loss of fluorescently labelled CA from fluorescently labelled integrase, the SunTag system measures uncoating by when the cytoplasmically expressed scFv-sfGFP antibody is able to enter the

disassembling capsid core to bind to the epitope peptide array. Thus, analysis was performed on the kinetics over time in the fluctuations of scFv-sfGFP bound SunTag arrays (green spots). Although CA staining may have provided a useful reference/normalisation point for the assay, due to the labour intensiveness in the acquisition of two-channel images (approximately 18 h per data set for acquisition of the dual-labelled viral uncoating in **section 3.14**), we dispensed with the capsid stain and focused on the appearance and loss of SunTag spots as indicators of uncoating. As the scFv-sfGFP can be expressed within cells, the eventual objective was to use this system in live cell imaging, which precludes the immunofluorescent staining of CA.

Few spots were observed in cells fixed directly after spinoculation (**Fig. 25A-E**), consistent with the virus initiating fusion with the target cell, and uncoating having not yet taken place. This was followed by a sharp increase in spots, with a peak number of spots per cell recorded from 30 to 60 minutes p.s. The addition of nevirapine delayed the peak in spots per cell recorded in two of the time courses, but a similar kinetic as the DMSO control was observed in two more experiments (**Fig. 25B-E**). When the graphs were compiled, however, a significant delay in the peak number of spots per cells was observed with the addition of nevirapine (120 min p.s) compared to the DMSO control (45 min p.s) (**Fig. 25F**).

3.3.1 24xSunTag analysis with Operetta High-Content Imaging

One of the drawbacks of measuring uncoating using confocal microscopy was the requirement to fix the samples, meaning that the images acquired between time points were of different cell populations. To track the viral particles within the same cells throughout the time course, a series of experiments was performed using the Operetta High-Content Imaging System. Viruses were prepared using pNL4-3 pseudotyped with VSV-G envelope. HeLa P4 clone cells stably expressing scFv-sfGFP were seeded into 96-well cell carrier plates, and transduced with IN-24xST trans-incorporated viruses. Viral supernatant was replaced with warm fluorobrite media directly after spinoculation and the plate was transferred to the Operetta for image acquisition. Images were acquired at 5-15 minute intervals using the 40x objective, Xenon laser and the standard Alexa 488 filter set.

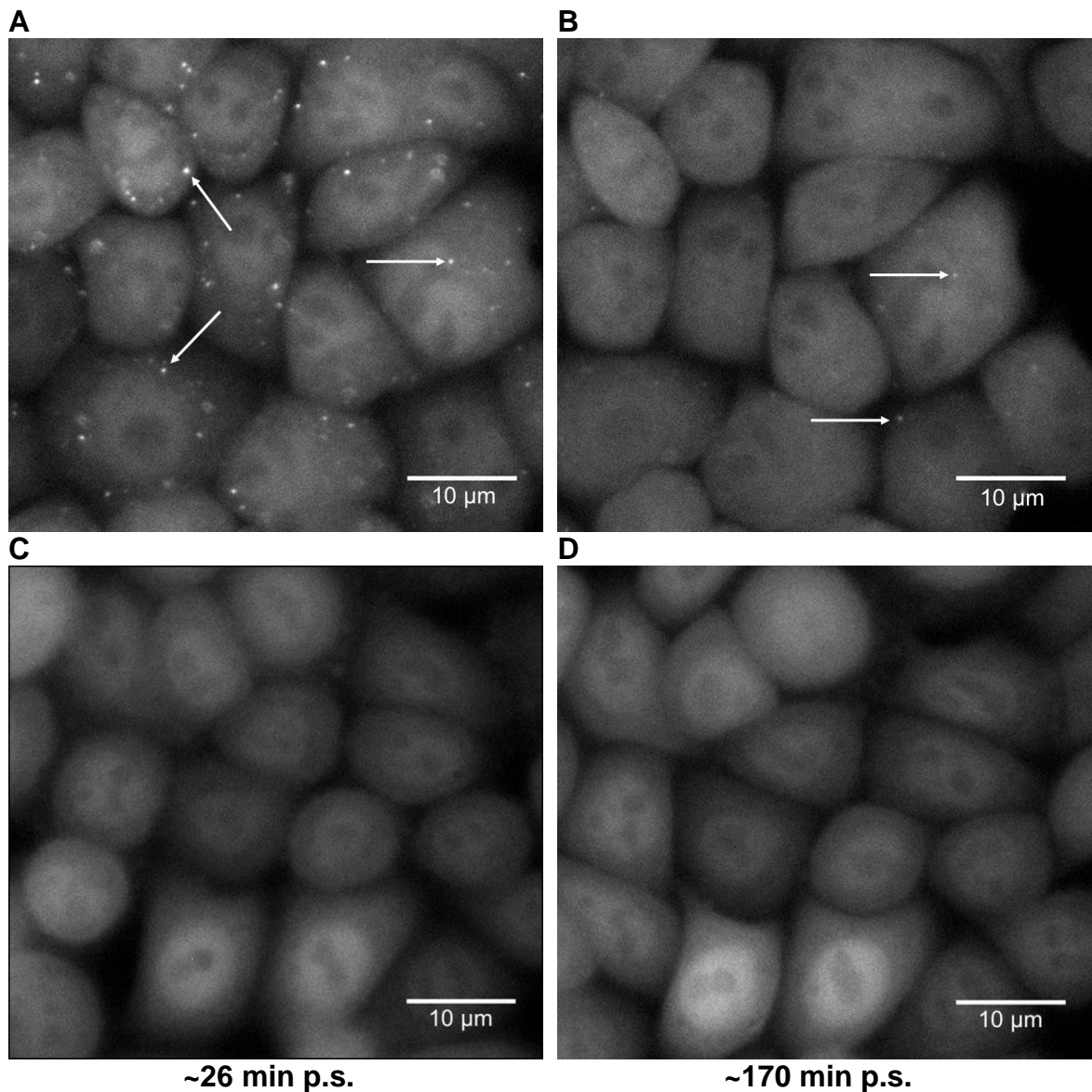


Figure 26. Detection of IN-24xST labelled viruses in HeLa P4 cells using the Operetta high-content imaging system. HeLa P4 cells stably expressing the scFv-sfGFP intrabody were transduced with ~0.6 RTU of IN-24xST labelled virus (A and B) or NL4.3 + VSV-G CTRL virus (C and D) and imaged at regular intervals p.s. Arrows indicate examples of IN-24xST spots. (A) Many spots were observed in cells transduced with the IN-24xST labelled virus at ~26 min p.s., far fewer spots were observed ~170 min p.s. (B). Little to no spots observed in the NL4-3 + VSV-G CTRL (C and D).

Fluorescent puncta were clearly evident within the cytoplasm of infected cells 25 min p.s. (**Fig. 26A**), indicating successful fusion and uncoating of the IN-24xST trans-incorporated virus. Fewer spots were observed 170 min p.s. suggesting most of the viruses had uncoated (**Fig. 26B**). A 24xST signal profile in relation to background levels of scFv-sfGFP over time, indicated that bleaching of the signal was not occurring (**Fig. S2**).

Repeat time courses were conducted comparing the original IN-24xST virus along with viruses containing CA mutations making the capsid core less stable (K203A) and more stable (E45A and E128A/R132A) compared to WT CA, a virus containing a mutation in the active site of RT (D110E), and the addition of the inhibitory compounds nevirapine, ebselen and PF74. After live acquisition the cells and fluorescent puncta were segmented and analysed using the Harmony High-Content Imaging and Analysis Software (**section 2.9.1**). Transduction with a VSV-G pseudotyped pNL4-3 virus without IN-24xST provided a negative control from which we could optimise the spot segmentation, removing the pseudo-spots derived from autofluorescence.

As with confocal imaging, few fluorescent puncta were observed in the initial time point, from 4-10 min p.s., however, a consistent peak in the number of spots per cell was detected from 20 to 30 min p.s. (**Fig. 27A and B**). This is in concordance with the reports on the 50% capsid uncoating time recorded with VSV-G pseudotyped viruses [127][67]. A sharp drop in the number of spots per cell was observed thereafter, which levelled off at approximately 60 to 80 min p.s. to a population just above that of the WT control.

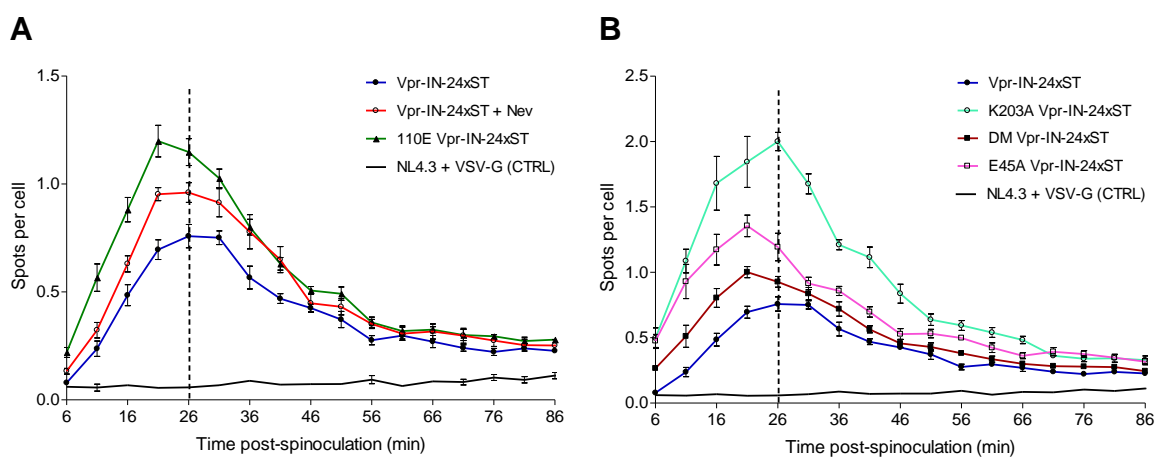


Figure 27. Number of SunTag spots per cell time post-spinoculation. HeLa P4 cells stably expressing the scFv-sfGFP intrabody were transduced with ~0.15 RTU IN-24xST labelled virus preparations and imaged at 5 min intervals p.s. (A) \pm capsid restriction compounds and a RT mutant. (B) CA mutations. Error bars indicate the SEM of 6 technical and 2 biological repeats.

Similar kinetics were observed with all the viruses \pm the CA mutations or restriction compounds, with a sharp peak in the number of spots per cell from 21-26 min p.s., followed by a sharp decline, levelling off to a point just above that of

the WT control at the end of the time course (**Fig. 27A and B**). The latter, suggesting that uncoating was occurring right up until the end of the time course. No significant difference was observed for the time point with the peak number of spots per cell between the IN-24xST trans-incorporated virus \pm nevirapine or the RT mutant (**Fig. 27A**), or with the addition of ebselen and PF74 (**Fig. 28A**). Viruses containing CA mutations also failed to elicit any significant difference in peak uncoating (**Fig. 27B**).

To establish whether the fluorescent puncta observed were fluorescently labelled virus particles and not VSV-G enveloped vesicles [124], IN-24xST particles pseudotyped with VSV-G were prepared without the pNL4-3 provirus. Trans-incorporated viruses were also prepared with the HXB2 envelope as earlier experiments had shown that these viruses only enter cells expressing the CD4 receptor (**Fig. 12**). As expected, background levels of fluorescence similar to that of the WT control (minus IN-24xST) were observed with the particles prepared with IN-24xST but without the viral genome (**Fig. 28A**). Fewer puncta were detected with viruses prepared with HXB2 envelope compared to VSV-G pseudotyped viruses (**Fig. 28B**), with approximately 1 spot for every 3 cells, but this is in accordance with the reports of lower fusion efficiency with the WT envelope [216]. However, the peak in the number of SunTag spots per cell occurred within the same time frame as that recorded with VSV-G pseudotyped particles (22 min p.s.), which is in contrast to that observed by Hulme and co-workers [67], who reported a delay in fusion of 23 min with WT envelope. Apart from the more pronounced peak seen with the VSV-G pseudotyped virus, the overall kinetics were similar, with a levelling off after 60 min of around 1 spot for every 4 cells with HXB2 enveloped viruses, and 1 spot every 2-3 cells with VSV-G. Background levels of fluorescence were observed with viruses prepared without an envelope (**Fig. 28B**).

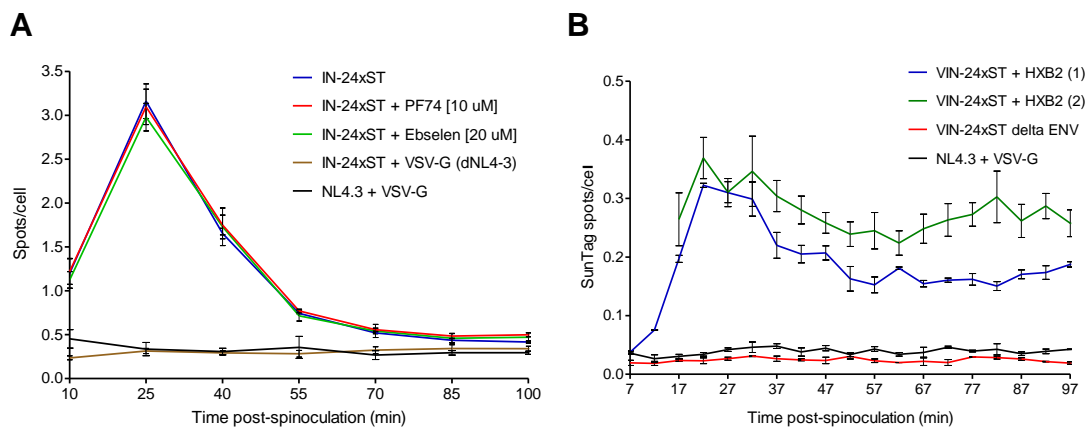


Figure 28. Number of SunTag spots per cell time post-spinoculation with addition of HIV-1 restriction compounds, ± the HXB2 envelope and viruses prepared without the NL4-3 provirus. HeLa P4 cells stably expressing the scFv-sfGFP intrabody were transduced with ~0.15 RTU IN-24xST labelled virus preparations. (A) Number of IN-24xST spots per cell over time ± the restriction compounds PF74 and ebselen, and a vector prepared without the NL4-3 provirus. (B) Number of SunTag spots per cell with vectors prepared ± HXB2 envelope. Error bars indicate the SEM of 3 technical repeats.

A number of experiments were conducted to try to generate a change in the time when the peak number of spots per cell were observed to verify if we were actually tracking uncoating events. Trans-incorporated viruses were produced in the presence of saquinavir, a protease inhibitor, to restrict the development of a mature capsid core; without a functional capsid core we expected scFv-sfGFP SunTag bound spots to be seen immediately upon fusion. A scFv-sfGFP expression clone was also developed using the TZM-bl cell line stably expressing the TRIM-CypA fusion protein, which is reported to bind to intact capsid cores triggering premature uncoating events [209]. Neither of these tests, however, significantly altered the time at which the peak number of spots per cell was observed (**Fig. S3**).

3.4 Studying uncoating with APOBEC3-24xSunTag

As it was difficult to establish whether the spots observed with Vpr-integrase trans-incorporation of the SunTag were derived from uncoating events of real infective viruses, we decided to test an alternative method for the insertion of the repeat peptide epitope array into the viral capsid core. Burdick and co-workers managed to track HIV-1 PICs by the fusion of a yellow fluorescent protein on to

the C-terminus of the APOBEC human cytidine deaminases APOBEC3F (A3F) and APOBEC3G (A3G) (**section 1.10.1**) [124]. The A3F/G proteins are thought to be encapsulated within HIV-1 viral cores through interaction with viral RNA and the nucleocapsid domain of the Gag protein [217][195][218]. Although the proteins actively restrict Vif-deficient HIV-1 replication [219][220], as uncoating occurs in the early phase of infection we reasoned the viral ribonucleoprotein targeting properties of A3F/G would provide a suitable alternative method for the incorporation the 24xSunTag array into the capsid core.

The 24xSunTag peptide array was fused to the C-terminus of A3F and an A3G E259Q mutant (A3G*) reported to reduce the HIV-1 restriction properties of this protein [124]. These vectors were used in the production of viruses, along with the Vif negative pHR-SIN-Luc molecular clone [221], the Δ 8.91 packaging vector and VSV-G envelope. The viruses were used to infect HeLa P4 scFv-sfGFP stable clone cells in 96-well tissue culture plates and analysed using Operetta high-content imaging (**Fig. 29**).

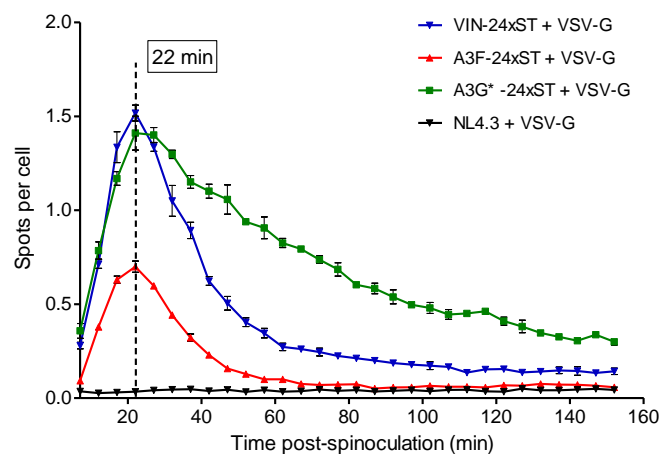


Figure 29. Number of SunTag spots per cell time post-spinoculation with APOBEC3F/G* trans-incorporated viruses. HeLa P4 cells stably expressing the scFv-sfGFP intrabody were transduced with ~0.15 RTU APOBEC3F/G*-24xST labelled virus preparations and imaged at 5 min intervals p.s. Error bars indicate the SEM of 3 technical repeats.

As with the Vpr-IN-24xST system, few spots were observed in the initial time points p.s., but a sharp increase in spots per cell were seen hereafter, with a peak in the number of spots recorded 22 min p.s. This was in the range of the peak in spots per cell recorded with Vpr incorporation of the 24xST (20 to 30

min), and also other reports on the 50% uncoating time of VSV-G pseudotyped viruses [67][127]. In contrast to the Vpr incorporated SunTag, a slower reduction in spots per cells was observed with the A3G*-24xST trans-incorporated virus.

3.5 Operetta High-Content Imaging using a 60x objective

In the above experiments (**section 3.3 and 3.4**) the images were acquired using a 40x objective, and it was suspected that the lower resolution compared to confocal acquisition using the 63x objective, meant that some of the subtler aspects of uncoating were being lost. This may have contributed to the consistent peak of spots per cell observed in the presence of restriction compounds and CA mutants. Thus, analysis of the Vpr-IN/A3F-24xST vectors was repeated with the Operetta high-content imaging system using a 60x objective (**Fig. 30**). Repeat experiments in the presence of nevirapine or the DMSO control showed a significant delay in the reduction of the number of spots detected per cell, after the initial peak, in the presence of nevirapine (**Fig. 30A, B and C**). This levelled off to a point just above that of the DMSO control, suggesting that in the presence of nevirapine spots were being detected, or uncoating was occurring, at a higher rate than with the DMSO control, right up to the end of the time course. A less stable CA mutant (K203A) was also analysed alongside the non-mutated IN-24xST vector, and a significantly premature peak in uncoating (15 min as opposed to 23 min p.s.) was observed with the less stable capsid core (**Fig. 30D**).

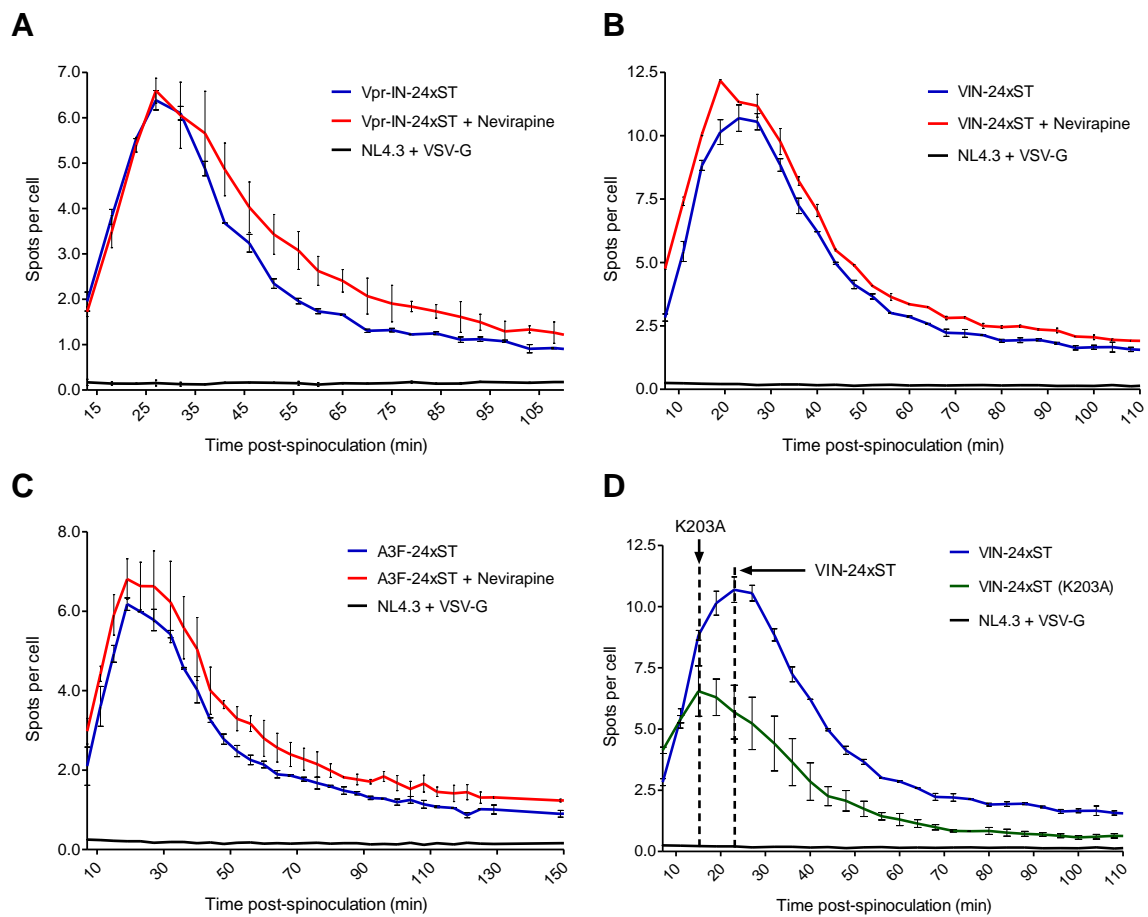


Figure 30. Number of SunTag spots per cell time post-spinoculation with Operetta High-Content Imaging using a 60x objective. HeLa P4 cells stably expressing the scFv-sfGFP intrabody were transduced with ~1 RTU Vpr-IN/A3F-24xST labelled virus preparations and uncoating analysed using a 60x objective. (A and B) Number of IN-24xST spots per cell over time \pm nevirapine. (C) Number of A3F-24xST spots per cell over time \pm nevirapine. (D) Number of Vpr-IN-24xST compared to a virus prepared with a less stable (K203A) capsid core. SEM of 3 technical repeats.

3.6 NanoBiT luciferase analysis of HIV-1 uncoating

As there was little significant difference in the timing for the peak number of spots per cell observed with the two 24xSunTag array capsid uncoating systems, we decided to try an alternative strategy for studying uncoating. One of the perceived drawbacks to the 24xST repeat epitope was the size of the non-bound ~63 kDa SunTag array, and what effect this would have on the assembly of the capsid core. NanoLuc Binary Technology (NanoBiT) is a two-subunit system used for intracellular detection of protein:protein interactions using an engineered luciferase (**section 1.10.3**) [222][200]. Luminescence is achieved upon binding of the 1.3 kDa peptide (HiBiT) with the 18 kDa polypeptide (LgBiT), in the presence of substrate. The small size (19 kDa) and stability of the enzyme made it an attractive option to use as an alternative to the SunTag.

The 11 aa HiBiT peptide was cloned on to the c-terminus of the A3F/G* proteins, and the LgBiT peptide inserted into a pAIB provirus and used in the production of HeLa P4 cells stably expressing the LgBiT. Because of the small size of the HiBiT we also decided to insert it onto the C-terminus of integrase in the pNL4-3 proviral vector, as similar sized peptides had previously been inserted here without affecting the infectivity of the virus [204]. The fusion of the HiBiT to a proviral vector would prevent the formation of labelled VSV-G pseudotyped vesicles which may have been present in the previous systems. Viruses were prepared using the pHR-SIN-GFP molecular clone and the Δ 8.91 packaging vector for the A3F/G* trans-incorporated HiBiT or with pNL4-3-HiBiT proviral vector alone, and pseudotyped with VSV-G or HXB2 envelope. HeLa P4 cells expressing the LgBiT were seeded into 96-well tissue culture plates and transduced using spinoculation. Viruses prepared without the HiBiT and transfection with the HiBiT containing plasmids were used as negative and positive controls, respectively. Nano-Glo Live Cell reagent was added immediately after spinoculation and the cells analysed using a TECAN Infinite M200 microplate reader for 150 min at 5 min intervals (**Fig. 30**).

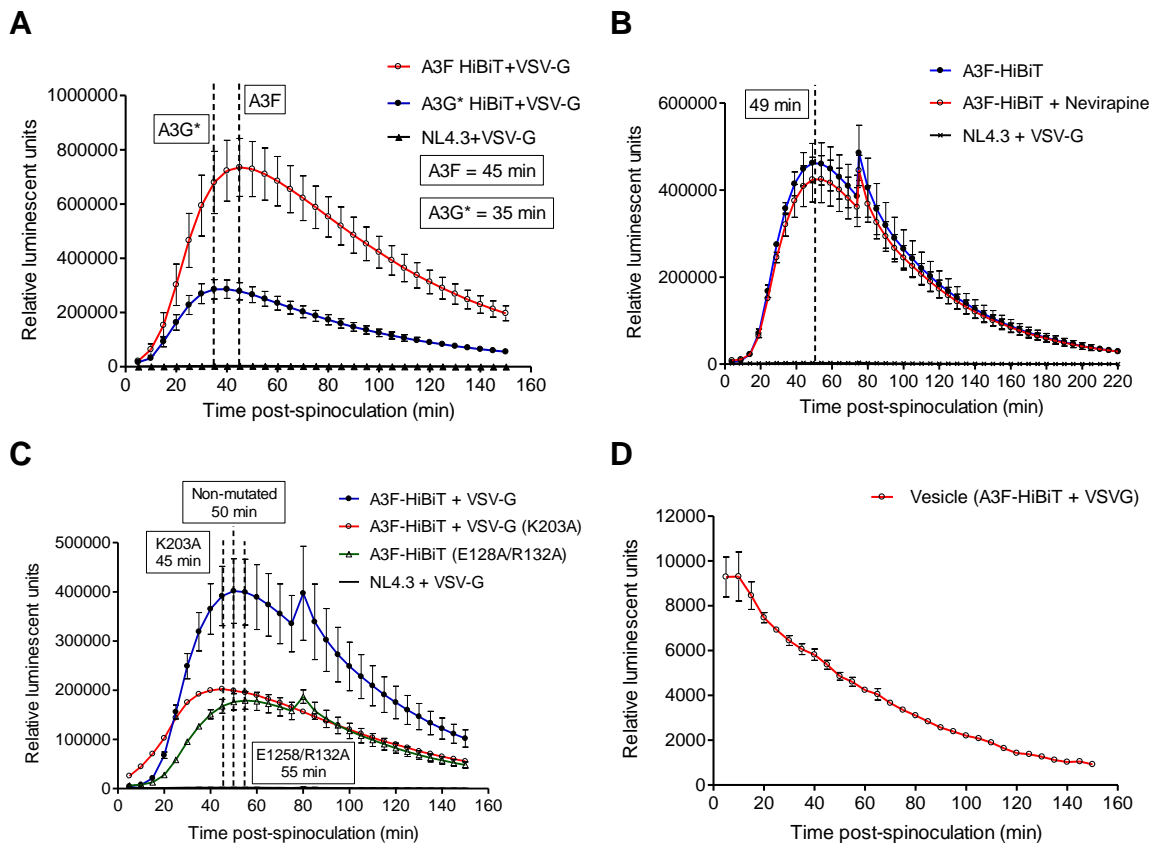


Figure 31. Relative luminescent units (RLU) time post-spinoculation for APOBEC3F/G*-HiBiT trans-incorporated viruses. HeLa P4 cells expressing the Large Bit (LgBiT) enzyme fragment were transduced with 1.2 RTU VSV-G pseudotyped A3F/G*-HiBiT labelled virus preparations and the plates analysed at 5 min intervals p.s. with the TECAN Infinite M200 microplate reader. (A) A3F/G*-HiBiT (n = 3 biological repeats). (B) A3F-HiBiT virus \pm nevirapine [10 μ M (n = 3 technical repeats)]. (C) A3F-HiBiT alongside a less stable (K203A) or more stable (E128A/R132A) capsid mutant (n = 3 technical repeats). (D) A vector prepared without the viral genome (2 biological repeats). Error bars show the SEM.

A pronounced peak in RLU was observed with both the A3G* and A3F-HiBiT viruses at 35 min and 45 min p.s., respectively, with a slower decline in RLU after this point (**Fig. 31A**). RLU double of that for the A3G*-HiBiT virus were recorded with the A3F-HiBiT trans-incorporated virus. The addition of nevirapine to the samples failed to change the kinetics of the curve with the A3F-HiBiT (**Fig. 31B**). CA mutations in the Δ 8.91 packaging vector which destabilised (K203A) and stabilised (E128A/R132A) the viral core, showed an earlier and delayed peak in RLU, respectively, compared to the non-mutated virus (**Fig. 31C**). A 50% decrease in RLU was also recorded with the CA mutants. The sharp peak in RLU at ~80 min p.s. was a result of an extra orbital shake upon the addition of fresh Nano-Glo substrate in one of the wells (**Fig. S4**). Vectors prepared lacking the

viral genome (VLPs) exhibited different RLU kinetics compared to true viruses (**Fig. 31D**), suggesting that the initial increase in RLU observed with normal viral vectors (**Fig. 31A, B and C**) was a result of capsid uncoating rather than VLP fusion events.

Preliminary studies using the HiBiT moiety cloned onto the C-terminus of integrase in NL4-3 showed a similar peak in RLU to the A3F/G*-HiBiT, at around 37 min p.s. (**Fig. 32**). This suggested that the peak in luciferase was a result of capsid uncoating, and not through fusion with VSV-G pseudotyped vesicles. A shift in the kinetics of the peaks in the presence of capsid restriction compounds was also observed. A delay of ~10 min was observed in the presence of PF74 compared to the DMSO control with both the WT (HXB2) envelope and the VSV-G pseudotyped viruses (**Fig. 32A and B**). A premature peak in RLU (~10 min) was observed in the presence of ebselen compared to the DMSO control, with the VSV-G pseudotyped virus (**Fig. 32B**). The addition of nevirapine had little effect on the peak in the RLU, with only a ~5 min delay compared to the DMSO control in viruses prepared with the WT envelope (**Fig. 32A**).

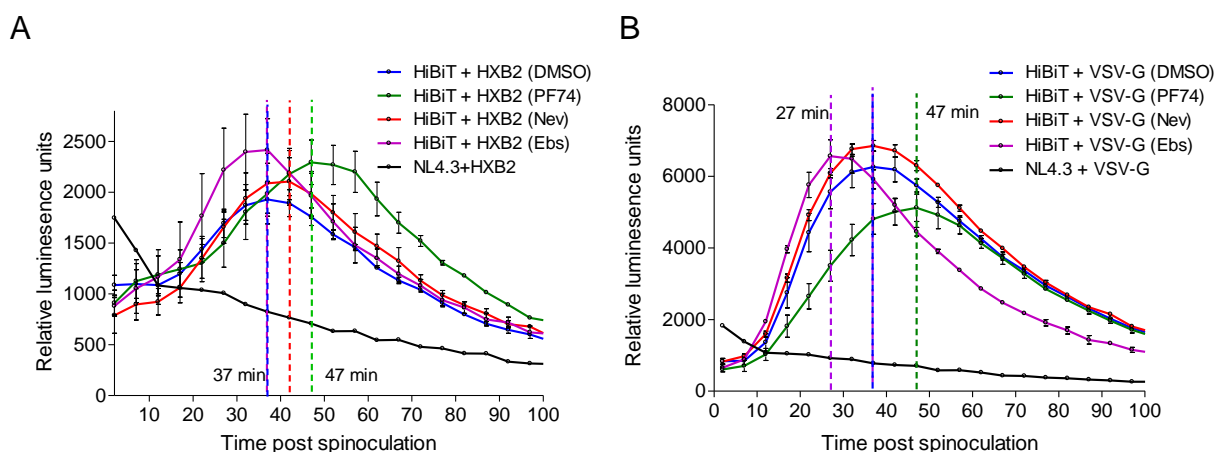


Figure 32. Relative luminescent units (RLU) time post-spinoculation for pNL4-3.Luc.R-E-HiBiT trans-incorporated viruses. HeLa P4 cells expressing the Large Bit (LgBiT) enzyme fragment were transduced with HXB2 (WT) enveloped [8 RTU] or VSV-G pseudotyped [3 RTU] NL4-3-HiBiT labelled viruses, in the presence of the restriction compounds nevirapine, ebselen, PF74 or the DMSO control. The cells were analysed at 5 min intervals p.s. with the TECAN Infinite M200 microplate reader. (A) NL4-3-HiBiT + HXB2 (WT) envelope. (B) NL4-3-HiBiT + VSV-G. SEM of n = 3 technical repeats.

DISCUSSION

The early phase of HIV-1 infection has been intensively studied over the past 35 years, and it is becoming increasingly clear that the viral capsid (the individual proteins and the assembled fullerene core) plays a fundamental role in productive infection [44][160][85][94]. Initially, the viral core was thought to be solely a vessel for the containment and effective transport of the viral ribonucleoprotein into the target cell [15]. However, investigations into HIV-1 trafficking pathways and integration site preferences using wholesale genomic knockdown studies and CA mutations [54][56][58][65][88][89][91][103], emphasise the intrinsic role of CA in multiple steps leading up to incorporation with the host genome. These insights must have an impact on the historical interpretation of uncoating as solely the process by which the capsid core dissociates from the RTC [44][223]. Thus, the process of uncoating should be understood in the wider context of the large number of host factors with which CA interacts during cytoplasmic trafficking and nuclear import of the viral genome.

The principal aim of this project was to devise a system with which to study the process of uncoating within the spatial and temporal context of the cell, to help clarify some of the questions regarding where, when and how the capsid disassembles after productive cellular fusion. For this purpose we developed three uncoating assays, with each one encompassing different properties which in combination would give a more comprehensive picture of *in situ* CA disassembly: 1) a dual-labelled virus, in which uncoating could be measured by the separation of fluorescent labels fused to the CTD of both CA and IN; 2) capsid incorporation of a repeat peptide array (SunTag), which facilitates signal detection through attachment of cytoplasmically expressed, fluorescently labelled antibodies after breaching of the capsid core; and 3) capsid incorporation of a small peptide from a split luciferase system, which generates luminescence upon fusion with the cytoplasmically expressed polypeptide moiety (in the presence of substrate). By approaching capsid uncoating using different techniques it was possible to get a more holistic understanding of this process, which can otherwise lead to a biased interpretation when using individual systems of

analysis. A table summarising the advantages/disadvantages of each system can be seen at the end of the discussion (**Table 2**).

4.1 A dual-fluorescent system for studying uncoating

The labelling of proteins with fluorescent probes is a well-established method for studying intracellular events using high resolution microscopy [187]. This has enabled the direct visualisation of interactions between HIV-1 and cellular proteins, providing a wealth of information regarding the physical location and temporal aspects of these exchanges. Although *in vivo* analysis of HIV-1 infection had been performed through the fluorescent labelling of other regions of the Gag gene [187], this was the first study whereby a fluorophore was fused directly to the CTD of CA. The capsid core is notorious for its sensitivity to CA mutations, with even point mutations effecting the stability and consequently the infectivity of the virus [65][112]. It has also been reported that the peptides/proteins, and the correct cleavage events of the Gag polyprotein, downstream from CA can have a direct effect on the proper assembly and functioning of the capsid core [207][212][213]. The production of viable capsid cores containing CA monomers with fluorophores fused to the CTD of the protein was made possible by the ability of the Gag protein to multimerise (primarily through interactions with the CTD of CA) at the cellular membrane before viral assembly and budding [36][224]. Thus, through the co-transfection of a vector containing the gene for a full Gag polyprotein (pNL4-3) and the vector containing a fluorophore fused to the CTD of CA, it was possible to produce infectious virions with correctly assembled, fluorescently labelled, capsid core. A system for tracking the RTC/PIC up to and including nuclear entry had already been developed by Albanese and co-workers, through the fusion of a fluorophore on to the CTD of IN [125]. This, in turn, was fused to HIV-1 Vpr, with the inclusion of a proteolytic cleavage site, which enabled the efficient trans-incorporation of the fluorescently labelled IN into the assembling capsid core through protease activation during viral maturation. A titration assay was performed to determine the optimal concentration of vectors to use in the production of CA and IN fluorescently labelled (dual-labelled) viruses (**Fig. 10**). A plasmid transfection concentration was selected which limited the loss of infectivity to 18% of that compared to WT virus. Although this was significantly lower than the WT virus,

subsequent confocal analysis ensured that enough fluorescently labelled virus was present for visualisation of colocalisation (**Fig. 12**).

Western blot analysis of viral supernatant produced when transfecting with increasing concentrations of MA-CA-GFP vector, revealed bands corresponding to the expected cleavage products (**Fig. 11**), including CA-GFP (~52 kDa). A large proportion of the matrix, however, remained attached to CA-GFP. This may have been due to the presence of immature viruses within the viral supernatant. Alternatively, the MA-CA-GFP protein may have been overly expressed in the producer cells and was in excess to that which could be processed by the NL4-3 protease. The absence of the proteins downstream from the MA-CA-GFP vector may also have had an effect on the upstream protease cleavage [206][207].

When the dual-labelled virus was pseudotyped with an HXB2 (WT) envelope and used to infect cell lines stably expressing the CD4 receptor (HeLa P4) or WT HeLa cells, CA-GFP and IN-mCherry colocalised particles were observed only in the CD4 expressing cell line (**Fig. 12**). The lack of fluorescent spots within WT HeLa cells indicated that the spots observed within the HeLa P4 cells entered productively through fusion with the CD4 receptor, rather than through endocytosis. A high percentage of colocalisation could also be observed between the CA-GFP and IN-mCherry signals, and the subsequent loss of colocalisation when imaging the dual-labelled virus at later time points post-infection lent further evidence for its potential use for the tracking of uncoating events (**Fig. 13**).

4.1.1 Validation of dual-labelled virus

A series of time courses were performed with the dual-labelled virus in the presence of CA-targeting restrictive compounds, and with the addition of mutations in the CA known to affect the stability of the capsid (**Fig. 14**). These were performed to verify whether the loss of colocalisation between the CA-GFP and IN-mCherry was a marker of real uncoating events, and from this to ascertain whether the dual-labelled virus was functioning like WT HIV-1 virus. Analysis in conjunction with a Vpr-IN-mCherry only trans-incorporated virus, stained with an anti-p24^{CA} antibody, showed a similar trend in loss of

colocalisation over time (**Fig. 14A**), with both viruses containing a residual proportion of the population that retained CA up until the end of the time course. This could also be observed directly under the confocal microscope (**Fig. 13D**). Visibly larger fluorescent puncta were obtained with the p24^{CA} stain compared to the fluorescently labelled CA, probably due to stoichiometric effects i.e. only a portion of the CA monomers present within the capsid core would be directly labelled by the fluorophore (trans-incorporation along with WT CA), whereas a higher percentage would be available for staining. This would account for the constantly higher percentage of colocalisation observed over time for the CA stained particles.

The addition of restriction compounds had a similar effect on the uncoating of the dual-labelled virus as has been reported in other uncoating assays [67][111][127]. The addition of the RT inhibitor, nevirapine, significantly delayed uncoating (**Fig. 14B**), in accordance with reports of a functional link between reverse transcription and CA disassembly [67][127][129]. The addition of PF74 [10 µM] promoted a moderate but significant increase in uncoating at 60 min prior to that of the DMSO control (**Fig. 14C**), consistent with reports that the capsid core destabilises in the presence of high concentrations [≥5µM] of PF74 [47][115][130][225]. A 50% half-time of uncoating was observed for both viruses at the 180 min time point post-trypsinisation. PF74 has also been reported to inhibit the binding of CA with the phenylalanine-glycine (FG) repeats of Nup358 and Nup153, impeding the interaction of these Nups with capsid at the nuclear envelope [46][91][105][130][131][176]. This may account for the levelling-off of colocalisation observed from 180 to 240 min post-trypsinisation in the presence of PF74 compared to the DMSO control.

The infection of TZM-bl cells stably expressing the TRIM-CypA restriction factor and a dual-labelled virus containing a less stable capsid core (K203A), both showed premature uncoating compared to the control viruses, in agreement with other reports (**Fig. 14D and E**) [67][127]. TRIM-CypA has been reported to target intact capsid cores soon after viral cellular entry, leading to premature capsid uncoating [122][123]. Both conditions exhibited increased uncoating at the '0 min plus trypsin' compared to the '0 min minus trypsin' time point. In our assay, we allowed a 50 min incubation period post-spinoculation before trypsinisation, for

the optimal fusion of the HXB2 (WT) envelope with the cellular membrane. This is in line with previous experiments and a report on the half-time for HXB2 fusion [67]. However, a large amount of virus was still entering the cells before the '0 min' time point, and these studies suggest that uncoating was occurring almost immediately after viral entry (before the 30 min post-trypsinisation time point). Compared to the directly fixed non-trypsinised cells (0 min minus trypsin), which would contain a large proportion of colocalised virions outside of the cell, a significant increase in uncoating could be observed within the trypsinised cells. Although spinoculation at 16°C increased the synchronisation of viral fusion events, these experiments highlight the dynamic kinetics of HIV-1 fusion, and the complications entailed in studying the uncoating events of bulk populations of viruses.

Finally, a double mutation (E128A/R132A) was introduced into the CA of the dual-labelled virus which has been reported to increase the stability of the capsid core, leading to delayed uncoating kinetics [65][67][124]. When assayed alongside a non-mutated dual-labelled virus, a similar trend in uncoating kinetics could be observed with both viruses (**Fig. 14F**). However, when the threshold for CA colocalisation with IN was raised (i.e. a higher intensity of CA within the segmented IN region was required to establish colocalisation) an almost 3-fold lower colocalisation (represented by the area under the curve – AUC) was observed with WT compared to the CA mutant virus (**Fig. 14G**). This means that a significantly larger proportion of capsid was remaining with the viral genome with the CA mutant compared to with the WT capsid, suggesting that the mutation was also affecting the stability of the remaining core after the initial uncoating event. This is similar to what was observed by Xu and co-workers [111].

A relative increase in colocalisation was occasionally observed at the end of the time course with this assay (**Fig. 14 A, F/G**), and visual inspection of the images revealed a number of colocalised particles. Some authors have reported a delayed uncoating at the periphery of the nucleus [15][86][142]. As the percentage of colocalisation using the 3D manager plugin was determined by the number of colocalised particles divided by the total number of IN-labelled particles, what we may be observing here is a loss of IN-labelled particles from

previously uncoated PICs (through diffusion or proteasome degradation) in comparison to the colocalised 'intact' capsid particles, which are remaining relatively stable in numbers. Thus, we are not actually observing an increase in total colocalisation, but an increase compared to the number of IN-labelled particles.

Taken together, these results show a decrease in colocalisation (capsid uncoating) over time, with a proportion of the CA remaining colocalised with IN up until the end of the time course - up to 6 hr post-spinoculation in some of the time courses (**Fig. 14A, B, D and F/G**). This is the period when most of the PICs were observed associated within the nucleus in a study performed by Albanese and co-workers [125]. There is the possibility that the colocalised particles observed at the end of the time course were aberrant viruses, and one of the current drawbacks in using imaging methods for tracking HIV-1 uncoating is the inability to distinguish between these and the particles which will eventually lead to productive infection [44][226]. However, it is tempting to speculate that the PICs containing a residual amount of CA may be the ones that lead to nuclear translocation, and subsequent integration into the host genome.

4.1.2 High-throughput analysis of uncoating

The tracking of the dual-labelled viruses using confocal microscopy was a very labour intensive process, taking up to 18 h just to acquire the images for a data set. To speed up the process a pipeline was devised using DeconvolutionLab open source software (ImageJ), which performed the automatic deconvolution, segmentation, counting and colocalisation of the images (**Fig. 17**). The IN-mCherry fluorophore was replaced with sfGFP, and the CA-GFP fluorophore subsequently swapped for mKO. In combination, these fluorophores provided a brighter fluorescence, enabling the reduction of the pinhole from 1.5 to 1.0 AU (**Table 1; Fig. 15**). This, in turn, reduced the background signal in the images, and resulted in smaller and more defined puncta. Time courses were repeated with the dual-fluorescent virus in the presence of nevirapine or the DMSO control. This enabled the use of the same virus stock between conditions, reducing the confounding effects associated with using two different viruses (i.e. those prepared with CA mutations). Again, the optimal segmentation

thresholding had to be adjusted manually, due to slight differences in the SNR between data sets (**Fig. 18**). This system drastically reduced the time it took to analyse the images (from a few days to a few hours). The accuracy of the DeconvolutionLab analysis was assessed by manual counting. Uncoating was determined by both the loss of the absolute number of CA-mKO and IN-sfGFP colocalised spots over time (**Fig. 19A**), and the number of colocalised spots divided by either the total number of CA-mKO (**Fig. 19B**) or IN-sfGFP spots. A clear drop in colocalisation, similar to that seen in **Fig. 14**, was observed over time using DeconvolutionLab analysis (**Fig. 19**). When assessing the absolute number of colocalised spots, a 50% half-time of uncoating was observed between the 110 and 170 min time points post-trypsinisation for both the nevirapine and the DMSO control samples (**Fig. 19A**). An additional sampling between these two time points may have enabled the elucidation of the capsid stabilising effects of nevirapine. However, when assessing the ratio of colocalised spots a significant delay in uncoating was recorded in the presence of nevirapine compared to the DMSO control at the 170 to 230 min time points (**Fig. 19B**). The disparity in results derived from these different systems for calculating uncoating can be explained by the fact that the first system considers solely the total number of colocalised spots, without addressing the uncoated particles. As the spot counts were derived from separate cell populations at different time points, it is highly likely that there were fluctuations in the number of viral particles per cell between disparate time points i.e. it is unlikely that each cell will be infected with exactly the same number of viral particles. When calculating the ratio of colocalisation, however, the method considers the number of CA-mKO or IN-sfGFP puncta in relation to the total number of colocalised particles, which should not be effected by disparities in cellular infection.

Although high-throughput analysis drastically reduced the time it took to analyse samples, and a clear difference in uncoating kinetics could be observed for the dual-labelled virus plus/minus the addition of nevirapine (**Fig. 19B**), a large deviation in the percentage/ratio of colocalisation was detected between separate time courses (**Fig. 19A and B**). There are many factors involved in an experiment of this sort – differences between viral productions, quality of the cells, even disparities through confocal acquisition on separate days. The

analysis of different cell populations within separate time points presented an additional factor that could lead to fluctuations within biological repeats.

4.1.3 Colocalisation within the nucleus

Contrary to some of the early studies, suggesting a model of complete capsid uncoating from the VNC directly after cellular entry of the virus [16][50], two groups have recently published the first images of CA particles colocalised with IN within the nucleus [55][57]. Both groups used the Vpr-IN-GFP system for labelling the PIC, and capsid colocalisation was detected using p24^{CA} antibody staining. Super-resolution microscopy was required in both cases because of the low levels of CA associated with the PICs in the nuclear compartment, with Peng and co-workers using photoactivated localisation microscopy (PALM) alongside direct stochastic optical reconstruction microscopy (dSTORM), whilst the Hulme group employed high resolution structured illumination microscopy (SIM). Using CA-mKO in conjunction with IN-sfGFP, we were also able to detect capsid particles colocalised with IN within the nucleus using conventional confocal microscopy and Huygens Remote Manager deconvolution software (**Fig. 20**). However, with the dual-fluorescently labelled virus it should be possible to track the translocation of the PIC through the nuclear membrane in real time, enabling live visualisation of the interaction of CA with the proteins involved in the nuclear import pathway (Nup358, Nup153, TNPO2, CPSF6). This presents many exciting possibilities for the further elucidation of viral interactions at the nuclear pore, and may confirm the growing literature reports suggesting a link with HIV-1 CA and PIC nuclear translocation and integration [85][86][87][91].

4.2 SuperNova tagging (SunTag) system – CA-SunTag

Reports that interfering with the protease cleavage sites and proteins downstream of the CA protein of Gag [207][212][213] might affect the maturation and assembly of a correctly functioning capsid core, led us to try an alternative method for labelling the capsid core. The SunTag provided an attractive alternative system for labelling of the capsid core because of its relatively small size 19 aa (2.3 kDa) compared to a fluorophore (27 kDa) [193]. The fluorescently labelled reporter antibody (scFv-sfGFP) was ideally suited for targeting the

SunTag, because the fused light and heavy chains of its epitope-binding regions enabled its productive expression within cells – facilitating its use in live microscopy. The CypA-binding loop was selected as the site for the incorporation of the SunTag peptide because of its prominent location on the surface of the capsid core, and literature reviews and protein folding algorithms suggested minimum impact for peptide insertion within this domain [65][112][215][214]. A mature capsid core is composed of approximately 1500 CA monomers [39][43]. Thus, it was reasoned that trans-incorporation of a viral vector containing the CA SunTag in conjunction with a standard viral vector, would provide enough sites for the binding of the fluorescently labelled antibody (scFv-sfGFP) for confocal visualisation, and the binding of cellular factors (e.g. CypA) necessary for productive infection.

Viral infectivity was significantly reduced for the CA-SunTag incorporated virus, but this could be rescued to almost half of the WT infectivity levels through co-transfection with greater ratios of a non-tagged packaging vector (**Fig. 22A**). When infecting HeLa P4 cells stably expressing scFv-sfGFP, very few spots were observed at various time points post-spinoculation (**Fig. 22B**). However, many spots could be observed in target cells when the CA-SunTag virus was produced in 293T cells stably expressing the scFv-sfGFP antibody (**Fig. 22C**). This may have been due to increased accessibility of the CA-SunTag epitope to the scFv-sfGFP antibodies during viral production. These spots were also shown to colocalise with a p24^{CA} antibody stain, which meant that the CA-SunTag system did not interfere with AG3.0 antibody binding. Finally, no CA-SunTag spots were observed when WT virus was produced in 293T cells expressing the scFv-sfGFP, and used to infect HeLa P4 cells (**Fig. 22D**); confirming that antibody incorporation was epitope specific.

Western blot analysis, however, revealed that proper protease cleavage was not occurring in viruses produced solely using the viral vector containing the CA-SunTag (**Fig. 23**). Bands of the correct size were observed when the CA-SunTag was co-transfected together with a non-mutated packaging vector, but these may just represent the cleavage products derived from the non-mutated vector. If the polyproteins derived from the CA-SunTag vector were not being correctly cleaved, then properly assembled capsid cores would not be formed, and the

CA-SunTag spots observed colocalised with the p24^{CA} antibody stain likely contained amalgamations of cleaved and non-cleaved Gag products. Many studies report the sensitivity of CA to mutations [65][112][227][129], and so it was decided to try an alternative strategy for studying capsid uncoating which did not involve manipulation of the CA protein.

4.3 Non-capsid based reporter assays

An alternative strategy for determining initial capsid uncoating events, is to label a component of the VNC within the capsid core that can produce a signal upon binding with an externalised capsid component. The SunTag system was ideally suited for this as the small epitopes could be linked together to form an array containing up to 24 repeats of this peptide [193]. Studies showed that the peptide epitopes within the array could be fully occupied by the fluorescently labelled antibody without steric hindrance, enabling massive signal amplification. The use of the scFv antibody fused to sfGFP also enabled successful expression in soluble form within the cell, with limited aggregation, facilitating its use in live cell microscopy. The 24x repeat peptide array was fused to both the CTD of Vpr-IN (IN-24xST) and the APOBEC 3F/3G* proteins (A3F/G*-24xST), for incorporation into the capsid core via interactions with the Gag p6 domain [183][184] and viral RNA [195][228], respectively. The principle behind this system was that when the capsid core started to disassemble, the fluorescently labelled antibodies present within the cytoplasm of the cell would be able to enter the capsid and bind to the SunTag peptide array, creating a signal.

Preliminary studies showed this to be a creditable candidate for studying uncoating, with many more spots observed in HeLa P4 cells at 60 min compared to 0 min post-infection with the 24xST virus, suggestive of uncoating events (**Fig. 24**). Staining with a p24^{CA} antibody revealed colocalised and CA only stained puncta, indicative of newly uncoated and intact cores, respectively. The IN-24xST system was initially tested in fixed cells using confocal microscopy, with viruses prepared in the presence of DMSO or nevirapine (**Fig. 25**). Five biological replicates showed an initial peak of uncoating in the DMSO control from 30 to 60 min post-spinoculation (**Fig. 25A-C**). The addition of nevirapine delayed the uncoating kinetics in two of the replicates (**Fig. 25C and E**), but no

significant difference compared to the DMSO control was observed in two more experiments (**Fig. 25B and D**). When the data sets were combined, however, a significant delay in peak uncoating from 45 to 120 mins p.s. (75 min) could be observed in the presence of nevirapine compared to the DMSO control (**Fig. 25F**). This was almost exactly the same delay recorded by Hulme and co-workers in the presence of nevirapine (73 min) when using the CsA washout assay for studying uncoating [67]. This also correlates with the delay in uncoating recorded with the dual-labelled virus in the presence of nevirapine, with a delay of 85 min and 60 min observed when using 3D manager (**Fig. 14B**), or DeconvolutionLab (**Fig. 19B**) for establishing colocalisation, respectively. Interestingly, uncoating events were still observed with the 24xST system right up to the end of the time course, 240 min post-spinoculation.

4.4 High-throughput analysis of uncoating

4.4.1 Analysis of the 24xSunTag with High-content imaging

The considerable signal amplification provided by the 24x repeat array opened up new options for image acquisition, including Operetta High-Content Imaging. Although Operetta has a lower resolution capacity compared to confocal microscopy, a wide field of view enables the imaging of many cells within the specimen area. Also, an inbuilt temperature and CO₂ regulator allows the tracking of viruses within the same cells over time, thus dispensing with the issue of different infection levels within different sampling populations associated with fixed cell analysis. Many well-defined spots could be observed at the initial time points, with a loss of spots per cell clearly seen over time (**Fig. 26**). Repeat time courses showed a significant peak in the number of spots per cell from approximately 20 to 30 minutes p.s., followed by a sharp decline to a level just above the negative control (**Fig. 27**). This peak is consistent with the 50% half-time recorded when using the CsA washout method for studying uncoating [67], suggesting that with this system the peak in spots per cell determines the half-time of uncoating. However, in contrast to the CsA washout study, no significant difference in the peak number of spots per cell was observed with the introduction of various CA mutants known to effect capsid stability, or the introduction of restriction compounds reported to alter the kinetics of capsid

uncoating (**Fig. 27, and 28A**). In fact, a slightly premature peak was observed with the more stable CA mutants (E45A and E128A/R132A) compared to the non-mutated virus (**Fig. 27B**). This lack of kinetic change raised concerns that we were observing viral fusion, rather than actual uncoating events. However, repeating the assay with vectors prepared without a viral genome, which produces VSV-G enveloped vesicles without a capsid core, elicited a response equal to that of the negative control (**Fig. 28A**).

Viruses were produced in the presence of saquinavir, a protease inhibitor which obstructs the cleavage of the Gag and Pol polyproteins by HIV-1 protease, preventing the formation of capsid cores. The rationale behind this being that prevention of capsid core formation would lead to the production of SunTag spots directly after viral fusion with the cellular membrane. Unfortunately, no shift in peak spot formation kinetics was observed in this experiment (**Fig. S3A**). This may in part be due, however, to issues with viral quantification, as protease inhibition also prevented the production of the RT used in PERT analysis. As such, equivalent volumes of viral preparation were used in both the control viruses, and those produced in the presence of saquinavir. As a result, a 6-fold increase in the number of SunTag spots was observed with the latter, which may have influenced the kinetics of spot formation. To properly analyse the effects of saquinavir, the experiment needs to be repeated with viral stocks adjusted to allow for the equivalent numbers of SunTag spots.

Hope and co-workers also reported a delay in uncoating kinetics when using a HIV-1 WT envelope as opposed to VSV-G pseudotyped viruses [67], which they attributed to the slower viral fusion with the cellular membrane. However, viruses prepared with an HXB2 envelope showed a similar, albeit less pronounced, peak with Operetta analysis (**Fig. 28B**). Interestingly, unlike VSV-G pseudotyped viruses, no sharp decline in spots per cell was observed with the HXB2 enveloped viruses, with more of a low, residual count over time; but this may be due to the low efficiency in infectivity recorded with WT as opposed to VSV-G pseudotyped particles [216].

In an alternative strategy to confirm whether the spots observed in this assay were depicting real uncoating events, we made use of the viral RNA binding

priorities of the APOBEC proteins for the incorporation of the SunTag into the capsid core [124]. Fascinatingly, a peak in the number of spots per cell was recorded within the same time frame for the APOBEC3 incorporation of the 24x repeat array, as with Vpr-IN incorporation (**Fig. 29**). The only difference in the kinetics between these two systems being a slower decline after the peak with APOBEC3G* incorporation of the SunTag.

The use of the Operetta high-content imaging system with a 60x objective increased the resolution of the images, enabling the discernment of a small but significant change in the kinetics of SunTag spot formation in the presence of nevirapine, after the initial peak (**Fig. 30A-C**). A premature peak in the number of SunTag spots per cell was also observed with a less stable CA mutant (K203A), indicative of earlier capsid uncoating (**Fig. 30D**). It is possible that the 40x objective was only able to detect the larger, bulk events of capsid uncoating, and the more intricate events detected using confocal acquisition (**Fig. 25**) were missed. Unfortunately, further analysis with the 60x objective was curtailed as the objective was available on a short-term lease.

Taken together, the 24x SunTag system seems to suggest a prominent initial uncoating event occurring soon after (20-60 min) viral fusion (**Fig. 25, 27-30**), with further uncoating events occurring towards the end of the time course, as ascertained by confocal microscopy (**Fig. 25**); the resolution of the Operetta being too low to capture these later events. Further validation of the 24x SunTag needs to be carried out, but this system would be ideally suited for live microscopy performed with higher resolution.

4.4.2 Luciferase analysis of capsid uncoating using the NanoBiT

Capsid uncoating was also analysed using the NanoBiT split luciferase system, with the small bit (HiBiT) of the split enzyme fused to both the ABOPEC3F/G* proteins, and to the CTD of IN in a viral vector. A HeLa P4 cell line was prepared stably expressing the large polypeptide (LgBiT). Similar to the SunTag peptide array system, uncoating was measured upon capsid disassembly, in this case allowing the entry and binding of the cytoplasmic LgBiT with the capsid internalised HiBiT, eliciting luminescence in the presence of the NanoLuc substrate.

Initial tests showed very repeatable peaks of luciferase (representing uncoating) at approximately 35 min and 45 min p.s. with the HiBiT fused to A3G* and A3F, respectively (**Fig. 31A**). An explanation for the difference could be the action of the A3F cytidine deaminase inhibiting minus strand DNA transcription, thus impeding uncoating. Cytidine deaminase activity was restricted with the A3G* mutant [124], therefore reverse transcription and uncoating could proceed as normal [67]. Further analysis of the A3F incorporated HiBiT revealed no difference in the RLU in the presence of nevirapine compared to a DMSO control (**Fig. 31B**). As reverse transcription may already be affected with this cytidine deaminase, further studies using the NNRTI might be more appropriate with A3G* HiBiT incorporation. The introduction of the destabilising (K203A) and stabilising (E128A/R132A) CA mutations caused slightly premature and delayed peaks in RLU, respectively, compared to the non-mutated CA (**Fig. 31C**).

Replications of the assay using vectors lacking the viral genome generated different RLU kinetics compared to true viruses (**Fig. 31D**), indicating the observation of uncoating events rather than the fusion of VLPs. This was also substantiated by transfection with the A3F/G* plasmid alone, which showed similar RLU kinetics as the VLPs (**Fig. S4**).

The HiBiT moiety fused directly to the integrase domain of the molecular clone resulted in similar peaks in RLU as those derived from the A3F/G* incorporated HiBiT (~37 min p.s.) (**Fig. 32**), indicating that the luminescence kinetics were derived from the disassembly of the capsid core, rather than from non-specific events consequent of VSV-G pseudotyped vesicles. A change in the luminescent kinetics in the presence of restriction compounds known to affect the timing of uncoating, lent further support to the validity of this assay in tracking capsid uncoating events. Although some studies suggest that PF74 has a destabilising effect on the capsid core at high concentrations ($\geq 5 \mu\text{M}$) [111][115][130] (**Fig. 14C**), and we observed a delay in uncoating indicative of capsid stabilisation with this assay, recent work by Saito and co-workers have suggested a multi-modal action of PF74 on capsid uncoating, depending on the concentrations used [131]. This highlights the complexity surrounding this process, which is likely to be cell

line dependent, and the requirement for further validation of this assay, also within distinct cell lines.

The table below (**Table 2**) highlights some of the strengths and weaknesses of the three capsid uncoating systems developed in this project.

Method	Criteria	Score	Comments
CA-GFP/mKO + Vpr-Integrase (Confocal)	Sensitivity/ Specificity	✓✓✓	Very sensitive (x,y resolution <300 nm), detects restriction compound/CA mutant specific changes in uncoating kinetics
	Robustness	✓	Imaging different cell sets over time, large difference in kinetics between biological replicates
	High-throughput	✗	Preparation of samples on separate coverslips and confocal acquisition of individual time points very labour intensive; two conditions per assay
	Cost-effectiveness	✓✓	Standard reagents used (with the exception of microscope slides and VECTASHIELD mounting medium)
24xSunTag (Operetta)	Sensitivity/ Specificity	✓	Limited kinetic changes upon addition of restriction compounds or capsid mutations
	Robustness	✓✓	Similar fluorescence kinetics between assays
	High-throughput	✓✓✓	96-well plate, many conditions per assay
	Cost-effectiveness	✓	Requires use of CellCarrier-96-well, tissue culture-treated plates with optically clear base
HiBiT (Tecan)	Sensitivity/ Specificity	✓✓	Small kinetic changes upon addition of restriction compounds or capsid mutations
	Robustness	✓✓	Similar luminescence kinetics between assays
	High-throughput	✓✓✓	96-well plate, many conditions per assay
	Cost-effectiveness	✗	Requires use of 96 well plates, white flat bottom tissue culture plates and Nano-Glo® Live Cell Reagent

Table 2. Summary of the three systems developed for studying capsid uncoating. The table shows a qualitative summary of the strengths and weaknesses of the three assays developed in this project, using the criteria – sensitivity and specificity, robustness, high-throughput capability and cost-effectiveness. Sensitivity and specificity was judged on the response of the capsid uncoating assay to CA mutations and restriction compounds and, in the case of the dual-labelled assay, comparison with manual counting of spots for false positives/negatives.

CONCLUSION

Much is yet unknown about the process of capsid uncoating. The fragility of the capsid core and its sensitivity to structural and chemical manipulation make it very difficult to study *in vivo*, which can be attested to by the diverse techniques that have been employed to investigate capsid uncoating (**section 1.7**). Different results can be obtained depending upon the system employed to study it, which is why three models of uncoating have been proposed (**section 1.5**). Capsid disassembly can also vary depending on the cell type infected, and is affected by the envelope used for pseudotyping (**Fig. 28**) [67][150][229]. This is likely to be due to the large number of cellular host factors that CA has been reported to bind and interact with (**section 1.8.3**) [58][54][56], which would be expressed in variable amounts depending on the cell line used. Using three distinct systems for studying uncoating: 1) dual-fluorescent labelling, 2) incorporation of a SunTag peptide array, and 3) a split luciferase reporter, we have shown that capsid uncoating is likely to be a biphasic process, with an initial peak of uncoating shortly after cellular entry (**Fig. 25, 27-32**) followed by a more gradual disassembly as the PIC traffics towards the nucleus (**Fig. 14 and 19**). A portion of the capsid is likely to remain with the PIC to facilitate docking with nuclear proteins at the NPC (**section 1.4.5**). This may explain the observation of CA colocalisation with IN at the end of the time courses, when studying uncoating with the dual-fluorescently labelled virus using confocal microscopy (**Fig. 14**). That a portion of the capsid remains with the PIC until nuclear translocation, fits well with the view that the capsid core may act as a shield to protect the viral genome from detection by cellular innate immune sensors (**section 1.4.2**). The visualisation of CA colocalised with IN in the nucleus of infected cells (**Fig. 20**), also lends further evidence to the notion of a potential role for CA in the nuclear import and integration of the PIC (**section 1.4.5/6**).

Finally, preliminary studies using the split-luciferase system for measuring capsid uncoating, show great potential for the development of a high-throughput assay for screening candidate compounds that restrict HIV-1 infection by targeting the stability of the capsid core. The conservative nature of the viral core and the large number of cellular factors it has been shown to associate with, suggests that it is very unlikely to be able to evolve resistance to restriction factors, making

it an ideal target for therapeutic intervention. Restriction compounds that speed up uncoating would be particularly effective, as this would have the twofold action of impairing infection due to the close interconnectedness between timely uncoating and optimal integration; and the activation of an innate cellular antiviral response through the exposure of the viral genome.

FUTURE PERSPECTIVES

All three systems developed for analysing uncoating need further validation to determine the sensitivity and specificity of these assays. Analysis of these assays within separate cells lines will also determine the robustness of these systems, and provide essential new understanding on the host-specific effects on uncoating.

The dual-labelled virus and the 24xSunTag assays will be further optimised for use with high-resolution live microscopy, such as the TILL Photonics iMic2 total internal reflection (TIRF) system. This will enable more sensitive live analysis of the uncoating events occurring towards the end of the time courses, at the point at which the PIC attaches to the NPC.

Further investigation of the dual-labelled virus in conjunction with protein knockdowns or the fluorescent labelling of cellular proteins (e.g. CypA, Nup358, Nup153, TNPO3 and CPSF6) would be useful for analysis of the interaction of CA with these proteins during nuclear import and viral integration.

High-resolution live microscopy of the repeat peptide SunTag system with viruses prepared with the S15-mCherry membrane marker (a fluorescently labelled fusion protein containing the 15 N-terminal amino acid membrane targeting domain of the Src tyrosine kinase p60^{c-Src} [192]), would allow better elucidation of the uncoating events occurring directly after membrane fusion.

Finally, further analysis needs to be done on the split-luciferase system of analysing uncoating, including additional tests with the HiBiT peptide fused directly to the CTD of IN in the NL4.3 molecular clone. The advantage of the latter being that VLPs are less likely to be produced when using full length viral vectors in the production of viruses. The speed, sensitivity and reproducibility of the split-luciferase capsid uncoating assay, makes this an ideal system for the screening of candidate compounds restricting one of the more conserved events of the HIV-1 lifecycle.

REFERENCES

- [1] Centers for Disease Control (CDC), "Kaposi's sarcoma and Pneumocystis pneumonia among homosexual men - New York and California," *Morb. Mortal. Wkly. Rep.*, vol. 30, no. 25, pp. 305–308, 1981.
- [2] D. T. Durack, "Opportunistic infections and Kaposi's sarcoma in homosexual men," *N Engl J Med*, vol. 305, no. 24, pp. 1465–1467, 1981.
- [3] K. Hymes, J. Greene, A. Marcus, D. William, T. Cheung, N. Prose, H. Ballard, and L. Laubenstein, "Kaposi'S Sarcoma in Homosexual Men—a Report of Eight Cases," *Lancet*, vol. 318, no. 8247, pp. 598–600, 1981.
- [4] F. Barre-Sinoussi, J. C. Chermann, F. Rey, M. T. Nugeyre, S. Chamarat, J. Gruest, C. Dautet, C. Axler-Blin, F. Vezinet-Brun, C. Rouzioux, W. Rozenbaum, and L. Montagnier, "Isolation of a T-lymphotropic retrovirus from a patient at risk for acquired immune deficiency syndrome (AIDS).," *Science (80-.)*, vol. 220(4599), pp. 868–71, 1983.
- [5] R. C. Gallo, S. Z. Salahuddin, M. Popovic, G. M. Shearer, M. Kaplan, B. F. Haynes, T. J. Palker, R. Redfield, J. Oleske, B. Safai, and al. et, "Frequent detection and isolation of cytopathic retroviruses (HTLV-III) from patients with AIDS and at risk for AIDS.," *Science*, vol. 224, no. 4648, pp. 500–3, 1984.
- [6] M. Popovic, M. G. Sarngadharan, E. Read, and R. C. Gallo, "Detection, isolation, and continuous production of cytopathic retroviruses (HTLV-III) from patients with AIDS and pre-AIDS.," *Science*, vol. 224, no. 4648, pp. 497–500, 1984.
- [7] K. Case, "Nomenclature: Human Immunodeficiency Virus," *Ann. Intern. Med.*, vol. 105, no. 1, pp. 133–133, 1986.
- [8] M. H. Merson, J. O'Malley, D. Serwadda, and C. Apisuk, "The history and challenge of HIV prevention," *The Lancet*, vol. 372, no. 9637. pp. 475–488, 2008.
- [9] B. N. Fields, P. M, D. E, G. Editor, R. A, L. Editor, M. A, M. Editor, R. Editor, S. E, S. Editor, D. M, Knipe, E. By, L. Williams, A. J. Levine, R. C. Condit, S. C. Harrison, L. A. Ball, N. Fields, B. N. Fields, D. M. Knipe, and P. M. Howley, *Field Virology*, 4th ed. Lippincott Williams & Wilkins, 2001.

- [10] J. M. Watts, K. K. Dang, R. J. Gorelick, C. W. Leonard, J. W. Bess, R. Swanstrom, C. L. Burch, and K. M. Weeks, "Architecture and secondary structure of an entire HIV-1 RNA genome.," *Nature*, vol. 460, no. 7256, pp. 711–6, 2009.
- [11] B. M. Peterlin and D. Trono, "Hide, shield and strike back: how HIV-infected cells avoid immune eradication," *Nat. Rev. Immunol.*, vol. 3, no. 2, pp. 97–107, 2003.
- [12] Y. Kobayashi, J. Zhuang, S. Peltz, and J. Dougherty, "Identification of a cellular factor that modulates HIV-1 programmed ribosomal frameshifting," *J. Biol. Chem.*, vol. 285, no. 26, pp. 19776–19784, 2010.
- [13] P. Biswas, X. Jiang, A. L. Pacchia, J. P. Dougherty, and S. W. Peltz, "The human immunodeficiency virus type 1 ribosomal frameshifting site is an invariant sequence determinant and an important target for antiviral therapy.," *J. Virol.*, vol. 78, no. 4, pp. 2082–7, 2004.
- [14] R. W. Doms and D. Trono, "The plasma membrane as a combat zone in the HIV battlefield," *Genes and Development*, vol. 14, no. 21, pp. 2677–2688, 2000.
- [15] N. Arhel, "Revisiting HIV-1 uncoating.," *Retrovirology*, vol. 7, no. 1, p. 96, Jan. 2010.
- [16] M. D. Miller, C. M. Farnet, and F. D. Bushman, "Human immunodeficiency virus type 1 preintegration complexes: studies of organization and composition.," *J. Virol.*, vol. 71, no. 7, pp. 5382–5390, 1997.
- [17] Y. Suzuki and R. Craigie, "The road to chromatin - nuclear entry of retroviruses.," *Nat. Rev. Microbiol.*, vol. 5, no. 3, pp. 187–96, 2007.
- [18] A. Trkola, "HIV-host interactions: Vital to the virus and key to its inhibition," *Current Opinion in Microbiology*, vol. 7, no. 4, pp. 407–411, 2004.
- [19] D. F. Purcell and M. A. Martin, "Alternative splicing of human immunodeficiency virus type 1 mRNA modulates viral protein expression, replication, and infectivity.," *J. Virol.*, vol. 67, no. 11, pp. 6365–6378, 1993.
- [20] C. Hellmund and A. M. L. Lever, "Coordination of genomic RNA packaging with viral assembly in HIV-1," *Viruses*, vol. 8, no. 7, 2016.
- [21] D. Muriaux, J. Mirro, D. Harvin, and A. Rein, "RNA is a structural element in retrovirus particles.," *Proc. Natl. Acad. Sci. U. S. A.*, vol. 98, no. 9, pp. 5246–51, 2001.

- [22] S. Campbell and A. Rein, "In Vitro Assembly Properties of Human Immunodeficiency Virus Type 1 Gag Protein Lacking the p6 Domain," *J. Virol.*, vol. 73, no. 3, pp. 2270–2279, 1999.
- [23] A. Cimarelli, S. Sandin, S. Höglund, and J. Luban, "Basic Residues in Human Immunodeficiency Virus Type 1 Nucleocapsid Promote Virion Assembly via Interaction with RNA," *J. Virol.*, vol. 74, no. 7, pp. 3046–3057, 2000.
- [24] E. Mailler, S. Bernacchi, R. Marquet, J.-C. Paillart, V. Vivet-Boudou, and R. P. Smyth, "The Life-Cycle of the HIV-1 Gag-RNA Complex.," *Viruses*, vol. 8, no. 9, Sep. 2016.
- [25] J. S. Saad, J. Miller, J. Tai, A. Kim, R. H. Ghanam, and M. F. Summers, "Structural basis for targeting HIV-1 Gag proteins to the plasma membrane for virus assembly.," *Proc. Natl. Acad. Sci. U. S. A.*, vol. 103, no. 30, pp. 11364–9, 2006.
- [26] V. Chukkapalli and A. Ono, "Molecular determinants that regulate plasma membrane association of HIV-1 Gag," *Journal of Molecular Biology*, vol. 410, no. 4, pp. 512–524, 2011.
- [27] S. E. El Meshri, D. Dujardin, J. Godet, L. Richert, C. Boudier, J. L. Darlix, P. Didier, Y. Mély, and H. De Rocquigny, "Role of the nucleocapsid domain in HIV-1 gag oligomerization and trafficking to the plasma membrane: A fluorescence lifetime imaging microscopy investigation," *J. Mol. Biol.*, vol. 427, no. 6, pp. 1480–1494, 2015.
- [28] J. Chen, S. A. Rahman, O. A. Nikolaitchik, D. Grunwald, L. Sardo, R. C. Burdick, S. Plisov, E. Liang, S. Tai, V. K. Pathak, and W.-S. Hu, "HIV-1 RNA genome dimerizes on the plasma membrane in the presence of Gag protein.," *Proc. Natl. Acad. Sci. U. S. A.*, vol. 113, no. 2, pp. E201-8, 2016.
- [29] L. VerPlank, F. Bouamr, T. J. LaGrassa, B. Agresta, A. Kikonyogo, J. Leis, and C. A. Carter, "Tsg101, a homologue of ubiquitin-conjugating (E2) enzymes, binds the L domain in HIV type 1 Pr55(Gag).," *Proc. Natl. Acad. Sci. U. S. A.*, vol. 98, no. 14, pp. 7724–9, 2001.
- [30] B. Strack, A. Calistri, S. Craig, E. Popova, and H. G. Göttlinger, "AIP1/ALIX is a binding partner for HIV-1 p6 and EIAV p9 functioning in virus budding," *Cell*, vol. 114, no. 6, pp. 689–699, 2003.
- [31] W. I. Sundquist and H. G. Krausslich, "HIV-1 assembly, budding, and maturation," *Cold Spring Harb. Perspect. Med.*, vol. 2, pp. 1–24, 2012.

- [32] Y. Suzuki and Y. Suzuki, "Gene Regulatable Lentiviral Vector System," in *Viral Gene Therapy*, InTech, 2011.
- [33] A. H. Kaplan, M. Manchester, and R. Swanstrom, "The activity of the protease of human immunodeficiency virus type 1 is initiated at the membrane of infected cells before the release of viral proteins and is required for release to occur with maximum efficiency.," *J. Virol.*, vol. 68, no. 10, pp. 6782–6, Oct. 1994.
- [34] S. K. Lee, M. Potempa, and R. Swanstrom, "The choreography of HIV-1 proteolytic processing and virion assembly," *Journal of Biological Chemistry*, vol. 287, no. 49. pp. 40867–40874, 2012.
- [35] S. Mattei, F. K. Schur, and J. A. Briggs, "Retrovirus maturation - An extraordinary structural transformation," *Curr. Opin. Virol.*, vol. 18, pp. 27–35, 2016.
- [36] W. I. Sundquist and H.-G. Kräusslich, "HIV-1 assembly, budding, and maturation.," *Cold Spring Harb. Perspect. Med.*, vol. 2, no. 7, p. a006924, Jul. 2012.
- [37] S. Mattei, M. Anders, J. Konvalinka, H.-G. Kräusslich, J. A. G. Briggs, and B. Müller, "Induced maturation of human immunodeficiency virus.," *J. Virol.*, vol. 88, no. 23, pp. 13722–31, 2014.
- [38] K. Wieggers, G. Rutter, H. Kottler, U. Tessmer, H. Hohenberg, and H. G. Kräusslich, "Sequential steps in human immunodeficiency virus particle maturation revealed by alterations of individual Gag polyprotein cleavage sites.," *J. Virol.*, vol. 72, no. 4, pp. 2846–2854, 1998.
- [39] B. K. Ganser-Pornillos, A. Cheng, and M. Yeager, "Structure of Full-Length HIV-1 CA: A Model for the Mature Capsid Lattice," *Cell*, vol. 131, no. 1, pp. 70–79, 2007.
- [40] S. Thenin-Houssier, I. M. S. De Vera, L. Pedro-Rosa, A. Brady, A. Richard, B. Konnick, S. Opp, C. Buffone, J. Fuhrmann, S. Kota, B. Billack, M. Pietka-Ottlik, T. Tellinghuisen, H. Choe, T. Spicer, L. Scampavia, F. Diaz-Griffero, D. J. Kojetin, and S. T. Valentea, "Ebselen, a small-molecule capsid inhibitor of HIV-1 replication," *Antimicrob. Agents Chemother.*, vol. 60, no. January, pp. 2195–2208, 2016.
- [41] T. Galal, P. Nardin, and J. Mignot, *An analysis for solar central receiver systems with terminal concentrators or variable apertures*, vol. 41, no. 2. 1988.

- [42] F. K. M. Schur, W. J. H. Hagen, M. Rumlová, T. Ruml, B. Müller, H.-G. Kräusslich, and J. a G. Briggs, "Structure of the immature HIV-1 capsid in intact virus particles at 8.8 Å resolution.," *Nature*, vol. 517, pp. 505–508, 2015.
- [43] J. a G. Briggs, M. N. Simon, I. Gross, H.-G. Kräusslich, S. D. Fuller, V. M. Vogt, and M. C. Johnson, "The stoichiometry of Gag protein in HIV-1.," *Nat. Struct. Mol. Biol.*, vol. 11, no. 7, pp. 672–675, 2004.
- [44] E. M. Campbell and T. J. Hope, "HIV-1 capsid: the multifaceted key player in HIV-1 infection," *Nat. Rev. Microbiol.*, vol. 13, no. 8, pp. 471–483, 2015.
- [45] L. Lamorte, S. Titolo, C. T. Lemke, N. Goudreau, J. F. Mercier, E. Wardrop, V. B. Shah, U. K. Von Schwedler, C. Langelier, S. S. R. Banik, C. Aiken, W. I. Sundquist, and S. W. Mason, "Discovery of novel small-molecule HIV-1 replication inhibitors that stabilize capsid complexes," *Antimicrob. Agents Chemother.*, vol. 57, no. 10, pp. 4622–4631, 2013.
- [46] A. J. Price, D. A. Jacques, W. A. McEwan, A. J. Fletcher, S. Essig, J. W. Chin, U. D. Halambage, C. Aiken, and L. C. James, "Host Cofactors and Pharmacologic Ligands Share an Essential Interface in HIV-1 Capsid That Is Lost upon Disassembly," *PLoS Pathog.*, vol. 10, no. 10, 2014.
- [47] W. S. Blair, C. Pickford, S. L. Irving, D. G. Brown, M. Anderson, R. Bazin, J. Cao, G. Ciaramella, J. Isaacson, L. Jackson, R. Hunt, A. Kjerrstrom, J. A. Nieman, A. K. Patick, M. Perros, A. D. Scott, K. Whitby, H. Wu, and S. L. Butler, "HIV capsid is a tractable target for small molecule therapeutic intervention," *PLoS Pathog.*, vol. 6, no. 12, 2010.
- [48] Z. Zhang, 1, F. Zhang, 1, C. Yang, 1, J. Qi, 1, S. Gao, 1, S. Li, 2 1, Y. Gu, 2 1, and * and Ningshao Xia, "HIV-1 Capsid as a Target for Antiviral Therapy," *J. AIDS Clin. Res.*, vol. 7, no. 1, pp. 1–6, 2011.
- [49] O. Pornillos, B. K. Ganser-Pornillos, and M. Yeager, "Atomic-level modelling of the HIV capsid.," *Nature*, vol. 469, no. 7330, pp. 424–7, 2011.
- [50] A. Fassati and S. P. Goff, "Characterization of intracellular reverse transcription complexes of human immunodeficiency virus type 1," *J Virol*, vol. 75, no. 8, pp. 3626–3635, 2001.

- [51] N. K. Heinzinger, M. I. Bukrinsky, S. A. Haggerty, A. M. Ragland, V. Kewalramani, M. A. Lee, H. E. Gendelman, L. Ratner, M. Stevenson, and M. Emerman, "The Vpr protein of human immunodeficiency virus type 1 influences nuclear localization of viral nucleic acids in nondividing host cells.," *Proc. Natl. Acad. Sci. U. S. A.*, vol. 91, no. 15, pp. 7311–5, Jul. 1994.
- [52] M. I. Bukrinsky, N. Sharova, T. L. McDonald, T. Pushkarskaya, W. G. Tarpley, and M. Stevenson, "Association of integrase, matrix, and reverse transcriptase antigens of human immunodeficiency virus type 1 with viral nucleic acids following acute infection.," *Proc. Natl. Acad. Sci. U. S. A.*, vol. 90, no. July, pp. 6125–6129, 1993.
- [53] D. McDonald, M. A. Vodicka, G. Lucero, T. M. Svitkina, G. G. Borisy, M. Emerman, and T. J. Hope, "Visualization of the intracellular behavior of HIV in living cells.," *J. Cell Biol.*, vol. 159, no. 3, pp. 441–52, Nov. 2002.
- [54] R. König, Y. Zhou, D. Elleder, T. L. Diamond, G. M. C. Bonamy, J. T. Ireland, C.-Y. Chiang, B. P. Tu, P. D. De Jesus, C. E. Lilley, S. Seidel, A. M. Opaluch, J. S. Caldwell, M. D. Weitzman, K. L. Kuhlen, S. Bandyopadhyay, T. Ideker, A. P. Orth, L. J. Miraglia, F. D. Bushman, J. a Young, and S. K. Chanda, "Global analysis of host-pathogen interactions that regulate early-stage HIV-1 replication.," *Cell*, vol. 135, no. 1, pp. 49–60, Oct. 2008.
- [55] A. E. Hulme, Z. Kelley, D. Foley, and T. J. Hope, "Complementary Assays Reveal a Low Level of CA Associated with Viral Complexes in the Nuclei of HIV-1-Infected Cells.," *J. Virol.*, vol. 89, no. March, pp. 5350–61, 2015.
- [56] A. L. Brass, D. M. Dykxhoorn, Y. Benita, N. Yan, A. Engelman, R. J. Xavier, J. Lieberman, and S. J. Elledge, "Identification of host proteins required for HIV infection through a functional genomic screen," *Science (80-.)*, vol. 319, no. 5865, pp. 921–926, 2008.
- [57] K. Peng, W. Muranyi, B. Glass, V. Laketa, S. R. Yant, L. Tsai, T. Cihlar, B. Müller, and H.-G. Kräusslich, "Quantitative microscopy of functional HIV post-entry complexes reveals association of replication with the viral capsid.," *Elife*, vol. 3, no. 2013, p. e04114, 2014.
- [58] H. Zhou, M. Xu, Q. Huang, A. T. Gates, X. D. Zhang, J. C. Castle, E. Stec, M. Ferrer, B. Strulovici, D. J. Hazuda, and A. S. Espeseth, "Genome-Scale RNAi Screen for Host Factors Required for HIV Replication," *Cell Host Microbe*, vol. 4, no. 5, pp. 495–504, 2008.

- [59] R. Welker, H. Hohenberg, U. Tessmer, C. Huckhagel, and H. G. Kräusslich, "Biochemical and structural analysis of isolated mature cores of human immunodeficiency virus type 1.," *J. Virol.*, vol. 74, no. 3, pp. 1168–77, 2000.
- [60] J. Rasaiyaah, C. P. Tan, A. J. Fletcher, A. J. Price, C. Blondeau, L. Hilditch, D. A. Jacques, D. L. Selwood, L. C. James, M. Noursadeghi, and G. J. Towers, "HIV-1 evades innate immune recognition through specific cofactor recruitment.," *Nature*, vol. 503, no. 7476, pp. 402–5, Nov. 2013.
- [61] D. Gao, J. Wu, Y.-T. Wu, F. Du, C. Aroh, N. Yan, L. Sun, and Z. J. Chen, "Cyclic GMP-AMP synthase is an innate immune sensor of HIV and other retroviruses.," *Science*, vol. 341, no. 6148, pp. 903–906, 2013.
- [62] N. Yan, A. D. Regalado-Magdos, B. Stiggelbout, M. A. Lee-Kirsch, and J. Lieberman, "The cytosolic exonuclease TREX1 inhibits the innate immune response to human immunodeficiency virus type 1.," *Nat. Immunol.*, vol. 11, no. 11, pp. 1005–13, 2010.
- [63] X. Lahaye, T. Satoh, M. Gentili, S. Cerboni, C. Conrad, I. Hurbain, A. El Marjou, C. Lacabaratz, J.-D. Lelièvre, and N. Manel, "The capsids of HIV-1 and HIV-2 determine immune detection of the viral cDNA by the innate sensor cGAS in dendritic cells.," *Immunity*, vol. 39, no. 6, pp. 1132–42, Dec. 2013.
- [64] J. Melchjorsen, "Learning from the messengers: Innate sensing of viruses and cytokine regulation of immunity-clues for treatments and vaccines," *Viruses*, vol. 5, no. 2, pp. 470–527, 2013.
- [65] B. M. Forshey, U. von Schwedler, W. I. Sundquist, and C. Aiken, "Formation of a human immunodeficiency virus type 1 core of optimal stability is crucial for viral replication.," *J. Virol.*, vol. 76, no. 11, pp. 5667–77, 2002.
- [66] G. J. Klarmann, C. A. Schaubert, and B. D. Preston, "Template-directed pausing of DNA synthesis by HIV-1 reverse transcriptase during polymerization of HIV-1 sequences in vitro," *J. Biol. Chem.*, vol. 268, no. 13, pp. 9793–9802, 1993.
- [67] A. E. Hulme, O. Perez, and T. J. Hope, "Complementary assays reveal a relationship between HIV-1 uncoating and reverse transcription.," *Proc. Natl. Acad. Sci. U. S. A.*, vol. 108, no. 24, pp. 9975–80, 2011.

- [68] Y. Yang, T. Fricke, and F. Diaz-Griffero, "Inhibition of reverse transcriptase activity increases stability of the HIV-1 core.," *J. Virol.*, vol. 87, no. 1, pp. 683–7, 2013.
- [69] S. J. Rihn, S. J. Wilson, N. J. Loman, M. Alim, S. E. Bakker, D. Bhella, R. J. Gifford, F. J. Rixon, and P. D. Bieniasz, "Extreme Genetic Fragility of the HIV-1 Capsid," *PLoS Pathog.*, vol. 9, no. 6, 2013.
- [70] U. K. von Schwedler, K. M. Stray, J. E. Garrus, and W. I. Sundquist, "Functional Surfaces of the Human Immunodeficiency Virus Type 1 Capsid Protein," *J. Virol.*, vol. 77, no. 9, pp. 5439–5450, 2003.
- [71] K. Warren, T. Wei, D. Li, F. Qin, D. Warrillow, M.-H. Lin, H. Sivakumaran, A. Apolloni, C. M. Abbott, A. Jones, J. L. Anderson, and D. Harrich, "Eukaryotic elongation factor 1 complex subunits are critical HIV-1 reverse transcription cofactors.," *Proc. Natl. Acad. Sci. U. S. A.*, vol. 109, no. 24, pp. 9587–92, 2012.
- [72] D. Warrillow, G. Tachedjian, and D. Harrich, "Maturation of the HIV reverse transcription complex: Putting the jigsaw together," *Reviews in Medical Virology*, vol. 19, no. 6, pp. 324–337, 2009.
- [73] S. Li, C. P. Hill, W. I. Sundquist, and J. T. Finch, "Image reconstructions of helical assemblies of the HIV-1 CA protein.," *Nature*, vol. 407, no. 6802, pp. 409–413, 2000.
- [74] M. P. Dodding and M. Way, "Coupling viruses to dynein and kinesin-1," *EMBO J.*, vol. 30, no. 17, pp. 3527–3539, 2011.
- [75] Z. Lukic, A. Dharan, T. Fricke, F. Diaz-Griffero, and E. M. Campbell, "HIV-1 uncoating is facilitated by dynein and kinesin 1.," *J. Virol.*, vol. 88, no. 23, pp. 13613–25, 2014.
- [76] V. Malikov, E. S. da Silva, V. Jovasevic, G. Bennett, D. a. de Souza Aranha Vieira, B. Schulte, F. Diaz-Griffero, D. Walsh, and M. H. Naghavi, "HIV-1 capsids bind and exploit the kinesin-1 adaptor FEZ1 for inward movement to the nucleus," *Nat. Commun.*, vol. 6, p. 6660, 2015.
- [77] Y. Sabo, D. Walsh, D. S. Barry, S. Tinaztepe, K. D. L. Santos, S. P. Goff, G. G. Gundersen, and M. H. Naghavi, "NIH Public Access," vol. 14, no. 5, 2014.

- [78] N. Arhel, A. Genovesio, K.-A. Kim, S. Miko, E. Perret, J.-C. Olivo-Marin, S. Shorte, and P. Charneau, "Quantitative four-dimensional tracking of cytoplasmic and nuclear HIV-1 complexes.," *Nat. Methods*, vol. 3, no. 10, pp. 817–824, 2006.
- [79] M. Yamashita and M. Emerman, "Capsid Is a Dominant Determinant of Retrovirus Infectivity in Nondividing Cells," *J. Virol.*, vol. 78, no. 11, pp. 5670–5678, 2004.
- [80] P. F. Lewis¹ and M. Emerman², "Passage through Mitosis Is Required for Oncoretroviruses but Not for the Human Immunodeficiency Virus," *J. Virol.*, vol. 68, no. 1, pp. 510–516, 1994.
- [81] T. Roe, T. C. Reynolds, G. Yu, and P. O. Brown, "Integration of murine leukemia virus DNA depends on mitosis.," *EMBO J.*, vol. 12, no. 5, pp. 2099–2108, 1993.
- [82] A. Fassati, "HIV infection of non-dividing cells: a divisive problem.," *Retrovirology*, vol. 3, p. 74, 2006.
- [83] R. A. Katz, J. G. Greger, and A. M. Skalka, "Effects of cell cycle status on early events in retroviral replication," *Journal of Cellular Biochemistry*, vol. 94, no. 5, pp. 880–889, 2005.
- [84] M. Yamashita and M. Emerman, "Retroviral infection of non-dividing cells: Old and new perspectives," *Virology*, vol. 344, no. 1, pp. 88–93, 2006.
- [85] K. a. Matreyek and A. Engelman, "Viral and cellular requirements for the nuclear entry of retroviral preintegration nucleoprotein complexes," *Viruses*, vol. 5, pp. 2483–2511, 2013.
- [86] L. Hilditch and G. J. Towers, "A model for cofactor use during HIV-1 reverse transcription and nuclear entry," *Curr. Opin. Virol.*, vol. 4, pp. 32–36, 2014.
- [87] Z. Ambrose and C. Aiken, "HIV-1 uncoating: Connection to nuclear entry and regulation by host proteins," *Virology*, vol. 454–455, no. 1, pp. 371–379, 2014.
- [88] M. Yamashita, O. Perez, T. J. Hope, and M. Emerman, "Evidence for direct involvement of the capsid protein in HIV infection of nondividing cells," *PLoS Pathog.*, vol. 3, no. 10, pp. 1502–1510, 2007.

- [89] D. J. Dismuke and C. Aiken, "Evidence for a Functional Link between Uncoating of the Human Immunodeficiency Virus Type 1 Core and Nuclear Import of the Viral Preintegration Complex," *J. Virol.*, vol. 80, no. 8, pp. 3712–3720, 2006.
- [90] K. E. Lee, Z. Ambrose, T. D. Martin, I. Oztop, A. Mulky, J. G. Julias, N. Vandegraaff, J. G. Baumann, R. Wang, W. Yuen, T. Takemura, K. Shelton, I. Taniuchi, Y. Li, J. Sodroski, D. R. Littman, J. M. Coffin, S. H. Hughes, D. Unutmaz, A. Engelman, and V. N. KewalRamani, "Flexible Use of Nuclear Import Pathways by HIV-1," *Cell Host Microbe*, vol. 7, no. 3, pp. 221–233, 2010.
- [91] T. Schaller, K. E. Ocwieja, J. Rasaiyaah, A. J. Price, T. L. Brady, S. L. Roth, S. Hué, A. J. Fletcher, K. Lee, V. N. KewalRamani, M. Noursadeghi, R. G. Jenner, L. C. James, F. D. Bushman, and G. J. Towers, "HIV-1 capsid-cyclophilin interactions determine nuclear import pathway, integration targeting and replication efficiency," *PLoS Pathog.*, vol. 7, no. 12, 2011.
- [92] K. a Matreyek and A. Engelman, "The requirement for nucleoporin NUP153 during human immunodeficiency virus type 1 infection is determined by the viral capsid.," *J. Virol.*, vol. 85, no. 15, pp. 7818–7827, 2011.
- [93] A. De Iaco, F. Santoni, A. Vannier, M. Guipponi, S. Antonarakis, and J. Luban, "TNPO3 protects HIV-1 replication from CPSF6-mediated capsid stabilization in the host cell cytoplasm.," *Retrovirology*, vol. 10, no. 1, p. 20, 2013.
- [94] A. Fassati, "Multiple roles of the capsid protein in the early steps of HIV-1 infection," *Virus Research*, vol. 170, no. 1–2, pp. 15–24, 2012.
- [95] A. R. W. Schröder, P. Shinn, H. Chen, C. Berry, J. R. Ecker, and F. Bushman, "HIV-1 integration in the human genome favors active genes and local hotspots," *Cell*, vol. 110, no. 4, pp. 521–529, 2002.
- [96] A. Ciuffi, M. Llano, E. Poeschla, C. Hoffmann, J. Leipzig, P. Shinn, J. R. Ecker, and F. Bushman, "A role for LEDGF/p75 in targeting HIV DNA integration.," *Nat. Med.*, vol. 11, no. 12, pp. 1287–1289, 2005.

- [97] M. C. Shun, N. K. Raghavendra, N. Vandegraaff, J. E. Daigle, S. Hughes, P. Kellam, P. Cherepanov, and A. Engelman, "LEDGF/p75 functions downstream from preintegration complex formation to effect gene-specific HIV-1 integration," *Genes Dev.*, vol. 21, no. 14, pp. 1767–1778, 2007.
- [98] G. A. Sowd, E. Serrao, H. Wang, W. Wang, H. J. Fadel, E. M. Poeschla, and A. N. Engelman, "A critical role for alternative polyadenylation factor CPSF6 in targeting HIV-1 integration to transcriptionally active chromatin.," *Proc. Natl. Acad. Sci. U. S. A.*, vol. 113, no. 8, pp. E1054-63, 2016.
- [99] C. R. Chin, J. M. Ferreira, G. Savidis, J. M. Portmann, A. M. Aker, E. M. Feeley, M. C. Smith, and A. L. Brass, "Direct Visualization of HIV-1 Replication Intermediates Shows that Capsid and CPSF6 Modulate HIV-1 Intra-nuclear Invasion and Integration," *Cell Rep.*, vol. 13, no. 8, pp. 1717–1731, 2015.
- [100] F. Di Nunzio, T. Fricke, A. Miccio, J. C. Valle-Casuso, P. Perez, P. Souque, E. Rizzi, M. Severgnini, F. Mavilio, P. Charneau, and F. Diaz-Griffero, "Nup153 and Nup98 bind the HIV-1 core and contribute to the early steps of HIV-1 replication," *Virology*, vol. 440, no. 1, pp. 8–18, 2013.
- [101] K. E. Ocwieja, T. L. Brady, K. Ronen, A. Huegel, S. L. Roth, T. Schaller, L. C. James, G. J. Towers, J. A. T. Young, S. K. Chanda, R. König, N. Malani, C. C. Berry, and F. D. Bushman, "HIV integration targeting: A pathway involving transportin-3 and the nuclear pore protein RanBP2," *PLoS Pathog.*, vol. 7, no. 3, 2011.
- [102] Y. Koh, X. Wu, A. L. Ferris, K. a. Matreyek, S. J. Smith, K. Lee, V. N. KewalRamani, S. H. Hughes, and A. Engelman, "Differential Effects of Human Immunodeficiency Virus Type 1 Capsid and Cellular Factors Nucleoporin 153 and LEDGF/p75 on the Efficiency and Specificity of Viral DNA Integration," *Journal of Virology*, vol. 87, no. 1. pp. 648–658, 2012.
- [103] N.-Y. Chen, L. Zhou, P. J. Gane, S. Opp, N. J. Ball, G. Nicastro, M. Zufferey, C. Buffone, J. Luban, D. Selwood, F. Diaz-Griffero, I. Taylor, and A. Fassati, "HIV-1 capsid is involved in post-nuclear entry steps.," *Retrovirology*, vol. 13, p. 28, 2016.
- [104] C. Aiken, "Cell-free assays for HIV-1 uncoating," *Methods Mol. Biol.*, vol. 485, pp. 41–53, 2009.

- [105] K. A. Matreyek, S. S. Yücel, X. Li, and A. Engelman, "Nucleoporin NUP153 Phenylalanine-Glycine Motifs Engage a Common Binding Pocket within the HIV-1 Capsid Protein to Mediate Lentiviral Infectivity," *PLoS Pathog.*, vol. 9, no. 10, 2013.
- [106] A. R. Lowe, J. J. Siegel, P. Kalab, M. Siu, K. Weis, and J. T. Liphardt, "Selectivity mechanism of the nuclear pore complex characterized by single cargo tracking.," *Nature*, vol. 467, no. 7315, pp. 600–3, 2010.
- [107] N. Pante and M. Kann, "Nuclear Pore Complex Is Able to Transport Macromolecules with Diameters of 39 nm," *Mol. Biol. Cell*, vol. 13, no. 2, pp. 425–434, 2002.
- [108] M. Bukrinsky, "A hard way to the nucleus," *Mol. Med.*, vol. 10, no. 1–6, pp. 1–5, 2004.
- [109] J. Lehmann-Che and A. Saïb, "Early stages of HIV replication: How to hijack cellular functions for a successful infection," *AIDS Reviews*, vol. 6, no. 4. pp. 199–207, 2004.
- [110] J. D. Dvorin and M. H. Malim, "Intracellular trafficking of HIV-1 cores: journey to the center of the cell," *Curr Top Microbiol Immunol*, vol. 281, pp. 179–208, 2003.
- [111] H. Xu, T. Franks, G. Gibson, K. Huber, N. Rahm, C. Strambio De Castillia, J. Luban, C. Aiken, S. Watkins, N. Sluis-Cremer, and Z. Ambrose, "Evidence for biphasic uncoating during HIV-1 infection from a novel imaging assay.," *Retrovirology*, vol. 10, no. 1, p. 70, 2013.
- [112] U. K. von Schwedler, K. M. Stray, J. E. Garrus, and W. I. Sundquist, "Functional surfaces of the human immunodeficiency virus type 1 capsid protein.," *J. Virol.*, vol. 77, no. 9, pp. 5439–50, 2003.
- [113] G. B. Mortuza, L. F. Haire, A. Stevens, S. J. Smerdon, J. P. Stoye, and I. a Taylor, "High-resolution structure of a retroviral capsid hexameric amino-terminal domain.," *Nature*, vol. 431, no. 2000, pp. 481–485, 2004.
- [114] O. Pornillos, B. K. Ganser-Pornillos, B. N. Kelly, Y. Hua, F. G. Whitby, C. D. Stout, W. I. Sundquist, C. P. Hill, and M. Yeager, "X-Ray Structures of the Hexameric Building Block of the HIV Capsid," *Cell*, vol. 137, no. 7, pp. 1282–1292, 2009.
- [115] J. Shi, J. Zhou, V. B. Shah, C. Aiken, and K. Whitby, "Small-molecule inhibition of human immunodeficiency virus type 1 infection by virus capsid destabilization," *J. Virol.*, vol. 85, no. 1, pp. 542–549, 2011.

- [116] V. B. Shah and C. Aiken, “*In vitro* Uncoating of HIV-1 Cores,” *J. Vis. Exp.*, no. November, pp. 2–5, 2011.
- [117] M. Stremlau, M. Perron, M. Lee, Y. Li, B. Song, H. Javanbakht, F. Diaz-Griffero, D. J. Anderson, W. I. Sundquist, and J. Sodroski, “Specific recognition and accelerated uncoating of retroviral capsids by the TRIM5 α restriction factor.,” *Proc. Natl. Acad. Sci. U. S. A.*, vol. 103, no. 14, pp. 5514–9, 2006.
- [118] T. Fricke, T. E. White, B. Schulte, D. a de Souza Aranha Vieira, A. Dharan, E. M. Campbell, A. Brandariz-Nuñez, and F. Diaz-Griffero, “MxB binds to the HIV-1 core and prevents the uncoating process of HIV-1.,” *Retrovirology*, vol. 11, p. 68, 2014.
- [119] S. B. Kutluay, D. Perez-Caballero, and P. D. Bieniasz, “Fates of Retroviral Core Components during Unrestricted and TRIM5-Restricted Infection,” *PLoS Pathog.*, vol. 9, no. 3, 2013.
- [120] P. Pawlica and L. Berthoux, “Cytoplasmic dynein promotes HIV-1 uncoating,” *Viruses*, vol. 6, no. 11, pp. 4195–4211, 2014.
- [121] D. M. Sayah, E. Sokolskaja, L. Berthoux, and J. Luban, “Cyclophilin A retrotransposition into TRIM5 explains owl monkey resistance to HIV-1.,” *Nature*, vol. 430, no. 6999, pp. 569–573, 2004.
- [122] B. M. Forshey, J. Shi, and C. Aiken, “Structural requirements for recognition of the human immunodeficiency virus type 1 core during host restriction in owl monkey cells.,” *J. Virol.*, vol. 79, no. 2, pp. 869–75, 2005.
- [123] J. Sastri and E. M. Campbell, “Recent insights into the mechanism and consequences of TRIM5 α retroviral restriction.,” *AIDS Res. Hum. Retroviruses*, vol. 27, no. 3, pp. 231–238, 2011.
- [124] R. C. Burdick, W.-S. Hu, and V. K. Pathak, “Nuclear import of APOBEC3F-labeled HIV-1 preintegration complexes.,” *Proc. Natl. Acad. Sci. U. S. A.*, vol. 110, pp. E4780-9, 2013.
- [125] A. Albanese, D. Arosio, M. Terreni, and A. Cereseto, “HIV-1 pre-integration complexes selectively target decondensed chromatin in the nuclear periphery,” *PLoS One*, vol. 3, no. 6, 2008.
- [126] E. M. Campbell, O. Perez, J. L. Anderson, and T. J. Hope, “Visualization of a proteasome-independent intermediate during restriction of HIV-1 by rhesus TRIM5 α .,” *J. Cell Biol.*, vol. 180, no. 3, pp. 549–61, Feb. 2008.

- [127] A. C. Francis, M. Marin, J. Shi, C. Aiken, and G. B. Melikyan, "Time-Resolved Imaging of Single HIV-1 Uncoating In Vitro and in Living Cells," *PLoS Pathog.*, vol. 12, no. 6, 2016.
- [128] A. S. Reicin, A. Ohagen, L. Yin, S. Hoglund, and S. P. Goff, "The role of Gag in human immunodeficiency virus type 1 virion morphogenesis and early steps of the viral life cycle.," *J. Virol.*, vol. 70, no. 12, pp. 8645–52, Dec. 1996.
- [129] A. E. Hulme, Z. Kelley, E. a Okocha, and T. J. Hope, "Identification of capsid mutations that alter the rate of HIV-1 uncoating in infected cells.," *J. Virol.*, vol. 89, no. 1, pp. 643–51, 2015.
- [130] A. Bhattacharya, S. L. Alam, T. Fricke, K. Zadrozny, J. Sedzicki, A. B. Taylor, B. Demeler, O. Pornillos, B. K. Ganser-Pornillos, F. Diaz-Griffero, D. N. Ivanov, and M. Yeager, "Structural basis of HIV-1 capsid recognition by PF74 and CPSF6.," *Proc. Natl. Acad. Sci. U. S. A.*, vol. 111, no. 52, pp. 18625–30, 2014.
- [131] A. Saito, D. Ferhadian, G. A. Sowd, E. Serrao, J. Shi, U. D. Halambage, S. Teng, J. Soto, M. A. Siddiqui, A. N. Engelman, C. Aiken, and M. Yamashita, "Roles of capsid-interacting host factors in multimodal inhibition of HIV-1 by PF74.," *J. Virol.*, vol. 90, no. 12, pp. 5808–5823, 2016.
- [132] S. Thenin-Houssier, I. M. S. de Vera, L. Pedro-Rosa, A. Brady, A. Richard, B. Konnick, S. Opp, C. Buffone, J. Fuhrmann, S. Kota, B. Billack, M. Pietka-Ottlik, T. Tellinghuisen, H. Choe, T. Spicer, L. Scampavia, F. Diaz-Griffero, D. J. Kojetin, and S. T. Valente, "Ebselen, a small molecule capsid-inhibitor of HIV-1 replication," *Antimicrob. Agents Chemother.*, no. JANUARY, p. AAC.02574-15, 2016.
- [133] K. Das, S. E. Martinez, J. D. Bauman, and E. Arnold, "HIV-1 reverse transcriptase complex with DNA and nevirapine reveals non-nucleoside inhibition mechanism," *Nat. Struct. Mol. Biol.*, vol. 19, no. 2, pp. 253–259, 2012.
- [134] V. J. Merluzzi, K. D. Hargrave, M. Labadia, K. Grozinger, M. Skoog, J. C. Wu, C. K. Shih, K. Eckner, S. Hattox, and J. Adams, "Inhibition of HIV-1 replication by a nonnucleoside reverse transcriptase inhibitor.," *Science*, vol. 250, no. 4986, pp. 1411–1413, 1990.

- [135] O. Cosnefroy, P. J. Murray, and K. N. Bishop, "HIV-1 capsid uncoating initiates after the first strand transfer of reverse transcription.," *Retrovirology*, vol. 13, no. 1, p. 58, 2016.
- [136] R. Li and G. G. Gundersen, "Beyond polymer polarity: how the cytoskeleton builds a polarized cell.," *Nat. Rev. Mol. Cell Biol.*, vol. 9, no. 11, pp. 860–73, 2008.
- [137] M. A. Welte, "Bidirectional transport along microtubules," *Current Biology*, vol. 14, no. 13. 2004.
- [138] E. M. Campbell and T. J. Hope, "Gene therapy progress and prospects: viral trafficking during infection.," *Gene Ther.*, vol. 12, no. 18, pp. 1353–1359, 2005.
- [139] M. H. Naghavi and S. P. Goff, "Retroviral proteins that interact with the host cell cytoskeleton," *Current Opinion in Immunology*, vol. 19, no. 4. pp. 402–407, 2007.
- [140] a Bukrinskaya, B. Brichacek, a Mann, and M. Stevenson, "Establishment of a functional human immunodeficiency virus type 1 (HIV-1) reverse transcription complex involves the cytoskeleton.," *J. Exp. Med.*, vol. 188, no. 11, pp. 2113–2125, 1998.
- [141] X. Contreras, O. Mzoughi, F. Gaston, M. B. Peterlin, and E. Bahraoui, "Protein kinase C-delta regulates HIV-1 replication at an early post-entry step in macrophages.," *Retrovirology*, vol. 9, p. 37, 2012.
- [142] N. J. Arhel, S. Souquere-Besse, S. Munier, P. Souque, S. Guadagnini, S. Rutherford, M.-C. Prévost, T. D. Allen, and P. Charneau, "HIV-1 DNA Flap formation promotes uncoating of the pre-integration complex at the nuclear pore.," *EMBO J.*, vol. 26, no. 12, pp. 3025–37, 2007.
- [143] G. Fischer, B. Wittmann-Liebold, K. Lang, T. Kiefhaber, and F. X. Schmid, "Cyclophilin and peptidyl-prolyl cis-trans isomerase are probably identical proteins.," *Nature*, vol. 337, no. 6206. pp. 476–478, 1989.
- [144] T. R. Gamble, F. F. Vajdos, S. Yoo, D. K. Worthylake, M. Houseweart, W. I. Sundquist, and C. P. Hill, "Crystal structure of human cyclophilin A bound to the amino-terminal domain of HIV-1 capsid," *Cell*, vol. 87, no. 7, pp. 1285–1294, 1996.
- [145] J. Luban, K. L. Bossolt, E. K. Franke, G. V Kalpana, and S. P. Goff, "Human immunodeficiency virus type 1 Gag protein binds to cyclophilins A and B.," *Cell*, vol. 73, no. 6, pp. 1067–1078, 1993.

- [146] E. Sokolskaja, D. M. Sayah, and J. Luban, "Target cell cyclophilin A modulates human immunodeficiency virus type 1 infectivity.," *J. Virol.*, vol. 78, no. 23, pp. 12800–8, 2004.
- [147] T. Hatzioannou, D. Perez-Caballero, S. Cowan, and P. D. Bieniasz, "Cyclophilin interactions with incoming human immunodeficiency virus type 1 capsids with opposing effects on infectivity in human cells.," *J. Virol.*, vol. 79, no. 1, pp. 176–83, 2005.
- [148] D. a Bosco, E. Z. Eisenmesser, S. Pochapsky, W. I. Sundquist, and D. Kern, "Catalysis of cis/trans isomerization in native HIV-1 capsid by human cyclophilin A.," *Proc. Natl. Acad. Sci. U. S. A.*, vol. 99, no. 8, pp. 5247–52, 2002.
- [149] T. Fricke, A. Brandariz-Nuñez, X. Wang, A. B. Smith, and F. Diaz-Griffero, "Human cytosolic extracts stabilize the HIV-1 core.," *J. Virol.*, vol. 87, no. 19, pp. 10587–97, 2013.
- [150] V. B. Shah, J. Shi, D. R. Hout, I. Oztop, L. Krishnan, J. Ahn, M. S. Shotwell, a. Engelman, and C. Aiken, "The Host Proteins Transportin SR2/TNPO3 and Cyclophilin A Exert Opposing Effects on HIV-1 Uncoating," *J. Virol.*, vol. 87, no. 1, pp. 422–432, 2012.
- [151] C. Liu, J. R. Perilla, J. Ning, M. Lu, G. Hou, R. Ramalho, B. A. Himes, G. Zhao, G. J. Bedwell, I.-J. Byeon, J. Ahn, A. M. Gronenborn, P. E. Prevelige, I. Rousso, C. Aiken, T. Polenova, K. Schulten, and P. Zhang, "Cyclophilin A stabilizes the HIV-1 capsid through a novel non-canonical binding site.," *Nat. Commun.*, vol. 7, p. 10714, 2016.
- [152] Y. Li, A. K. Kar, and J. Sodroski, "Target cell type-dependent modulation of human immunodeficiency virus type 1 capsid disassembly by cyclophilin A.," *J. Virol.*, vol. 83, no. 21, pp. 10951–62, 2009.
- [153] S. Matsuoka, E. Dam, D. Lecossier, F. Clavel, and A. J. Hance, "Modulation of HIV-1 infectivity and cyclophilin A-dependence by Gag sequence and target cell type.," *Retrovirology*, vol. 6, p. 21, 2009.
- [154] D. Braaten, E. K. Franke, and J. Luban, "Cyclophilin A is required for an early step in the life cycle of human immunodeficiency virus type 1 before the initiation of reverse transcription.," *J. Virol.*, vol. 70, no. 6, pp. 3551–60, 1996.

- [155] E. K. Franke and J. Luban, "Inhibition of HIV-1 replication by cyclosporine A or related compounds correlates with the ability to disrupt the Gag-cyclophilin A interaction.," *Virology*, vol. 222, no. 1, pp. 279–282, 1996.
- [156] O. Haller and G. Kochs, "Human MxA Protein: An Interferon-Induced Dynamin-Like GTPase with Broad Antiviral Activity," *J. Interf. Cytokine Res.*, vol. 31, no. 1, pp. 79–87, 2011.
- [157] C. Goujon, O. Moncorgé, H. Bauby, T. Doyle, C. C. Ward, T. Schaller, S. Hué, W. S. Barclay, R. Schulz, and M. H. Malim, "Human MX2 is an interferon-induced post-entry inhibitor of HIV-1 infection," *Nature*, vol. 502, no. 7472, pp. 559–62, 2013.
- [158] M. Kane, S. S. Yadav, J. Bitzegeio, S. B. Kutluay, T. Zang, S. J. Wilson, J. W. Schoggins, C. M. Rice, M. Yamashita, T. Hatziioannou, and P. D. Bieniasz, "MX2 is an interferon-induced inhibitor of HIV-1 infection.," *Nature*, vol. 502, no. 7472, pp. 563–6, 2013.
- [159] Z. Liu, Q. Pan, S. Ding, J. Qian, F. Xu, J. Zhou, S. Cen, F. Guo, and C. Liang, "The interferon-inducible MxB protein inhibits HIV-1 infection," *Cell Host Microbe*, vol. 14, no. 4, pp. 398–410, 2013.
- [160] V. Le Sage, A. J. Moulard, and F. Valiente-Echeverría, "Roles of HIV-1 capsid in viral replication and immune evasion," *Virus Res.*, vol. 193, pp. 116–129, 2014.
- [161] F. Diaz-Griffero, "The Role of TNPO3 in HIV-1 Replication.," *Mol Biol Int*, vol. 2012, p. 868597, 2012.
- [162] N. Kataoka, J. L. Bachorik, and G. Dreyfuss, "Transportin-SR, a nuclear import receptor for SR proteins," *J. Cell Biol.*, vol. 145, no. 6, pp. 1145–1152, 1999.
- [163] L. Zhou, E. Sokolskaja, C. Jolly, W. James, S. A. Cowley, and A. Fassati, "Transportin 3 promotes a nuclear maturation step required for efficient HIV-1 integration," *PLoS Pathog.*, vol. 7, no. 8, 2011.
- [164] A. De Iaco and J. Luban, "Inhibition of HIV-1 infection by TNPO3 depletion is determined by capsid and detectable after viral cDNA enters the nucleus," *Retrovirology*, vol. 8, no. 1, p. 98, 2011.
- [165] J. C. Valle-Casuso, F. Di Nunzio, Y. Yang, N. Reszka, M. Lienlaf, N. Arhel, P. Perez, A. L. Brass, and F. Diaz-Griffero, "TNPO3 is required for HIV-1 replication after nuclear import but prior to integration and binds the HIV-1 core.," *J. Virol.*, vol. 86, no. 10, pp. 5931–6, 2012.

- [166] U. Rügsegger, D. Blank, and W. Keller, "Human Pre-mRNA Cleavage Factor I m Is Related to Spliceosomal SR Proteins and Can Be Reconstituted In Vitro from Recombinant Subunits," *Mol. Cell*, vol. 1, no. 2, pp. 243–253, 1998.
- [167] A. J. Price, A. J. Fletcher, T. Schaller, T. Elliott, K. E. Lee, V. N. KewalRamani, J. W. Chin, G. J. Towers, and L. C. James, "CPSF6 Defines a Conserved Capsid Interface that Modulates HIV-1 Replication," *PLoS Pathog.*, vol. 8, no. 8, 2012.
- [168] K. Lee, A. Mulky, W. Yuen, T. D. Martin, N. R. Meyerson, L. Choi, H. Yu, S. L. Sawyer, and V. N. Kewalramani, "HIV-1 capsid-targeting domain of cleavage and polyadenylation specificity factor 6.," *J. Virol.*, vol. 86, no. 7, pp. 3851–60, 2012.
- [169] T. Hori, H. Takeuchi, H. Saito, R. Sakuma, Y. Inagaki, and S. Yamaoka, "A carboxy-terminally truncated human CPSF6 lacking residues encoded by exon 6 inhibits HIV-1 cDNA synthesis and promotes capsid disassembly.," *J. Virol.*, vol. 87, no. 13, pp. 7726–36, 2013.
- [170] T. Fricke, J. C. Valle-Casuso, T. E. White, A. Brandariz-Nuñez, W. J. Bosche, N. Reszka, R. Gorelick, and F. Diaz-Griffero, "The ability of TNPO3-depleted cells to inhibit HIV-1 infection requires CPSF6.," *Retrovirology*, vol. 10, p. 46, 2013.
- [171] A. A. Labokha and A. F. Fassati, "Viruses challenge selectivity barrier of nuclear pores," *Viruses*, vol. 5, no. 10, pp. 2410–2423, 2013.
- [172] C. Strambio-De-Castillia, M. Niepel, and M. P. Rout, "The nuclear pore complex: bridging nuclear transport and gene regulation," *Nat Rev Mol Cell Biol*, vol. 11, no. 7, pp. 490–501, 2010.
- [173] J. Wu, M. J. Matunis, D. Kraemer, G. Blobel, and E. Coutavas, "Nup358, a cytoplasmically exposed nucleoporin with peptide repeats, Ran-GTP binding sites, zinc fingers, a cyclophilin A homologous domain, and a leucine-rich region," *J. Biol. Chem.*, vol. 270, no. 23, pp. 14209–14213, 1995.
- [174] D. H. Lin, S. Zimmermann, T. Stuwe, E. Stuwe, and A. Hoelz, "Structural and functional analysis of the C-terminal domain of Nup358/RanBP2," *J. Mol. Biol.*, vol. 425, no. 8, pp. 1318–1329, 2013.

- [175] K. Bichel, A. J. Price, T. Schaller, G. J. Towers, S. M. V Freund, and L. C. James, "HIV-1 capsid undergoes coupled binding and isomerization by the nuclear pore protein NUP358.," *Retrovirology*, vol. 10, no. 1, p. 81, 2013.
- [176] F. Di Nunzio, A. Danckaert, T. Fricke, P. Perez, J. Fernandez, E. Perret, P. Roux, S. Shorte, P. Charneau, F. Diaz-Griffero, and N. J. Arhel, "Human Nucleoporins Promote HIV-1 Docking at the Nuclear Pore, Nuclear Import and Integration," *PLoS One*, vol. 7, no. 9, 2012.
- [177] A. M. Meehan, D. T. Saenz, R. Guevera, J. H. Morrison, M. Peretz, H. J. Fadel, M. Hamada, J. van Deursen, and E. M. Poeschla, "A Cyclophilin Homology Domain-Independent Role for Nup358 in HIV-1 Infection," *PLoS Pathog.*, vol. 10, no. 2, 2014.
- [178] F. Bin Hamid, J. Kim, and C.-G. Shin, "Cellular and viral determinants of retroviral nuclear entry.," *Can. J. Microbiol.*, vol. 62, no. 1, pp. 1–15, 2015.
- [179] P. Enarson, M. Enarson, R. Bastos, and B. Burke, "Amino-terminal sequences that direct nucleoporin Nup153 to the inner surface of the nuclear envelope," *Chromosoma*, vol. 107, no. 4, pp. 228–236, 1998.
- [180] B. Fahrenkrog, B. Maco, A. M. Fager, J. Köser, U. Sauder, K. S. Ullman, and U. Aebi, "Domain-specific antibodies reveal multiple-site topology of Nup153 within the nuclear pore complex," in *Journal of Structural Biology*, 2002, vol. 140, no. 1–3, pp. 254–267.
- [181] R. Y. H. Lim, N.-P. P. Huang, J. Köser, J. Deng, K. H. A. Lau, K. Schwarz-Herion, B. Fahrenkrog, and U. Aebi, "Flexible phenylalanine-glycine nucleoporins as entropic barriers to nucleocytoplasmic transport," *Proc. Natl. Acad. Sci.*, vol. 103, no. 25, pp. 9512–9517, 2006.
- [182] S. M. Paulillo, E. M. Phillips, J. Köser, U. Sauder, K. S. Ullman, M. A. Powers, and B. Fahrenkrog, "Nucleoporin domain topology is linked to the transport status of the nuclear pore complex," *J. Mol. Biol.*, vol. 351, no. 4, pp. 784–798, 2005.
- [183] W. Paxton, R. I. Connor, and N. R. Landau, "Incorporation of Vpr into human immunodeficiency virus type 1 virions: requirement for the p6 region of gag and mutational analysis.," *J. Virol.*, vol. 67, no. 12, pp. 7229–37, 1993.

- [184] H. Wu, H. Liu, H. Xiao, J. Kim, P. Seshiah, G. Natsoulis, J. D. Boeke, B. H. Hahn, and J. C. Kappes, "Targeting foreign proteins to human immunodeficiency virus particles via fusion with Vpr and Vpx.," *J. Virol.*, vol. 69, no. 6, pp. 3389–3398, 1995.
- [185] B. Müller, U. Tessmer, U. Schubert, and H. G. Kräusslich, "Human immunodeficiency virus type 1 Vpr protein is incorporated into the virion in significantly smaller amounts than gag and is phosphorylated in infected cells.," *J. Virol.*, vol. 74, no. 20, pp. 9727–31, 2000.
- [186] S. P. Singh, P. Tungaturthi, M. Cartas, B. Tomkowicz, T. A. Rizvi, S. A. Khan, V. S. Kalyanaraman, and A. Srinivasan, "Virion-associated HIV-1 Vpr: variable amount in virus particles derived from cells upon virus infection or proviral DNA transfection.," *Virology*, vol. 283, no. 1, pp. 78–83, 2001.
- [187] C. M. Danielson and T. J. Hope, "Imaging of HIV/host protein interactions," *Current Topics in Microbiology and Immunology*, vol. 339, no. 1, pp. 103–123, 2009.
- [188] C. Hoffmann, G. Gaietta, A. Zürn, S. R. Adams, S. Terrillon, M. H. Ellisman, R. Y. Tsien, and M. J. Lohse, "Fluorescent labeling of tetracycline-tagged proteins in intact cells.," *Nat. Protoc.*, vol. 5, no. 10, pp. 1666–77, 2010.
- [189] B. A. Griffin, S. R. Adams, R. Y. Tsien, R. Y. Tsien, E. Kalef, C. Gitler, V. P. Whittaker, G. Merutka, W. Shalongo, E. Stellwagen, W. G. Lowe, C. S. Hamilton, C. Spang, F. T. Edelman, M. Noltemeyer, H. W. Roesky, R. Heim, R. Y. Tsien, A. Miyawaki, M. Ormö, F. Denizot, R. Lang, G. Zlokarnik, C. F. Ford, I. Suominen, C. E. Glatz, G. R. Crabtree, and S. L. Schreiber, "Specific covalent labeling of recombinant protein molecules inside live cells.," *Science*, vol. 281, no. 5374, pp. 269–72, 1998.
- [190] G. Gaietta, T. J. Deerinck, S. R. Adams, J. Bower, O. Tour, D. W. Laird, G. E. Sosinsky, R. Y. Tsien, and M. H. Ellisman, "Multicolor and electron microscopic imaging of connexin trafficking," *Science (80-.)*, vol. 296, no. 5567, pp. 503–507, 2002.
- [191] K. a Page, T. Liegler, and M. B. Feinberg, "Use of a green fluorescent protein as a marker for human immunodeficiency virus type 1 infection.," *AIDS Res. Hum. Retroviruses*, vol. 13, no. 13, pp. 1077–81, 1997.

- [192] E. M. Campbell, O. Perez, M. Melar, and T. J. Hope, "Labeling HIV-1 virions with two fluorescent proteins allows identification of virions that have productively entered the target cell," *Virology*, vol. 360, no. 2, pp. 286–293, 2007.
- [193] M. E. Tanenbaum, L. a. Gilbert, L. S. Qi, J. S. Weissman, and R. D. Vale, "A protein-tagging system for signal amplification in gene expression and fluorescence imaging," *Cell*, vol. 159, no. 3, pp. 635–646, 2014.
- [194] J. L. Smith, W. Bu, R. C. Burdick, and V. K. Pathak, "Multiple ways of targeting APOBEC3-virion infectivity factor interactions for anti-HIV-1 drug development," *Trends in Pharmacological Sciences*, vol. 30, no. 12, pp. 638–646, 2009.
- [195] L. Apolonia, R. Schulz, T. Curk, P. Rocha, C. M. Swanson, T. Schaller, J. Ule, and M. H. Malim, "Promiscuous RNA Binding Ensures Effective Encapsidation of APOBEC3 Proteins by HIV-1," *PLoS Pathog.*, vol. 11, no. 1, pp. 1–22, 2015.
- [196] J. L. Mbisa, W. Bu, and V. K. Pathak, "APOBEC3F and APOBEC3G inhibit HIV-1 DNA integration by different mechanisms.," *J. Virol.*, vol. 84, no. 10, pp. 5250–5259, 2010.
- [197] A. Wörn, A. A. Der Maur, D. Escher, A. Honegger, A. Barberis, and A. Plückthun, "Correlation between in vitro stability and in vivo performance of anti- GCN4 intrabodies as cytoplasmic inhibitors," *J. Biol. Chem.*, vol. 275, no. 4, pp. 2795–2803, 2000.
- [198] J.-D. Pédelacq, S. Cabantous, T. Tran, T. C. Terwilliger, and G. S. Waldo, "Engineering and characterization of a superfolder green fluorescent protein.," *Nat. Biotechnol.*, vol. 24, no. 1, pp. 79–88, 2006.
- [199] A. M. Gronenborn, D. R. Filpula, N. Z. Essig, A. Achari, M. Whitlow, P. T. Wingfield, and G. M. Clore, "A novel, highly stable fold of the immunoglobulin binding domain of streptococcal protein G.," *Science*, vol. 253, no. 5020, pp. 657–61, 1991.
- [200] M. P. Hall, J. Unch, B. F. Binkowski, M. P. Valley, B. L. Butler, M. G. Wood, P. Otto, K. Zimmerman, G. Vidugiris, T. Machleidt, M. B. Robers, H. A. Benink, C. T. Eggers, M. R. Slater, P. L. Meisenheimer, D. H. Klaubert, F. Fan, L. P. Encell, and K. V. Wood, "Engineered luciferase reporter from a deep sea shrimp utilizing a novel imidazopyrazinone substrate," *ACS Chem. Biol.*, vol. 7, no. 11, pp. 1848–1857, 2012.

- [201] A. S. Dixon, M. K. Schwinn, M. P. Hall, K. Zimmerman, P. Otto, T. H. Lubben, B. L. Butler, B. F. Binkowski, T. MacHleidt, T. a. Kirkland, M. G. Wood, C. T. Eggers, L. P. Encell, and K. V. Wood, "NanoLuc Complementation Reporter Optimized for Accurate Measurement of Protein Interactions in Cells," *ACS Chem. Biol.*, vol. 11, pp. 400–408, 2016.
- [202] J. Vermeire, E. Naessens, H. Vanderstraeten, A. Landi, V. Iannucci, A. Van Nuffel, T. Taghon, M. Pizzato, and B. Verhasselt, "Quantification of reverse transcriptase activity by real-time PCR as a fast and accurate method for titration of HIV, lenti- and retroviral vectors.," *PLoS One*, vol. 7, no. 12, p. e50859, 2012.
- [203] M. Pizzato, O. Erlwein, D. Bonsall, S. Kaye, D. Muir, and M. O. McClure, "A one-step SYBR Green I-based product-enhanced reverse transcriptase assay for the quantitation of retroviruses in cell culture supernatants.," *J. Virol. Methods*, vol. 156, no. 1–2, pp. 1–7, Mar. 2009.
- [204] C. Petit, O. Schwartz, and F. Mammano, "Oligomerization within virions and subcellular localization of human immunodeficiency virus type 1 integrase.," *J. Virol.*, vol. 73, no. 6, pp. 5079–88, 1999.
- [205] C. F. Pereira, P. C. Ellenberg, K. L. Jones, T. L. Fernandez, R. P. Smyth, D. J. Hawkes, M. Hijnen, V. Vivet-Boudou, R. Marquet, I. Johnson, and J. Mak, "Labeling of multiple HIV-1 proteins with the biarsenical-tetracysteine system," *PLoS One*, vol. 6, no. 2, 2011.
- [206] S. K. Lee, M. Potempa, M. Kolli, A. ??zen, C. A. Schiffer, and R. Swanstrom, "Context surrounding processing sites is crucial in determining cleavage rate of a subset of processing sites in HIV-1 gag and gag-pro-pol polyprotein precursors by viral protease," *J. Biol. Chem.*, vol. 287, no. 16, pp. 13279–13290, 2012.
- [207] S. C. Pettit, M. D. Moody, R. S. Wehbie, A. H. Kaplan, P. V Nantermet, C. A. Klein, and R. Swanstrom, "The p2 domain of human immunodeficiency virus type 1 Gag regulates sequential proteolytic processing and is required to produce fully infectious virions.," *J. Virol.*, vol. 68, no. 12, pp. 8017–27, 1994.
- [208] U. O'Doherty, W. J. Swiggard, and M. H. Malim, "Human immunodeficiency virus type 1 spinoculation enhances infection through virus binding.," *J. Virol.*, vol. 74, no. 21, pp. 10074–80, 2000.

- [209] M. R. Neagu, P. Ziegler, T. Pertel, C. Strambio-De-Castillia, C. Grütter, G. Martinetti, L. Mazzucchelli, M. Grütter, M. G. Manz, and J. Luban, "Potent inhibition of HIV-1 by TRIM5-cyclophilin fusion proteins engineered from human components," *J. Clin. Invest.*, vol. 119, no. 10, pp. 3035–3047, 2009.
- [210] N. C. Shaner, P. a Steinbach, and R. Y. Tsien, "A guide to choosing fluorescent proteins.," *Nat. Methods*, vol. 2, no. 12, pp. 905–909, 2005.
- [211] S. Karasawa, T. Araki, T. Nagai, H. Mizuno, and A. Miyawaki, "Cyan-emitting and orange-emitting fluorescent proteins as a donor/acceptor pair for fluorescence resonance energy transfer.," *Biochem. J.*, vol. 381, no. Pt 1, pp. 307–12, 2004.
- [212] H. G. Kräusslich, M. Fäcke, A. M. Heuser, J. Konvalinka, and H. Zentgraf, "The spacer peptide between human immunodeficiency virus capsid and nucleocapsid proteins is essential for ordered assembly and viral infectivity.," *J. Virol.*, vol. 69, no. 6, pp. 3407–19, 1995.
- [213] L. V Coren, J. A. Thomas, E. Chertova, R. C. Sowder, T. D. Gagliardi, R. J. Gorelick, and D. E. Ott, "Mutational analysis of the C-terminal gag cleavage sites in human immunodeficiency virus type 1," *J. Virol.*, vol. 81, no. 18, pp. 10047–10054, 2007.
- [214] G. Zhao, J. R. Perilla, E. L. Yufenyuy, X. Meng, B. Chen, J. Ning, J. Ahn, A. M. Gronenborn, K. Schulten, C. Aiken, and P. Zhang, "Mature HIV-1 capsid structure by cryo-electron microscopy and all-atom molecular dynamics.," *Nature*, vol. 497, no. 7451, pp. 643–646, 2013.
- [215] S. Abdurahman, S. Höglund, A. Höglund, and A. Vahlne, "Mutation in the loop C-terminal to the cyclophilin A binding site of HIV-1 capsid protein disrupts proper virus assembly and infectivity.," *Retrovirology*, vol. 4, p. 19, 2007.
- [216] C. Aiken, "Pseudotyping Human Immunodeficiency Virus Type 1 (HIV-1) by the Glycoprotein of Vesicular Stomatitis Virus Targets HIV-1 Entry to an Endocytic Pathway and Suppresses both the Requirement for Nef and the Sensitivity to Cyclosporin A," *J. Virol.*, vol. 71, no. 8, pp. 5871–5877, 1997.
- [217] K. Strebel and M. a Khan, "APOBEC3G encapsidation into HIV-1 virions: which RNA is it?," *Retrovirology*, vol. 5, p. 55, 2008.

- [218] X. Wang, X. Li, J. Ma, L. Zhang, L. Ma, Z. Mi, J. Zhou, F. Guo, L. Kleiman, and S. Cen, "Human APOBEC3F incorporation into human immunodeficiency virus type 1 particles," *Virus Res.*, vol. 191, no. 1, pp. 30–38, 2014.
- [219] Y.-L. Chiu and W. C. Greene, "APOBEC3G: an intracellular centurion.," *Philos. Trans. R. Soc. Lond. B. Biol. Sci.*, vol. 364, no. 1517, pp. 689–703, 2009.
- [220] Y.-H. Zheng, D. Irwin, T. Kurosu, K. Tokunaga, T. Sata, and B. M. Peterlin, "Human APOBEC3F is another host factor that blocks human immunodeficiency virus type 1 replication.," *J. Virol.*, vol. 78, no. 11, pp. 6073–6, 2004.
- [221] C. Demaison, K. Parsley, G. Brouns, M. Scherr, K. Battmer, C. Kinnon, M. Grez, and A. J. Thrasher, "High-level transduction and gene expression in hematopoietic repopulating cells using a human immunodeficiency [correction of immunodeficiency] virus type 1-based lentiviral vector containing an internal spleen focus forming virus promoter.," *Hum. Gene Ther.*, vol. 13, no. 7, pp. 803–13, May 2002.
- [222] A. S. Dixon, M. K. Schwinn, M. P. Hall, K. Zimmerman, P. Otto, T. H. Lubben, B. L. Butler, B. F. Binkowski, T. MacHleidt, T. A. Kirkland, M. G. Wood, C. T. Eggers, L. P. Encell, and K. V. Wood, "NanoLuc Complementation Reporter Optimized for Accurate Measurement of Protein Interactions in Cells," *ACS Chem. Biol.*, vol. 11, no. 2, pp. 400–408, 2016.
- [223] C. Aiken, "Viral and cellular factors that regulate HIV-1 uncoating.," *Curr. Opin. HIV AIDS*, vol. 1, pp. 194–199, 2006.
- [224] J. O. Maldonado, J. L. Martin, J. D. Mueller, W. Zhang, and L. M. Mansky, "New insights into retroviral Gag-Gag and Gag-membrane interactions," *Frontiers in Microbiology*, vol. 5, no. JUN. 2014.
- [225] T. Fricke, C. Buffone, S. Opp, J. Valle-Casuso, and F. Diaz-Griffero, "BI-2 destabilizes HIV-1 cores during infection and Prevents Binding of CPSF6 to the HIV-1 Capsid.," *Retrovirology*, vol. 11, p. 120, 2014.
- [226] J. a Thomas, D. E. Ott, and R. J. Gorelick, "Efficiency of human immunodeficiency virus type 1 postentry infection processes: evidence against disproportionate numbers of defective virions.," *J. Virol.*, vol. 81, no. 8, pp. 4367–70, 2007.

- [227] S. Manocheewa, J. E. Mittler, R. Samudrala, and J. I. Mullins, “Composite sequence-structure stability models as screening tools for identifying vulnerable targets for HIV drug and vaccine development,” *Viruses*, vol. 7, pp. 5718–5735, 2015.
- [228] A. York, S. B. Kutluay, M. Errando, and P. D. Bieniasz, “The RNA Binding Specificity of Human APOBEC3 Proteins Resembles That of HIV-1 Nucleocapsid.,” *PLoS Pathog.*, vol. 12, no. 8, p. e1005833, Aug. 2016.
- [229] S. Brun, M. Solignat, B. Gay, E. Bernard, L. Chaloin, D. Fenard, C. Devaux, N. Chazal, and L. Briant, “VSV-G pseudotyping rescues HIV-1 CA mutations that impair core assembly or stability.,” *Retrovirology*, vol. 5, p. 57, Jul. 2008.
- <http://www.who.int/mediacentre/factsheets/fs360/en/>

SUPPORTING INFORMATION

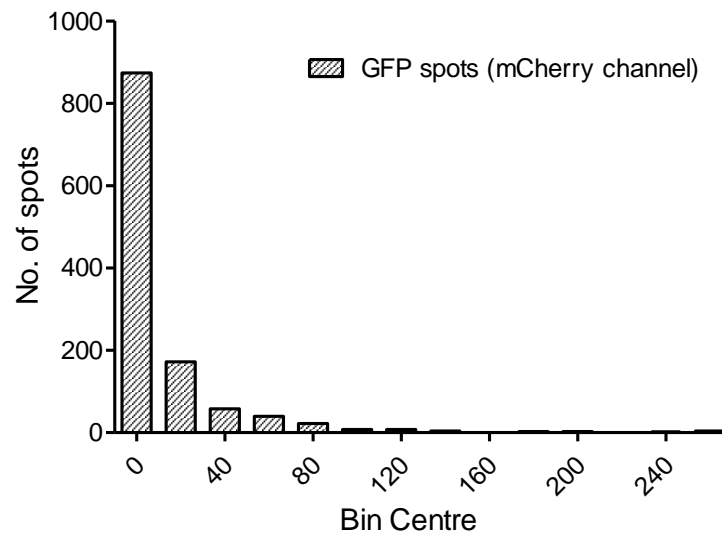


Figure S1. Graph showing the bleed-through from the GFP into the mCherry channel. HeLa P4 cells were transduced with 1 RTU of a HXB2 enveloped NL4-3 virus trans-incorporated with MA-CA-GFP only, and confocal images acquired using the standard settings for mCherry fluorophore acquisition (ex. at 543 nm, emission capture from 560 to 800 nm).

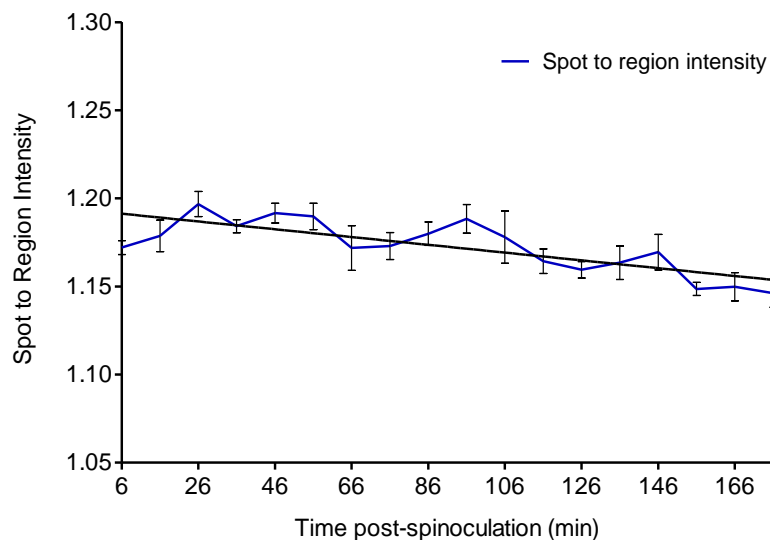


Figure S2. Bleaching profile of SunTag spots over time. HeLa P4 cells stably producing scFv-sfGFP were transduced with SunTag incorporated viruses and the spot intensity in relation to the background scFv-sfGFP in the cellular cytoplasm measured over time. SEM n = 4 technical repeats.

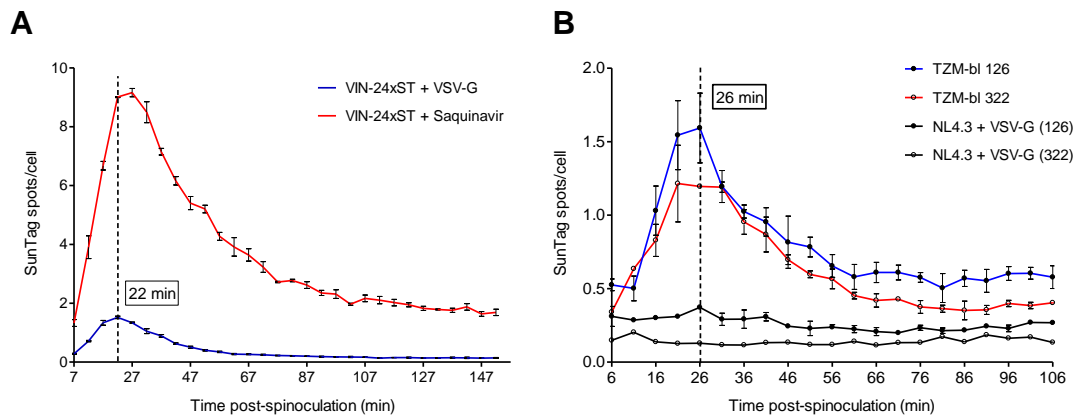


Figure S3. Number of SunTag spots per cell time post-spinoculation with viruses produced in the presence of saquinavir and in virus restricting TRIM-CypA producing cell lines. (A) IN-24xST viruses were produced in the presence of the protease inhibitor saquinavir and used to infect HeLa P4 cells stably producing the scFv-sfGFP antibody. **(B)** Transduction of scFv-sfGFP TZM-bl clone cells stably producing TRIMCypA or the TRIMCypA mutant. SEM n = 3 technical repeats.

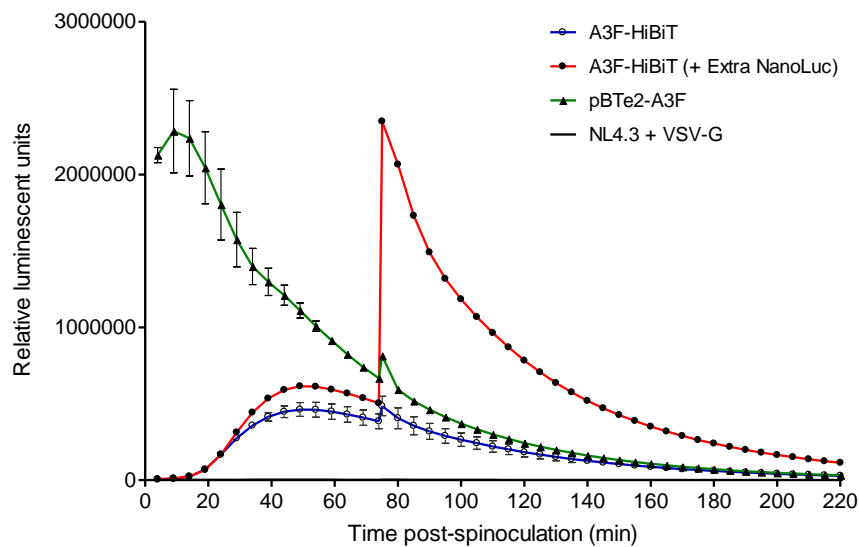


Figure S4. Depletion of Nano-Glo substrate. To ascertain whether we were observing the kinetics of capsid uncoating, and not the depletion of the Nano-Glo substrate, the experiment was repeated using the A3F-HiBiT virus with the addition of extra substrate at 75 min p.s. (when a reduction in signal in previous tests was detected). An immediate increase in signal was observed, with an instantaneous depletion in RLU after this time point, suggesting the addition of substrate fuelled the enzyme already present. Also shown is the pBTe2-A3F plasmid only positive control, which displays completely different RLU kinetics to the HiBiT incorporated viruses. SEM n = 3 technical repeats.

ACKNOWLEDGEMENTS

There are many people I would like to thank for their support during my PhD programme. Firstly, I would like to thank Anna Cereseto for giving me the opportunity to work within the Molecular Virology group, and for her continued support and guidance with this challenging project. I would also like to thank her for financing a 1 year extension, enabling me to explore the more recently developed systems for analysing capsid uncoating in greater detail. I would like to thank Ashwanth Francis, who supervised me at the beginning of my PhD and taught me many of the fundamental techniques employed in this project, and for the many hours he accompanied me during confocal acquisition. I would particularly like to thank Antonio Casini for his considerable intellectual input and prodigious assistance with the molecular aspects of the project, without which my thesis would have been a good deal shorter! I would also like to thank Gianluca Petris for his scientific expertise and helpful suggestions, and all the other members of the Molecular Virology group, past and present, for making it such an enjoyable and stimulating environment to work in, including Claudia Montagne, Giulia Maule, Giordano Reginato, Michele Olivieri, Ruben Maeso and Tiziana Coradin.

Outside of the Molecular Virology group I would like to thank Daniele Arosio, Jose Paredes, Marco Mina, and Giovanni Spagnolli for their valuable assistance with the technical and imaging aspects of the project.

Valuable technical support on this project was also provided by the CIBIO Core Facilities. I would particularly like to thank Valentina Adami and Michael Pancher from the High Throughput Screening facility, for their enthusiasm and expert assistance in the acquisition and analysis of images using the Operetta High-Content Imaging System. I would also like to thank Giorgina Scarduelli and Sara Leo from the Advanced Imaging group for their technical assistance with confocal microscopy and deconvolution.

I would like to express my very great appreciation to the Centre for Integrative Biology (CIBIO) of the University of Trento, which gave me the opportunity to work within this highly dynamic and stimulating research environment, and all the staff associated with the research centre - Paolo Macchi (former head of the PhD

programme) and the current coordinator Anna Cereseto; Betty Balduin (Secretariat of the PhD programme); Luca Andreetti, Marco Adami, Anna Helander and Paolo Struffi, and all the staff involved in the teaching and training provided by the International PhD programme.

Finally, I would like to express my deep gratitude to all my family and friends who have supported me during this time; for their incredible patience, generosity, understanding, encouragement and humour – many thanks!